OPTIMAL PRE AND POSTFILTERING OF NOISY SAMPLED SIGNALS-PARTICULAR APPLICATIONS TO PAM, PCM AND DPCM COMMUNICATION SYSTEMS

by

DONALD CHAN

B.A.Sc., University of British Columbia, 1964

M.A.Sc., University of British Columbia, 1967

A THESIS SUBMITTED IN PARTIAL FULFILMENT OF REQUIREMENTS FOR THE DEGREE OF

DOCTOR OF PHILOSOPHY

in the Department of Electrical Engineering

We accept this thesis as conforming to the required standard

Research Supervisor ....

Members of the Committee ....

....

....

Acting Head of the Department ....

Members of the Department of Electrical Engineering

THE UNIVERSITY OF BRITISH COLUMBIA

August, 1970

Department of ELECTRICAL ENGINEERING

The University of British Columbia
Vancouver 8, Canada

Date SEPT 1, 1970

ABSTRACT

In many control, data-processing, and communication systems, sampling is an inherent part of the system. If the time-continuous input signal is nonbandlimited, and noise is introduced in the system, an unavoidable error exists between the actual reconstructed signal and the desired time-continuous output signal. This error can be reduced by the suitable choice of prefilter prior to sampling and by the suitable choice of postfilter for reconstructing the time-continuous signal from the samples. In this thesis, an algorithm for determining the jointly optimal pre and postfilters which minimize the frequency weighted mean-integral-squared error of the system is presented, and the validity of the algorithm is proved. In the analysis, no restrictions are placed on the input signal spectrum or the noise spectrum, and the cross-correlation between signal and noise is taken into account.

Applications of the optimization algorithm to M-channel time-multiplexed PAM systems, PCM systems with digital channels errors, and DPCM systems are considered. Performance characteristics, showing mean-squared error and inband signal-to-noise ratio versus channel signal-to-noise ratio, are determined explicitly for optimal pre and postfiltered PAM and PCM systems with first-order Butterworth input spectrum. These characteristics are compared with those of PAM and PCM systems which use suboptimal filtering schemes and with the optimal performance theoretically attainable. Performance characteristics, showing mean-squared error versus channel capacity, are also determined for PAM, PCM, and DPCM systems when the systems parameters are optimized to yield the least mean-squared error for a given channel capacity.

Because of the subjective nature of speech, the effect of pre and postfilters in PAM, PCM and DPCM communication systems for speech transmission is studied by simulation methods and evaluated with subjective tests. Weak noise pre and postfilters (WNF), which yield virtually the same performance as optimal pre and postfilters, are considered in the subjective evaluation, in addition to lowpass pre and postfilters (LPF). The digital simulation facilities and the subjective testing methods are described, and the subjective results interpreted. It was observed that no significant subjective improvement resulted when WNF were used in place of LPF in PAM and DPCM systems. In PCM systems, significant differences in WNF and LPF subjective performances could exist. Using the analytical results, an explanation for the subjective behaviour is presented.

TABLE OF CONTENTS

Page

Page

LIST OF ILLUSTRATIONS

Page

LIST OF TABLES

ACKNOWLEDGEMENT

I am grateful to the Defence Research Board of Canada and the National Research Council of Canada for support received under Grants DRB 2801-26 and NRC A-3308, respectively. Grateful acknowledgement is also given to the National Research Council of Canada for NRC postgraduate scholarships received from 1967 to 1970.

I am particularly grateful to Dr. R.W. Donaldson for his valuable suggestions, generous counsel, and constant encouragement which were freely and readily given over the course of the research.

I am thankful to Messrs. E. Stanley, W. Dettwiler, and J. Stevens of the U.B.C. Computing Centre and Mr. M. Koombes of the U.B.C. Electrical Engineering Department for their assistance in the design, construction, and programming of the simulation facilities. I wish to thank Lenkurt Electric Company, Burnaby, Canada, for providing the lowpass and highpass filters used in the digital recording and playback systems. I also wish to express my sincere appreciation to Mr. A. MacKenzie for preparing the illustrations, and to Miss B. Harasymchuk and Miss H. DuBois for typing the manuscript.

Finally, in lieu of the time I might have otherwise spent with them, I would like to thank my wife, Patricia, and my daughters, Michelle, Elyse, and Nicole, for their patience and understanding.

1. INTRODUCTION

1.1 System Model

Widespread use of digital computers and the advent of low-priced integrated circuits have given great importance to the characterization of time-continuous signals in sampled format. In many control systems, data-processing systems, and communication systems, samples are taken of a time-continuous signal on input, and on output, a time-continuous signal is reconstructed. If the time-continuous input signal is tacitly assumed to be bandlimited to less than half the sampling frequency of the system, then straight-forward application of sampled data theory [1-3] can be used in the analysis and design of the system. Unfortunately, in many practical systems the input signal is not strictly bandlimited. Furthermore, if noise, necessarily introduced into the time-discrete signal, is also considered, an unavoidable error exists between the actual reconstructed signal and the desired continuous output signal. This error, however, can be reduced by the suitable choice of prefilter prior to sampling and by the suitable choice of postfilter for reconstruction from the time samples. A block diagram of the system under consideration is shown in Fig. 1. The research described in this thesis deals with the optimization of the pre and postfilters in Fig. 1 and the resulting applications.

Application of Fig. 1 to control systems results when digital controllers or digital filters are employed in place of continuous networks. If the computer operations are linear and time-invariant, then the digital computer program can be represented or included in the postfilter transfer function $G(f)$ [4,5]. Noise $n(t)$ can be interpreted at the error introduced by analog-to-digital conversion, and transfer function $A(f)$ as the continuous network which is to be simulated by the digital computer. For example, $A(f)$

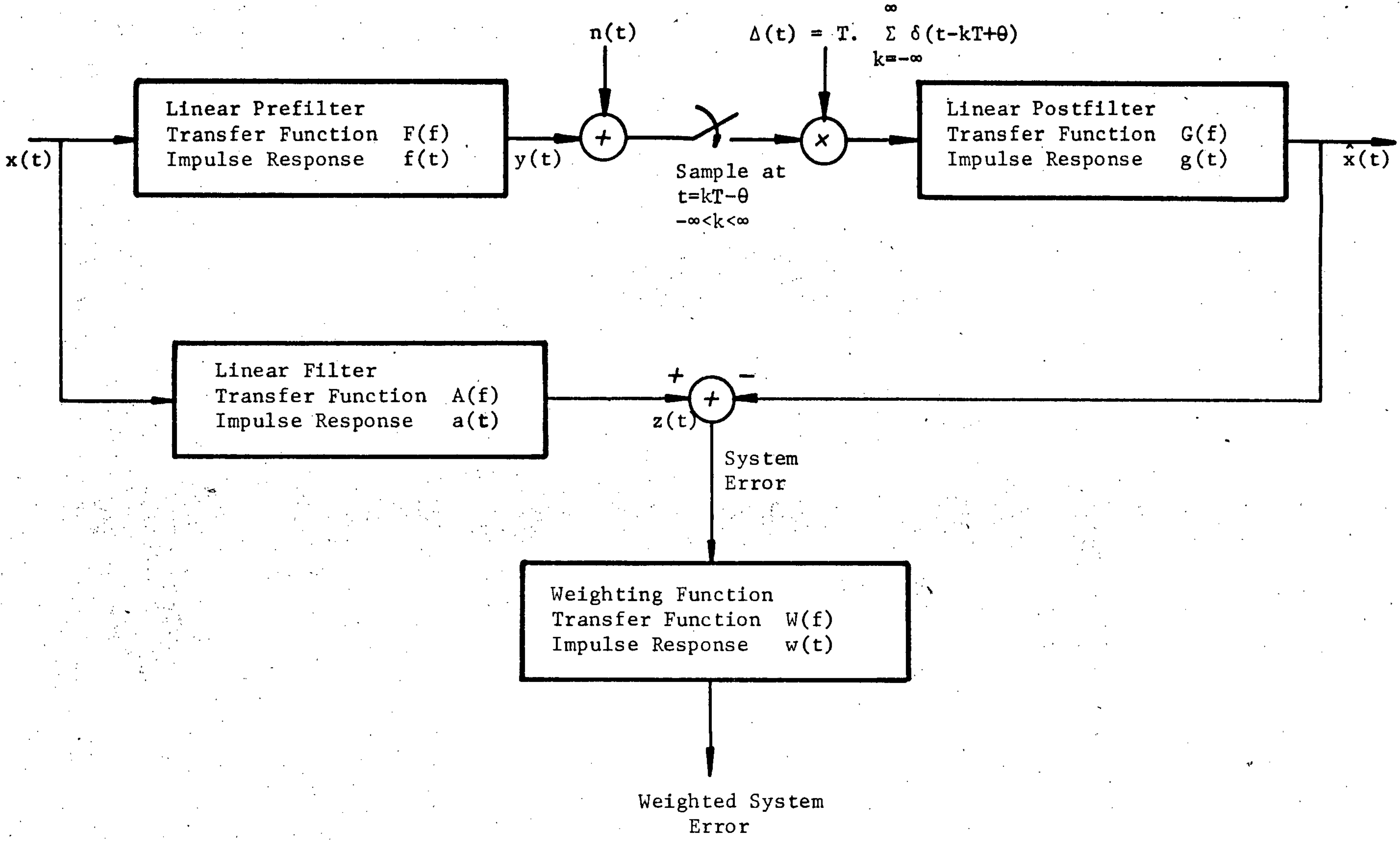

Fig. 1 Block diagram of a linear prefiltering and postfiltering system. Function $\delta(t)$ is the unit impulse. Phase angle θ is constant. Sampling period $T=1/f_s$ where f_s is the sampling frequency.

could be the transfer function of a compensating network. Although the advantages and disadvantages of utilizing a digital computer in control systems for continuous network simulation are dependent upon the particular application, it suffices to say that digital filters do not have the problems of drift, sensitivity and component tolerance that analog filters have. Furthermore, there are not real bounds on the accuracy that may be achieved in digital filter design.

In cases where Fig. 1 models a data-processing system, $x(t)$ may be a noisy version of some random function arising in the course of a measurement or observation, from which $z(t)$ is to be obtained by a linear operation. The prefilter, sampler, and noise process $n(t)$ may represent the analog-to-digital conversion process, and the postfilter might constitute a digital computer program.

When Fig. 1 depicts a communication system, $x(t)$ is the input message which is to be prefiltered, transmitted over a pulse modulation system and finally, postfiltered to yield the reconstructed time-continuous output $\hat{x}(t)$. Noise $n(t)$ is transmission and/or quantization noise arising from such pulse modulation systems as pulse amplitude modulation (PAM), pulse code modulation (PCM), and differential pulse code modulation (DPCM). The prefilter and the postfilter are chosen to make $\hat{x}(t)$ approximate the desired output $z(t)$, which is related to input $x(t)$ by a linear operation.

1.2 Review of Previous Research

Many significant contributions have been made to the optimal filtering problem since Wiener's original work [6]. The postfiltering problem of reconstructing continuous signal from time-discrete samples has been considered. Stewart [7] obtained the optimal reconstruction filter for noiseless samples, while Ruchkin [8] and Katzenelson [9] have determined the optimal postfilter for recovering an input signal from its quantized samples. Various aspects of the jointly optimal pre and postfiltering problem has been examined by numerous investigators. The first to examine the problem was Costas [10], who obtained the jointly optimal filters for wholly time-continuous systems. Tsybakov [11], Berger and Tufts [12], and Chang and Freeny [13] discussed the joint optimization of transmitter pulse-shaping filter and linear receiver filter in pulse transmission systems where the input and output signals are time-discrete random sequences. Other investigators, notably Robbins [14], De Russo [15], and Brown [16], have considered the joint optimization of pre and postfilters for data-processing and control applications. These systems were modelled as a concatenation of prefilter, sampler, and postfilter, in which the prefilter input consisted of signal plus noise.

As a communication system, the pre and postfiltering system shown in Fig. 1 has been analyzed with varying degrees of generality and rigor. Spilker [17] and Goodman and Drouilhet [18] determined the optimal filter pair when noise n(t) is white. Spilker considered input signals selected from a special class of nonbandlimited power spectra, while Goodman and Drouilhet treated bandlimited spectra. Kimme and Kuo [19], Bruce [20], and Brainard and Candy [21] are among some of the investigators who have analyzed systems which can essentially be reduced to the form shown in Fig. 1. However, in their investigations bandlimited input signals have been tacitly assumed. Nonbandlimited spectra have been considered by Kellogg [22], who utilized Brown's work [16] to obtain approximate optimal pre and postfilters for PCM systems. An unique feature in Kellogg's work is the inclusion of cross-correlation between the prefilter output signal and the quanization noise.

1.3 Scope of the Thesis

Although the previous works have developed fairly general solutions to the optimal filtering problem, they cannot be applied to nonbandlimited input and noise signals with arbitrary spectra. One of the purposes of this thesis is to derive expressions for the jointly optimal pre and postfilters under more general conditions. In the analysis of Chapter 2, no restrictions are placed on the input signal spectrum or the noise spectrum, and the cross-correlation between signal and noise is taken into account. Certain subtle and challenging difficulties arise in solving the necessary equations for the filters. First, the equations are nonlinear, and second, the equations along with the associated power constraint can be solved in an infinite number of ways. An algorithm for determining the solution which yields the least distortion is presented and proved to be optimal. The principal conclusion to be drawn from the algorithm is that the jointly optimal pre and postfilters are band-limited to a frequency set of total measure less than or equal to $1/T$, of which no two points coincide under frequency translation k/T for any integer $k \neq 0$. An important practical consequence of this conclusion is that the optimal prefilter and postfilter can be synthesized by combinations of analog bandpass and digital spectral-shaping filters. The fidelity criterion used in the analysis is the weighted integral of the system error spectrum. Frequency weighted mean-integral-squared error has been successfully employed by others as a measure of subjective goodness in television studies [19-21, 23].

In Chapter 3, optimal filtering is applied to some specific cases and various suboptimal filtering schemes are investigated. One scheme, designated as weak noise filtering, yields virtually the same performance as optimal filtering in many cases of interest, and has the practical advantage that the filter transfer characteristics are dependent only on the input signal spectrum and the relative spectrum of the noise.

Although the contents of the previous Chapters have more general applicability, only applications to PAM, PCM, and DPCM communication systems are considered in Chapter 4. The mean-squared error expression for a general M-channel time-multiplexed PAM system is derived. It is shown that if the requirement of distortionless transmission is imposed, which means that there is no intersymbol or interchannel distortion, then the time-multiplexed PAM system reduces to M independent systems of the form shown in Fig. 1. It is shown that PCM systems with digital channel errors can also be modelled by the system of Fig. 1. Correlation functions for quantized signals transmitted over discrete memoryless channels are derived and included as a necessary part of the filter optimization. Finally, it is shown that DPCM systems can also be reduced to the system depicted in Fig. 1. Once the major problem of modelling is solved, the results of Chapters 2 and 3 are easily applied. Optimal pre and postfiltering and some suboptimal filtering schemes which were presented in Chapter 3 are considered. System errors are evaluated and system parameters optimized to yield the least distortion for a channel of fixed capacity. The optimal performance theoretically attainable as derived from information theory arguments are computed and compared to the resulting performances achieved by the various filtering schemes utilized in the PAM, PCM, and DPCM communication systems.

In Chapter 5, two suboptimal filtering schemes discussed in Chapter 3, weak noise filtering and optimal prefiltering with constant amplitude postfiltering, are utilized in PAM, PCM, and DPCM speech communication systems which are simulated on a IBM 360/67 digital computer. Weak noise filters were simulated since they yield virtually the same performance as optimal pre and postfilters and have the practical advantage of relatively simple realization. The optimal prefilter-constant amplitude postfilter scheme was considered since under practical assumptions the filters are lowpass. The restrictions and assumptions used in the simulation are tabulated and an explanation of the simulation facilities, both hardware and software, is presented.

It is well known that the quality of speech cannot be judged by an objective measure alone. In fact, such a judgment may be quite misleading. The lack of an objective measure for speech quality necessitates the subjective measurements undertaken in Chapter 6, where a subjective testing method is developed for evaluating the subjective performances of PAM, PCM, and DPCM speech communication systems. The method is applied and the subjective results interpreted. It was observed that no significant subjective improvement resulted when weak noise filters (WNF) were used in place of lowpass filters (LPF) in the PAM and the DPCM systems. On the other hand, significant differences in subjective performance can exist between WNF and LPF in PCM systems. An heuristic explanation for this subjective behaviour is presented using the objective results of Chapter 4. Finally, a few concluding remarks are presented, including the feasibility of using a frequency weighted mean-integral-squared error criterion as an objective measure of speech quality, and the possibilities of using weak noise filters for television signals.

2. JOINT OPTIMIZATION OF THE PREFILTER AND THE POSTFILTER

In this Chapter the pre and postfilters shown in Fig. 1 are jointly optimized. The sampling operation is performed by a sampling gate in series with an impulse modulator. This results in no loss in generality since pulses of finite amplitude and duration can be converted to impulses by a linear pulse shaping filter included in the postfilter transfer function G(f). Filters having transfer functions A(f) and W(f) may not necessarily be physically realizeable. In addition, no a priori restrictions are placed on the power spectrum of the input signal or the noise, and the standard assumption of zero cross-correlation between signal and noise is not made. The figure of merit used for comparing system performance is the frequency weighted mean-integral-squared error criterion.

In Section 2.1, the error expression is derived and some necessary conditions for both realizeable and unrealizeable optimal filters presented. Section 2.2 is devoted to deriving further necessary conditions for unrealizeable filters. Unrealizeable filters provide a lower bound on the error obtained by linear time-invariant filters, and their characteristics can be approximated arbitrarily closely by physically realizeable filters if sufficient lag is permitted in the filter's impulse response. For many practical systems, such is the case, since reasonable time delay in the overall system response is usually not critical. In Section 2.3, an algorithm is presented for determining the characteristics and passbands of the optimal filters and in Section 2.4, the validity of the algorithm is established.

In the following analysis, E{ } denotes an ensemble average and $T = 1/f_s$ is the sampling period. Autocorrelation and cross-correlation functions are defined as $\phi_u(t,\tau) = E\{u(t)u(\tau)\}$ and $\phi_{uv}(t,\tau) = E\{u(t)v(\tau)\}$, respectively, where u(t) and v(t) are arbitrary random processes. If u(t) and v(t) are wide-sense stationary, then $\phi_u(t,\tau) = \phi_u(t-\tau)$ and $\phi_{uv}(t,\tau) = \phi_{uv}(t-\tau)$.

Fourier transform pairs are denoted by upper and lower case letters. For example, the power spectrum of u(t) is $\Phi_u(f) = \int_{-\infty}^{\infty} \phi_u(\tau)\, e^{-j2\pi f\tau} d\tau$ and the cross-power spectrum of u(t) and v(t) is $\Phi_{uv}(f) = \int_{-\infty}^{\infty} \phi_{uv}(\tau)\, e^{-j2\pi f\tau} d\tau$. Multiplication, convolution and complex conjugate are denoted by ".", "$\otimes$", "*", respectively.

2.1 Derivation of Weighted Mean-Integral-Squared Error Expression and Some Necessary Conditions

For the system shown in Fig. 1, the weighted mean-integral-squared error is given by

$$\varepsilon = E\{\frac{1}{T}\int_0^T (w(t) \otimes [z(t)-\hat{x}(t)])^2 dt\}$$

Substituting $\hat{x}(t) = g(t) \otimes [\Delta(t).(y(t)+n(t))]$ and $z(t) = a(t) \otimes x(t)$ and interchanging the order of integration and expectation yield

$$\varepsilon = \frac{1}{T}\int_0^T\{\iiiint_{-\infty}^{\infty} w(\beta_1)a(\beta_2)w(\beta_3)a(\beta_4)\phi_x(t-\beta_1-\beta_2,t-\beta_3-\beta_4)d\beta_1 d\beta_2 d\beta_3 d\beta_4$$

$$+ \iiiint_{-\infty}^{\infty} w(\beta_1)g(\beta_2)\Delta(t-\beta_1-\beta_2)w(\beta_3)g(\beta_4)\Delta(t-\beta_3-\beta_4)$$

$$\cdot[\phi_y(t-\beta_1-\beta_2,t-\beta_3-\beta_4) + \phi_{yn}(t-\beta_1-\beta_2,t-\beta_3-\beta_4)$$

$$+ \phi_{ny}(t-\beta_1-\beta_2,t-\beta_3-\beta_4) + \phi_n(t-\beta_1-\beta_2,t-\beta_3-\beta_4)]d\beta_1 d\beta_2 d\beta_3 d\beta_4$$

$$-2 \iiiint_{-\infty}^{\infty} w(\beta_1)a(\beta_2)w(\beta_3)g(\beta_4)\Delta(t-\beta_3-\beta_4)[\phi_{xy}(t-\beta_1-\beta_2,t-\beta_3-\beta_4)$$

$$+ \phi_{xn}(t-\beta_1-\beta_2,t-\beta_3-\beta_4)]d\beta_1 d\beta_2 d\beta_3 d\beta_4\}dt$$

Now, assume that x(t) and n(t) are stationary processes and the cross-correlation of y(t) and n(t) satisfy the relation $\phi_{yn}(\tau) = \hat{b}(\tau) \otimes \phi_y(\tau)$, where $\hat{b}(\tau)$ is a real function. It then follows that $\phi_{xn}(\tau) = \hat{b}(\tau)\otimes f(-\tau)\otimes\phi_x(\tau)$.

Substituting and integrating over t yield

$$\varepsilon = \iiiint_{-\infty}^{\infty} w(\beta_1)a(\beta_2)w(\beta_3)a(\beta_4)\phi_x(-\beta_1-\beta_2+\beta_3+\beta_4)d\beta_1 d\beta_2 d\beta_3 d\beta_4$$

$$+ \iiiint_{-\infty}^{\infty} w(\beta_1)g(\beta_2)w(\beta_3)g(\beta_4)\Delta(-\beta_1-\beta_2+\beta_3+\beta_4-\theta)[\Phi_n(-\beta_1-\beta_2+\beta_3+\beta_4)$$

$$+ \iiint_{-\infty}^{\infty} f(\beta_5)f(\beta_6)c(\beta_7)\phi_x(-\beta_1-\beta_2+\beta_3+\beta_4-\beta_5+\beta_6-\beta_7)d\beta_5 d\beta_6 d\beta_7]d\beta_1 d\beta_2 d\beta_3 d\beta_4$$

$$- 2 \int\!\!\int\!\!\int\!\!\int\!\!\int\!\!\int_{-\infty}^{\infty} w(\beta_1)a(\beta_2)w(\beta_3)g(\beta_4)f(\beta_5)b(\beta_6)\phi_x(-\beta_1-\beta_2+\beta_3+\beta_4+\beta_5-\beta_6)$$

$$d\beta_1 d\beta_2 d\beta_3 d\beta_4 d\beta_5 d\beta_6 \qquad (1)$$

where $b(\tau) = 1 + \hat{b}(\tau)$ and $c(\tau) = 1 + \hat{b}(\tau) + \hat{b}(-\tau)$.

Inspection of (1) leads to the conclusion that unless some restriction is placed on the prefilter output signal y(t), ε can be made arbitrarily small. In this regard, impose the following power constraint

$$E\{(k(t) \otimes y(t))^2\} = P$$

where k(t) is a real function. Taking expectation and expanding give

$$\iiiint_{-\infty}^{\infty} k(\beta_1)k(\beta_2)f(\beta_3)\ f(\beta_4)\ \phi_x(-\beta_1+\beta_2-\beta_3+\beta_4)d\beta_1 d\beta_2 d\beta_3 d\beta_4 = P \qquad (2)$$

The problem is to select filter impulse responses f(t) and g(t) such that ε in (1) is minimized subject to constraint (2). Use of variational calculus [24-26] shows that

$$\int\!\!\int\!\!\int\!\!\int\!\!\int\!\!\int_{-\infty}^{\infty} w(\beta_1)g(\beta_2)w(\beta_3)g(\beta_4)\Delta(-\beta_1-\beta_2+\beta_3+\beta_4-\theta)f(\beta_6)c(\beta_7)$$

$$\cdot\ \phi_x(-\beta_1-\beta_2+\beta_3+\beta_4-t+\beta_6-\beta_7)d\beta_1 d\beta_2 d\beta_3 d\beta_4 d\beta_6 d\beta_7$$

$$- \int\!\!\int\!\!\int\!\!\int\!\!\int_{-\infty}^{\infty} w(\beta_1)a(\beta_2)w(\beta_3)g(\beta_4)b(\beta_6)\phi_x(-\beta_1-\beta_2+\beta_3+\beta_4+t-\beta_6)d\beta_1 d\beta_2 d\beta_3 d\beta_4 d\beta_6$$

$$+ \lambda \iiint_{-\infty}^{\infty} k(\beta_1)k(\beta_2)f(\beta_4)\phi_x(-\beta_1+\beta_2-t+\beta_4)d\beta_1 d\beta_2 d\beta_4$$

$$= 0 \text{ for } \begin{cases} \text{all } t, \text{ unrealizeable filters} & (3a) \\ t \geq 0, \text{ realizeable filters} & (3b) \end{cases}$$

and that

$$\iint_{-\infty}^{\infty} \hat{f}(t)\hat{f}(\tau)\{\iiiint_{\infty}^{\infty} w(\beta_1)g(\beta_2)w(\beta_3)g(\beta_4)\Delta(-\beta_1-\beta_2+\beta_3+\beta_4-\theta)c(\beta_7)$$

$$\cdot\emptyset_x(-\beta_1-\beta_2+\beta_3+\beta_4-t+\tau-\beta_7)d\beta_1 d\beta_2 d\beta_3 d\beta_4 d\beta_7$$

$$+ \lambda \iint_{-\infty}^{\infty} k(\beta_1)k(\beta_2)\emptyset_x(-\beta_1+\beta_2-t+\tau)d\beta_1 d\beta_2\}dtd\tau > 0 \qquad (4)$$

are necessary and sufficient conditions for a prefilter impulse response $f(t)$ that minimizes ε for a fixed postfilter impulse response $g(t)$. The Lagrange multiplier λ must be chosen so that the solution of (3) for $f(t)$ satisfies (2). Assume $\lambda \geq 0$; then (4) is satisfied for all possible variations, $\hat{f}(t)$, of $f(t)$ when $C(f) > 0$, where $C(f)$ is the Fourier transform of $c(t)$. The assumption $\lambda \geq 0$ will be validated in Section 2.2. Similarly, it can be shown that

$$\iiint_{-\infty}^{\infty} w(\beta_1)w(\beta_3)g(\beta_4)\Delta(-\beta_1-t+\beta_3+\beta_4-\theta)[\emptyset_n(-\beta_1-t+\beta_3+\beta_4)$$

$$+ \iiint_{-\infty}^{\infty} f(\beta_5)f(\beta_6)c(\beta_7)\emptyset_x(-\beta_1-t+\beta_3+\beta_4-\beta_5+\beta_6-\beta_7)d\beta_5 d\beta_6 d\beta_7]d\beta_1 d\beta_3 d\beta_4$$

$$- \iiiiint_{-\infty}^{\infty} w(\beta_1)a(\beta_2)w(\beta_3)f(\beta_5)b(\beta_6)\emptyset_x(-\beta_1-\beta_2+\beta_3+t+\beta_5-\beta_6)d\beta_1 d\beta_2 d\beta_3 d\beta_5 d\beta_6$$

$$= 0 \text{ for } \begin{cases} \text{all } t, \text{ unrealizeable filters} & (5a) \\ t \geq 0, \text{ realizeable filters} & (5b) \end{cases}$$

and

$$\iint_{-\infty}^{\infty} \hat{g}(t)\hat{g}(\tau)\{\iint_{-\infty}^{\infty} w(\beta_1)w(\beta_3)\Delta(-\beta_1-t+\beta_3+\tau-\theta)[\emptyset_n(-\beta_1-t+\beta_3+\tau)$$

$$+ \iiint_{-\infty}^{\infty} f(\beta_5)f(\beta_6)c(\beta_7)\emptyset_x(-\beta_1-t+\beta_3+\tau-\beta_5+\beta_6-\beta_7)d\beta_5 d\beta_6 d\beta_7]d\beta_1 d\beta_3\}dtd\tau > 0 \qquad (6)$$

are the necessary and sufficient conditions for a postfilter impulse response $g(t)$ that minimizes ε for a fixed prefilter. Condition (6) is satisfied for all possible variations, $\hat{g}(t)$, of $g(t)$ when $C(f) > 0$. Therefore, assume the fixed and known real function $C(f) = 1 + \hat{B}(f) + \hat{B}^*(f)$ is positive. Then (3) and (5) constitute a set of necessary conditions that must be satisfied by $f(t)$ and $g(t)$ in order to be a solution to the joint optimization problem.

If the physical realizeability constraint is not imposed on the pre and postfilters, then the necessary conditions for the optimal prefilter and postfilter transfer functions can easily be obtained by taking the Fourier transforms of (3a) and (5a), respectively. On the other hand, if the filters are constrained to be physically realizeable, then the filter transfer functions can be obtained from Wiener-Hopf equations (3b) and (5b) by the method of spectral factorization [25,26]. In any case, from (3)

$$F(f) = A(f)B(f)G^*(f)|W(f)|^2\Phi_x(f)/D(f) \tag{7a}$$

and

$$F(f) = [1/D^+(f)][A(f)B(f)G^*(f)|W(f)|^2\Phi_x(f)/D^-(f)]_+ \tag{7b}$$

where

$$D(f) = \Phi_x(f)[\lambda|K(f)|^2+C(f)\sum_{k=-\infty}^{\infty}|G(f+kf_s)W(f+kf_s)|^2]$$

are the prefilter transfer functions for unrealizeable and realizeable optimal filters, respectively. Similarly, from (5)

$$G(f) = A(f)B(f)F^*(f)|W(f)|^2\Phi_x(f)/E(f) \tag{8a}$$

and

$$G(f) = [1/E^+(f)][A(f)B(f)F^*(f)|W(f)|^2\Phi_x(f)/E^-(f)]_+ \tag{8b}$$

where

$$E(f) = |W(f)|^2\sum_{k=-\infty}^{\infty}[\Phi_n(f+kf_s)+C(f+kf_s)|F(f+kf_s)|^2\Phi_x(f+kf_s)] \tag{8c}$$

are the transfer functions of the optimal unrealizeable and realizeable postfilters, respectively. Since there may be occasion to cancel the common factor $\Phi_x(f)$ from (7a) and the common factor $|W(f)|^2$ from (8a), $\Phi_x(f)$ and $|W(f)|^2$ are assumed positive almost everywhere. These assumptions are not critical since virtually all input signal power spectra and weighting functions of practical interest satisfy these conditions. In any case, $|W(f)|^2 = 0$ is meaningless since for this condition F(f) and G(f) can take on arbitrary values. Also, it is obvious that if $\Phi_x(f) = 0$ for some frequency f, the optimal filters have the trivial solution $F(f) = G(f) = 0$.

In both (7b) and (8b), $U^+(f)$ is used to denote all the left-half plane poles and zeros of any function U(f), and $U^-(f)$ is used to denote the right-half plane poles and zeros. Furthermore, $[V(f)/U^-(f)]_+ = \int_0^\infty q(\tau)e^{-j2\pi f\tau}d\tau$ where $q(\tau) = \int_{-\infty}^{\infty}[V(f)/U^-(f)]e^{j2\pi f\tau}df$.

At this point, it is essential to stress that simultaneous satisfaction of (7) and (8) is not a sufficient condition for an optimal system. In fact, it is the lack of a unique solution of the necessary conditions that necessitates the arguments in the remainder of this Chapter.

2.2 Further Necessary Conditions

Since the joint optimization problem is easier solved in the frequency domain, equations (1) and (2) are expressed in the following equivalent forms by repeated application of Parseval's theorem,

$$\varepsilon = \int_{-\infty}^{\infty}|A(f)W(f)|^2\Phi_x(f)df + \int_{-\infty}^{\infty}|G(f)W(f)|^2\sum_{k=-\infty}^{\infty}\Phi_n(f+kf_s)df$$

$$+\int_{-\infty}^{\infty}|G(f)W(f)|^2\sum_{k=-\infty}^{\infty}C(f+kf_s)|F(f+kf_s)|^2\Phi_x(f+kf_s)df$$

$$-2\int_{-\infty}^{\infty}A^*(f)B^*(f)F(f)G(f)|W(f)|^2\Phi_x(f)df \tag{9}$$

and $$\int_{-\infty}^{\infty}|F(f)K(f)|^2\Phi_x(f)df = P \tag{10}$$

where $B(f) = 1 + \hat{B}(f)$ and $C(f) = 1 + \hat{B}(f) + \hat{B}^*(f)$.

For the remainder of this Chapter, the optimal filters are assumed unrealizeable and functions $|K(f)|^2$, $B(f)$, and $C(f)$ are assumed periodic with period f_s. Also, $C(f) > 0$. In addition, we assume initially that $F(\alpha)$ and $G(\alpha)$ are non-zero at some frequency α. It then follows from (7a) and (8a) that for any integer k,

$$F(\alpha+kf_s)/F(\alpha) = A(\alpha+kf_s)G^*(\alpha+kf_s)|W(\alpha+kf_s)|^2/A(\alpha)G^*(\alpha)|W(\alpha)|^2 \tag{11}$$

$$G(\alpha+kf_s)/G(\alpha) = A(\alpha+kf_s)F^*(\alpha+kf_s)\Phi_x(\alpha+kf_s)/A(\alpha)F^*(\alpha)\Phi_x(\alpha) \tag{12}$$

Substituting (11) into (12) gives

$$G(\alpha+kf_s)/G(\alpha) = G(\alpha+kf_s)|A(\alpha+kf_s)W(\alpha+kf_s)|^2\Phi_x(\alpha+kf_s)/G(\alpha)|A(\alpha)W(\alpha)|^2\Phi_x(\alpha) \tag{13}$$

Equation (13) is satisfied if $F(\alpha+kf_s) = G(\alpha+kf_s) = 0$, or if

$$|A(\alpha+kf_s)W(\alpha+kf_s)|^2\Phi_x(\alpha+kf_s)/|A(\alpha)W(\alpha)|^2\Phi_x(\alpha) = 1 \tag{14}$$

In general, (14) is not satisfied for arbitrary integer values of k since $|A(f)W(f)|^2\Phi_x(f)$ is usually aperiodic. Hence, it may be concluded that the optimal F and G are non-zero for at most one frequency in the set $f+kf_s$, where k is any integer including zero. For those frequencies f where F and G are non-zero the optimal F and G are related as follows.

$$F(f) = A(f)B(f)G^*(f)|W(f)|^2/[\lambda|K(f)|^2+C(f)|G(f)W(f)|^2] \tag{15}$$

$$G(f) = A(f)B(f)F^*(f)\Phi_x(f)/[\Phi_{n_s}(f)+C(f)|F(f)|^2\Phi_x(f)] \tag{16a}$$

where $$\Phi_{n_s}(f) = \sum_{k=-\infty}^{\infty} \Phi_n(f+kf_s) \tag{16b}$$

From (15) and (16) it follows that

$$\lambda = |G(f)W(f)|^2\Phi_{n_s}(f)/|K(f)F(f)|^2\Phi_x(f)$$

Thus, λ is real and non-negative as assumed in Section 2.1 Substitution of (16) into (15) yields a quadratic equation in $|F|^2$, which, when solved gives

$$|F(f)|^2 = [1/C(f)][|A(f)B(f)W(f)/K(f)|\sqrt{\Phi_{n_s}(f)/\lambda\Phi_x(f)}-\Phi_{n_s}(f)/\Phi_x(f)] \quad (17)$$

Substitution of (15) into (16) gives

$$|G(f)|^2 = [1/C(f)][|A(f)B(f)K(f)/W(f)|\sqrt{\lambda\Phi_x(f)/\Phi_{n_s}(f)}-\lambda|K(f)|^2/|W(f)|^2] \quad (18)$$

The positive sign solutions of (17) and (18) are chosen for the quadratic equations because $|F|^2$ and $|G|^2$ must be non-negative for all f. For this reason, $|F|$ and $|G|$ are necessarily given by (17) and (18) at only those frequencies for which

$$|A(f)B(f)W(f)/K(f)| \geq \sqrt{\lambda\Phi_{n_s}(f)/\Phi_x(f)} \quad (19)$$

for all other frequencies, $F = G = 0$.

Let Ω be the set of frequencies for which F and G are non-zero. Substitution of (17) into (10) gives

$$1/\sqrt{\lambda} = (P+\int_\Omega[|K(f)|^2\Phi_{n_s}(f)/C(f)]df)/\int_\Omega|A(f)B(f)K(f)W(f)|\sqrt{\Phi_x(f)\Phi_{n_s}(f)}/C(f)df \quad (20)$$

Substitution of G(f) from (16) into (9) yields

$$\varepsilon = \int_{-\infty}^{\infty} \frac{|A(f)W(f)|^2\Phi_x(f)\{\Phi_{n_s}(f)+|F(f)|^2\Phi_x(f)[C(f)-|B(f)|^2]\}}{\Phi_{n_s}(f) + C(f)|F(f)|^2\Phi_x(f)}\, df$$

It follows that the phase of F has no effect on ε provided G is obtained from (16). Similarly, the phase of G is arbitrary provided F is obtained from (15). Substitution of (20) into (17) and the resulting equation into (21) yields

$$\varepsilon = \int_{\bar{\Omega}}|A(f)W(f)|^2\Phi_x(f)df + \int_\Omega|A(f)W(f)|^2\Phi_x(f)[1-|B(f)|^2/C(f)]df$$
$$+\{\int_\Omega|A(f)B(f)K(f)W(f)|\sqrt{\Phi_{n_s}(f)\Phi_x(f)}/C(f)df\}^2/\{P+\int_\Omega|K(f)|^2\Phi_{n_s}(f)/C(f)df\} \quad (22)$$

where $\bar{\Omega}$ contains all frequencies not included in Ω. The first integral in (22) results from filtering x(t). The other two integrals result from inband distortion.

2.3 Algorithm for Determining the Jointly Optimal Prefilter and Postfilter

It remains to select the frequency set Ω which minimizes ε in (22). Accordingly, define the frequency set $T_{max}=\{q:-f_s \leq q < f_s/2\}$ and let T be a subset of frequencies chosen from the set T_{max}. For each frequency $q\varepsilon T_{max}$ define the integer set I_q which contains exactly one element chosen from the set of all possible integer numbers. Frequency set Ω can now be defined as

$$\Omega = \left\{ \begin{array}{l} f:f = q+kf_s \text{ where } q\varepsilon T \text{ and } k\varepsilon I_q \text{ are chosen so (19)} \\ \text{is satisfied for all } f\varepsilon\Omega. \end{array} \right\} \tag{23}$$

The problem is to select the sets T and I_q to minimize ε in (22) subject to constraint (19). Based on the results of Section 2.4, the following algorithm is presented for determining the jointly optimal filters. Subscript "o" will designate the optimal Ω, T, I_q and λ.

1. Define for all $|q| < f_s/2$

$$I_{q_o} = \left\{ \begin{array}{l} k: |A(q+kf_s)W(q+kf_s)|^2 \Phi_x(q+kf_s) \text{ is maximized} \\ \text{where } q\varepsilon\ T_{max}. \end{array} \right\} \tag{24}$$

With $T = T_{max}$ and $k\varepsilon I_{q_o}$ calculate λ from (20).

If (19) is satisfied for all $f\varepsilon\Omega$, where Ω is defined by (23) with $T = T_{max}$ and $I_q = I_{q_o}$, set $\lambda_o=\lambda$, $T_o=T$ and $\Omega_o=\Omega$ and go to step 4. Otherwise go to step 2.

2. Define, for any λ

$$T_m(\lambda, I_{q_o}) = \left\{ \begin{array}{l} q:q\varepsilon\ T_{max} \text{ and (19) is satisfied for all} \\ f = q+kf_s \text{ where } k\,\varepsilon I_{q_o} \end{array} \right\} \tag{25}$$

Set λ equal to a positive real value. Calculate P_λ from

$$P_\lambda = \int_\Omega \{[|A(f)B(f)K(f)W(f)|\sqrt{\Phi_x(f)\Phi_{n_s}(f)/\lambda} - |K(f)|^2 \Phi_{n_s}(f)]/C(f)\}df \tag{26}$$

The integration in (26), obtained by solving (20) for P, is over the set Ω consisting of all $f=q+kf_s$ where $q\varepsilon T_m$ and $k\varepsilon I_{q_o}$.

3. Repeat step 2 for different values of λ, thereby obtaining P_λ vs λ. Choose as λ_o the value of λ which makes $P_\lambda = P$. Let the resulting $T_m = T_o$ and the resulting $\Omega=\Omega_o$.
4. At this point λ_o, T_o, I_{q_o}, and Ω_o are specified. For $f\varepsilon\bar{\Omega}_o$, set $F(f)=G(f)=0$. For $f\varepsilon\Omega_o$, determine $|F(f)|$ from (17); the phase of F is arbitrary, provided G(f) is obtained from (16). Alternatively, $|G(f)|$ may be obtained from (18) with the phase of G(f) being selected arbitrarily, provided F(f) is obtained from (15). A third alternative is to obtain $|F|$ and $|G|$ from (17) and (18), respectively, and to then select the phase of F and G to make FGA*B* real for all $f\varepsilon\Omega_o$. In any case, the resulting mimimum ε is given by (22) with $\Omega=\Omega_o$

2.4 Validity of the Optimization Algorithm[+]

In this Section, the validity of the preceding algorithm is established. From among all solutions of necessary conditions (17), (18), and (19) the recommended procedure determines the one that minimizes ε for a given λ. However, an optimal system was defined as one that minimizes ε for a given P, not a given λ. Thus, if we can show that there is no solution of the necessary conditions, regardless of the choice of Ω and λ, which simultaneously possesses power equal to, and error less than that obtainable using the algorithm, then the validity of the algorithm is proved.

For any positive real λ and any integer set I_q define

$$\Psi(\lambda,I_q) = \left\{ \begin{array}{l} q{:}q \text{ is contained in a subset of } T_{max} \text{ and (19) is} \\ \text{satisfied for all } f=q+kf_s \text{ where } k\varepsilon I_q. \end{array} \right\} \tag{27}$$

[+]The approach used here is not unlike that used by others [12,13] in optimizing the linear transmitter and receiver in pulse amplitude modulation systems.

Note that $\Psi(\lambda,I_q) \subset T_m(\lambda,I_{q_o})$ where I_{q_o} and $T_m(\lambda,I_{q_o})$ are defined by (24) and (25), respectively. It will now be shown that for any positive real λ, there exist no positive real $\hat{\lambda}\neq\lambda$ and no sets $I_q\neq I_{q_o}$ and $\Psi(\hat{\lambda},I_q)$ such that

$$P[\hat{\lambda},\Psi(\hat{\lambda},I_q), I_q] = P[\lambda, T_m(\lambda,I_{q_o}), I_{q_o}] \tag{28}$$

and

$$\varepsilon[\hat{\lambda},\Psi(\hat{\lambda},I_q), I_q] \not\leq \varepsilon[\lambda,T_m(\lambda,I_{q_o}), I_{q_o}] \tag{29}$$

where the dependence of ε in (22) and P in (26) on λ, I_q, $T(\lambda,I_q)$, and $\Psi(\lambda,I_q)$ has been made explicit.

Define for all $q\varepsilon\, T_{max}$

$$\rho(q) = |A(q+kf_s)B(q+kf_s)W(q+kf_s)|\sqrt{\Phi_x(q+kf_s)/C(q+kf_s)} \quad k\varepsilon I_{q_o} \tag{30}$$

$$\rho(q)-\Delta\rho(q) = |A(q+kf_s)B(q+kf_s)W(q+kf_s)|\sqrt{\Phi_x(q+kf_s)/C(q+kf_s)} \quad k\varepsilon I_q \tag{31}$$

$$\chi(q) = |K(q)|\sqrt{\Phi_{n_s}(q)/C(q)} \tag{32a}$$

Since $|K|$, Φ_{n_s}, and C are assumed periodic with period f_s

$$\chi(q+kf_s) = \chi(q) \tag{32b}$$

From the definition of I_{q_o}, $\Delta\rho(q) \geq 0$ for all $q\varepsilon\, T_{max}$. Define $J=T_m(\lambda,I_{q_o})$. Then any frequency set $\Psi(\lambda,I_q)$ in (27) can be expressed as $\Psi(\hat{\lambda},I_q) = J-\Delta J_1+\Delta J_2$, where $\Delta J_1 \subset J$ is a frequency set deleted from J and $\Delta J_2 \not\subset J$ is a frequency set added to J in order to compose $\Psi(\hat{\lambda},I_q)$.

Let $\gamma = \sqrt{\lambda}$ and $\gamma+\Delta\gamma = \sqrt{\hat{\lambda}}$. Use of (30), (31), (32), the constraint that P in (26) remain constant, as in (28), and the change of variable $f=q+kf_s$ yields

$$\begin{aligned}\gamma(\gamma+\Delta\gamma)\Delta P &= \gamma(\gamma+\Delta\gamma)[P(\gamma+\Delta\gamma,J-\Delta J_1+\Delta J_2,I_q)-P(\gamma,J,I_{q_o})] \\ &= \int_{J-\Delta J_1+\Delta J_2}[\gamma(\rho-\Delta\rho)\chi-\gamma(\gamma+\Delta\gamma)\chi^2]dq - \int_J[(\gamma+\Delta\gamma)\chi\rho-\gamma(\gamma+\Delta\gamma)\chi^2]dq \\ &= 0 \end{aligned} \tag{33}$$

From (20) and (22) it follows that

$$\varepsilon=\int_{-\infty}^{\infty}|A(f)W(f)|^2\Phi_x(f)df$$

$$-\int_{\Omega}\{[|A(f)B(f)W(f)|^2\Phi_x(f)-|A(f)B(f)K(f)W(f)|\sqrt{\lambda\Phi_x(f)\Phi_{n_s}(f)}]/C(f)\}df \tag{34}$$

Use of (30), (31), (32), (34) and the substitution $f=q+kf_s$ gives the following increment in ε.

$$\Delta\varepsilon = \varepsilon[\gamma+\Delta\gamma,J-\Delta J_1+\Delta J_2,I_q] - \varepsilon[\gamma,J,I_{q_o}]$$

$$= -\int_{J-\Delta J_1+\Delta J_2}(\rho-\Delta\rho)[(\rho-\Delta\rho) - (\gamma+\Delta\gamma)\chi]dq + \int_J\rho[\rho-\gamma\chi]dq \tag{35}$$

We now show that $\Delta\varepsilon \geq 0$ independent of whether $\Delta\gamma \geq 0$ or $\Delta\gamma < 0$. Consider first the case $\Delta\gamma \geq 0$. From (19), (24), (25), and (27) it follows that $J-\Delta J_1+\Delta J_2 = \Psi[\gamma+\Delta\gamma,\ I_q] \subset T_m(\gamma,I_{q_o}) = J$. Therefore, ΔJ_2 is an empty frequency set. Since (19) requires that both terms in square brackets in (35) be non-negative, and because $\Delta\rho \geq 0$, $\Delta\varepsilon \geq 0$ for $\Delta\gamma \geq 0$.

Finally, assume that $\Delta\gamma < 0$. Addition of (33) and (35) gives

$$\Delta\varepsilon = \Delta\varepsilon + \gamma(\gamma+\Delta\gamma)P$$

$$= \int_J[-(\rho-\Delta\rho)^2+(\gamma+\Delta\gamma)(\rho-\Delta\rho)\chi + \rho^2- \gamma\rho\chi+ \gamma(\rho-\Delta\rho)\chi$$

$$-\gamma(\gamma+\Delta\gamma)\chi^2 - (\gamma+\Delta\gamma)\rho\chi + \gamma(\gamma+\Delta\gamma)\chi^2]dq + \int_{-\Delta J_1+\Delta J_2}[(\rho-\Delta\rho)^2$$

$$+(\gamma+\Delta\gamma)(\rho-\Delta\rho)\chi + \gamma(\rho-\Delta\rho)\chi - \gamma(\gamma+\Delta\gamma)\chi^2]dq \tag{36}$$

Rearrangement of (36) gives

$$\Delta\varepsilon= \int_{J-\Delta J_1}\Delta\rho(\rho-\gamma\chi)dq + \int_{J-\Delta J_1+\Delta J_2}\Delta\rho[(\rho-\Delta\rho) - (\gamma+\Delta\gamma)\chi]dq + \int_{\Delta J_1}(\rho-\gamma\chi)^2dq$$

$$+\int_{\Delta J_1}(-\Delta\gamma)\chi(\rho-\Delta\gamma)dq + \int_{\Delta J_2}[-(\rho-\gamma\chi)[(\rho-\Delta\rho) - (\gamma+\Delta\gamma)\chi]dq \tag{37}$$

From (19), (25), (27), the periodicity of $\gamma\chi$ and the definitions of J, ΔJ_1 and J_2:

1. $\rho - \gamma\chi > 0 \ \forall q \varepsilon J$ and, therefore, $\forall q \varepsilon \Delta J_1$ and $\forall q \varepsilon J - \Delta J_1$

2. $(\rho - \Delta\rho) - (\gamma + \Delta\gamma)\chi > 0 \ \forall q \varepsilon J - \Delta J_1 + \Delta J_2$ and, therefore, $\forall \ q \varepsilon \Delta J_2$

3. $\rho - \gamma\chi \leq 0 \ \forall q \varepsilon \Delta J_2$ if J is a proper subset of T_{max}

4. ΔJ_2 is an empty set if $J = T_{max}$

It follows that $\Delta\varepsilon \geq 0$ as claimed, and that with I_{q_o} as given by (24), T_o is obtained by varying λ in (26) until a value $\lambda = \lambda_o$ is found such that $P[\lambda_o, T_m(\lambda_o, I_{q_o}), I_{q_o}] = P$. The optimal frequency set is then $T_o = T_m[\lambda_o, I_{q_o}] \subset T_{max}$.

3. ANALYSIS AND DISCUSSION OF SOME IMPORTANT FILTERING SCHEMES

3.1 Application of Optimal Filtering to Some Specific Cases

In this Section the optimal frequency set Ω_o is determined for some specific cases.

3.1.1 High Sampling Rate

In practice $\Phi_x(f) \to 0$ as $f \to \infty$, in which case Ω_o contains only frequencies for which $|f| < f_s/2$ if f_s is sufficiently large. If $A=B=C=|K| = |W| = 1$, for all $f \epsilon \Omega_o$, then the optimal filters and the resulting ε are identical to the results for unsampled systems [10].

The lowpass equivalent of the linearized analog modulation system in Fig. 2 can be represented as in Fig. 1 if G and H are combined and T = 0 in Fig. 1. For amplitude modulation P represents the power in the modulated signal, provided $|K(f)|^2=1$. For angle modulation $|K(f)|^2 = f^2$, in which case P equals the mean square bandwidth [27].

3.1.2 Lowpass Signals

A signal u(t) with power spectrum U(f) is lowpass if $dU/df<0$ for $f>0$. If $w(t)\otimes a(t)\otimes x(t)$ is lowpass, then from (24) it follows that for all $|q|<f_s/2$, I_{q_o} contains the integer zero. Also, if $d\{|B(f)/K(f)|/\sqrt{\Phi_{n_s}(f)}\}/df \le 0$ for $f>0$ application of the algorithm shows that Ω_o contains all frequencies $|f| \le W$. If the solution for V in the following equation, obtained by substituting (20) into (19), is less than $f_s/2$, then $W=V$.

$$\frac{\Phi_x(V)}{\Phi_{n_s}(V)} = \left|\frac{K(V)}{A(V)B(V)W(V)}\right| \frac{\int_{-V}^{V} [|A(f)B(f)K(f)W(f)|/C(f)]\sqrt{\Phi_{n_s}(f)\Phi_x(f)}\, df}{P + \int_{-V}^{V}[|K(f)|^2\Phi_{n_s}(f)/C(f)]\, df} \qquad (38)$$

If $V \ge f_s/2$ then $W = f_s/2$.

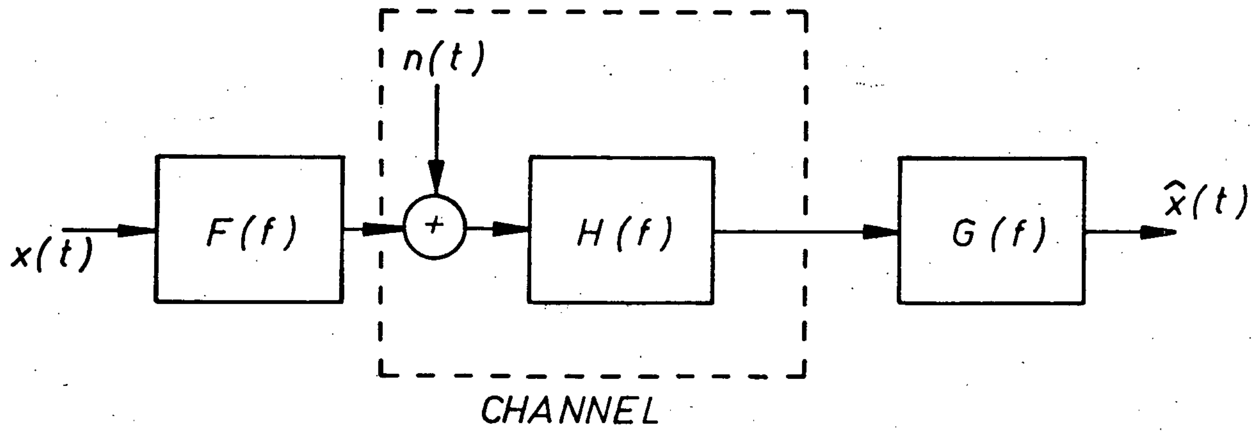

Fig. 2. Lowpass equivalent of a linearized analog modulation system.

3.1.3 Weak Noise

For $\Phi_{n_s}(f)$ sufficiently small inequality (19) is satisfied for all $f=q+kf_s$ where $|q|<f_s/2$ and $k\varepsilon I_{q_o}$. Hence, Ω_o will contain a frequency band whose total width equals f_s. The smaller $\Phi_{n_s}(f)$, the greater $|A(f)B(f)W(f)/K(f)|$ is, compared to $\sqrt{\lambda\Phi_{n_s}(f)/\Phi_x(f)}$, and the more accurate are the following approximate equations, obtained from (16), (17), (20), and (22).

$$1/\sqrt{\lambda_o} \simeq P/\int_{\Omega_o} [|A(f)B(f)K(f)W(f)|\sqrt{\Phi_{n_s}(f)\Phi_x(f)}/C(f)]\, df \tag{39a}$$

$$|F(f)|^2 \simeq |A(f)B(f)W(f)/K(f)|\sqrt{\Phi_{n_s}(f)/\lambda_o\Phi_x(f)}/C(f) \tag{39b}$$

$$\varepsilon \simeq \int_{\bar{\Omega}_o} |A(f)W(f)|^2\Phi_x(f)df + \int_{\Omega_o} |A(f)W(f)|^2\Phi_x(f)\ [1-|B(f)|^2/C(f)]df$$

$$+\{\int_{\Omega_o} [|A(f)B(f)K(f)W(f)|/C(f)]\sqrt{\Phi_{n_s}(f)\Phi_x(f)}\ df\}^2/P \tag{39c}$$

$$G(f) \simeq A(f)B(f)/C(f)F(f) \tag{39d}$$

If $A(f)B(f)/C(f)$ is constant, F and G become reciprocal filters. Also, if $\Phi_{n_s}(f)|W(f)/K(f)|^2$ is constant, then $|F(f)|^2$ is proportional to

$1/\sqrt{\Phi_x(f)}$, in which case F becomes a "half-whitening" filter [14].

3.1.4 Systems for which $\rho(f) = |A(f)B(f)W(f)/K(f)|\sqrt{\Phi_x(f)/\Phi_{n_s}(f)}$ is Constant

Let Γ denote the set of frequencies for which $|A(f)W(f)|^2\Phi_x(f) > 0$, and let $\rho(f) = \rho_o$ for all $f\varepsilon\Gamma$, where ρ_o is any constant. Substitution of ρ_o into (20) shows that (19) is always satisfied for any Ω which contains at most one frequency in the set $f=q+kf_s$ where $f\varepsilon\Gamma$, $|q| < f_s/2$ and k is any integer. It follows that if $W_\Gamma < f_s$ where W_Γ is the total width of the band of frequencies in Γ, and if no frequencies in Γ coincide under translation by kf_s where k is any non-zero integer, then $\Omega_o=\Gamma$. With $\rho(f) = \rho_o$ for all non-zero $\rho(f)$, (17) and (18) give

$$|F(f)|^2 = [\Phi_{n_s}(f)/\Phi_x(f)C(f)][\rho_o/\sqrt{\lambda_o}-1] \tag{40a}$$

$$|G(f)|^2 = [\lambda_o|K(f)|^2/C(f)|W(f)|^2[\rho_o/\sqrt{\lambda_o}-1] \tag{40b}$$

for all $f\varepsilon\Omega_o$. If $\Phi_{n_s}/C\Phi_x$ and $|K|^2/C|W|^2$ are constant for all $f\varepsilon\Omega_o$, then (40) shows that $|F|$ and $|G|$ are constant for all $f\varepsilon\Omega_o$.

3.2 Some Suboptimal Filtering Schemes

In the following discussion on suboptimal filtering schemes the frequency set Ω has the property that if $f\varepsilon\Omega$ then $f+kf_s\varepsilon\bar{\Omega}$ for any non-zero integer k, where Ω is as defined in (23).

3.2.1 Weak Noise Filters

When $|A(f)B(f)W(f)/K(f)|$ is sufficiently larger than $\sqrt{\lambda\Phi_{n_s}(f)/\Phi_x(f)}$ the optimal F and G are related approximately by (39d), in which case they will be called weak noise filters. With F and G constrained for $f\varepsilon\Omega$, and with

$F=G=0$ for $f\epsilon\bar{\Omega}$, it follows from substituting (39d) into (9) that

$$\epsilon = \int_{\bar{\Omega}}|A(f)W(f)|^2\Phi_x(f)df + \int_\Omega|A(f)W(f)|^2\Phi_x(f)[1-|B(f)|^2/C(f)]df$$

$$+ \int_\Omega[|A(f)B(f)W(f)|^2\Phi_{n_s}(f)/C^2(f)|F(f)|^2]df \tag{41}$$

From Schwartz's inequality

$$\int_\Omega[|A(f)B(f)W(f)|^2\Phi_{n_s}(f)/C^2(f)|F(f)|^2]df \int_\Omega|F(f)K(f)|^2\Phi_x(f)df$$

$$\geq \{\int_\Omega[|A(f)B(f)K(f)W(f)|\sqrt{\Phi_{n_s}(f)\Phi_x(f)}/C(f)]df\}^2$$

Equality holds if, and only if

$$\mu|F(f)|^2 = |A(f)B(f)W(f)/K(f)|\sqrt{\Phi_{n_s}(f)/\Phi_x(f)}/C(f) \tag{42}$$

where μ is any constant. Thus, to minimize (41) subject to (10) requires that $|F|^2$ satisfy (42) and, from (10), that

$$\mu = \int_\Omega[|A(f)B(f)K(f)|\sqrt{\Phi_{n_s}(f)\Phi_x(f)}/C(f)]df/P \tag{43}$$

The resulting mean-square error is given by

$$\epsilon = \int_{\bar{\Omega}}|A(f)W(f)|^2\Phi_x(f)df + \int_\Omega|A(f)W(f)|^2\Phi_x(f)[1-|B(f)|^2/C(f)]df$$

$$+ \{\int_\Omega[|A(f)B(f)K(f)W(f)|\sqrt{\Phi_{n_s}(f)\Phi_x(f)}/C(f)]df\}^2/P \tag{44}$$

If frequency sets Ω in (44) and (22) are identical then the two equations differ only that $\int_\Omega|K(f)|^2\Phi_{n_s}(f)/C(f)]df$ is missing from the denominator in the last term of (22). Whenever $P >> \int_\Omega[|K(f)|^2\Phi_{n_s}(f)/C(f)]df$, as is nearly always the case, the performance obtainable using weak noise filters is essentially equivalent to that obtainable using optimal filters.

Weak noise filters have a practical advantage which optimal filters do not have; their transfer characteristics are essentially dependent only on the relative power spectra of x(t) and n(t). Inspection of (17), (18), (39d), and (42) reveals that for optimal filters, precise knowledge of spectra $\Phi_x(f)$ and

$\Phi_{n_s}(f)$ is required, whereas for weak noise filters, only knowledge of their relative values is necessary to determine the filters to within a gain factor. Adjustment of the filter gains to satisfy power constraint can easily be accomplished during installation.

3.2.2 Optimal Prefilter; Constant Amplitude Postfilter

Let $A=A_1$, $B=B_1$, $C=C_1$, $|K|=K_1$, $|G|=G_1$, and $|W|=1$ for all $f\varepsilon\Omega$, where A_1, B_1, C_1, K_1 and G_1 are constants. From (7) it follows that the optimal $|F|= F_1$ for all $f\varepsilon\Omega$, and from (10) that

$$F_1 = (P/K_1^2 \int_\Omega \Phi_x(f)df)^{1/2} \tag{45}$$

Let the phase of F and G are such that $FG=F_1G_1$ for all $f\varepsilon\Omega$. Substitution of $|F|=F_1$, $|G|=G_1$ and $FG=F_1G_1$ into (9) yields the optimal G_1, as follows

$$G_1 = (A_1B_1P/K_1^2)/F_1(PC_1/K_1^2 + \int_\Omega \Phi_{n_s}(f)df) \tag{46}$$

The following equation gives the resulting error.

$$\varepsilon = A_1^2\int_{\bar{\Omega}} \Phi_x(f)df + A_1^2(1 - \frac{B_1^2}{C_1})\int_\Omega \Phi_x(f)df + \frac{A_1^2B_1^2}{C_1^2}\int_\Omega \Phi_x(f)df\int_\Omega \Phi_{n_s}(f)df/(\frac{P}{K_1^2} + \int_\Omega \frac{\Phi_{n_s}(f)}{C_1}df) \tag{47}$$

If the sets Ω in (22) and (47) are identical, ε in (47) exceeds ε in (22) because the numerator of the last term in (47) exceeds the numerator in the last term of (22), unless $\Phi_x(f)/\Phi_{n_s}(f)$ is constant for all $f\varepsilon\Omega$, in which case (22) and (47) give the same ε.

3.2.3 Constant Amplitude Prefilter; Optimal Postfilter

Let $A=A_1$, $B=B_1$, $C=C_1$, $|K|=K_1$, $|F|= F_1$, and $|W|=1$ for all $f\varepsilon\Omega$, where A_1, B_1, C_1, K_1 and F_1 are constants. From (10) F_1 is given by (45). Substitution of $|F|=F_1$ in (16) yields the optimal G as follows

$$G(f) = A_1B_1F^*(f)\Phi_x(f)/(\Phi_{n_s}(f) + C_1F_1^2\Phi_x(f)) \tag{48}$$

Substitution of (45) and (48) into (9) gives

$$\varepsilon=A_1^2\int_{\bar{\Omega}}\Phi_x(f)df+A_1^2\left(1-\frac{B_1^2}{C_1}\right)\int_{\Omega}\Phi_x(f)df+\frac{A_1^2B_1^2}{C_1^2}\int_{\Omega}\left[\Phi_{n_s}(f)\Phi_x(f)/\left(\frac{\Phi_{n_s}(f)}{C_1}+F_1^2\Phi_x(f)\right)\right]df \tag{49}$$

4 OPTIMAL AND SUBOPTIMAL FILTERING IN PAM, PCM, AND DPCM COMMUNICATION SYSTEMS

In this Chapter, optimal and suboptimal filtering schemes are applied to PAM, PCM and DPCM communication systems. System errors in PAM, PCM, and DPCM are evaluated for optimal pre and postfiltering, optimal pre-filtering only, and optimal postfiltering only schemes when the input power spectrum is first-order Butterworth. The resulting performances are compared with the optimum theoretically attainable as calculated from information theory.

4.1 Pulse Amplitude Modulation (PAM)

Fig. 3 depicts a multiplexed pulse amplitude modulation (PAM) system. Signals $x_1(t)$, $x_2(t)$, $\ldots,x_M(t)$ and $n_c(t)$ are assumed to be statistically independent random processes with power spectral densities $\Phi_{x_i}(f)$ $(i=1,2,\ldots,M)$ and $\Phi_{n_c}(f)$. Referring to the procedure used in Section 2.1 the mean-squared error ε_i (no weighting between $\hat{x}_i(t)$ and the desired i^{th} output $z_i(t)=a_i(t)\circledast x_i(t)$ is given by

$$\varepsilon_i = E\{\frac{1}{T}\int_0^T (z_i(t) - \hat{x}_i(t))^2 dt\}$$

In Fig. 3a let $\mathring{f}_i(t)$, $g_i(t)$, $o(t)$, $h(t)$ and $\ell(t)$ denote, respectively the impulse responses of filters having transfer functions $F_i(f)$, $G_i(f)$, $O(f)$, $H(f)$ and $L(f)$. Since $\hat{x}_i(t) = g_i(t)\circledast b_i(t)$ it follows that

$$\varepsilon_i=E\{\frac{1}{T}\int_0^T [z_i^2(t) - 2z_i(t)\hat{x}_i(t) + (\hat{x}_i(t))^2]dt\}$$

$$= \frac{1}{T}\int_0^T\{\phi_{z_i}(0)-2\int_{-\infty}^{\infty}g_i(\beta_1)\phi_{b_iz_i}(t-\beta_1,t)d\beta_1 +\int_{-\infty}^{\infty}\int_{-\infty}^{\infty} g_i(\beta_1)g_i(\beta_2)\phi_{b_i}(t-\beta_1,t-\beta_2)d\beta_1 d\beta_2\}dt$$

Since $b_i(t)=\Delta_i(t)\cdot[\ell(t)\circledast n_c(t) + \sum_{j=1}^{M} (y(t)\cdot\Delta_j(t))\circledast u(t)]$ where $u(t)=o(t)\circledast h(t)\circledast\ell(t)/M$, and since the y_i's and n_c are uncorrelated

$$\phi_{b_iz_i}(t,\tau)=\Delta_i(t)\int_{-\infty}^{\infty}\int_{-\infty}^{\infty}u(\beta_2)a_i(\beta_3)\Delta_i(t-\beta_2)\phi_{y_ix_i}(t-\beta_2,\tau-\beta_3)d\beta_2 d\beta_3$$

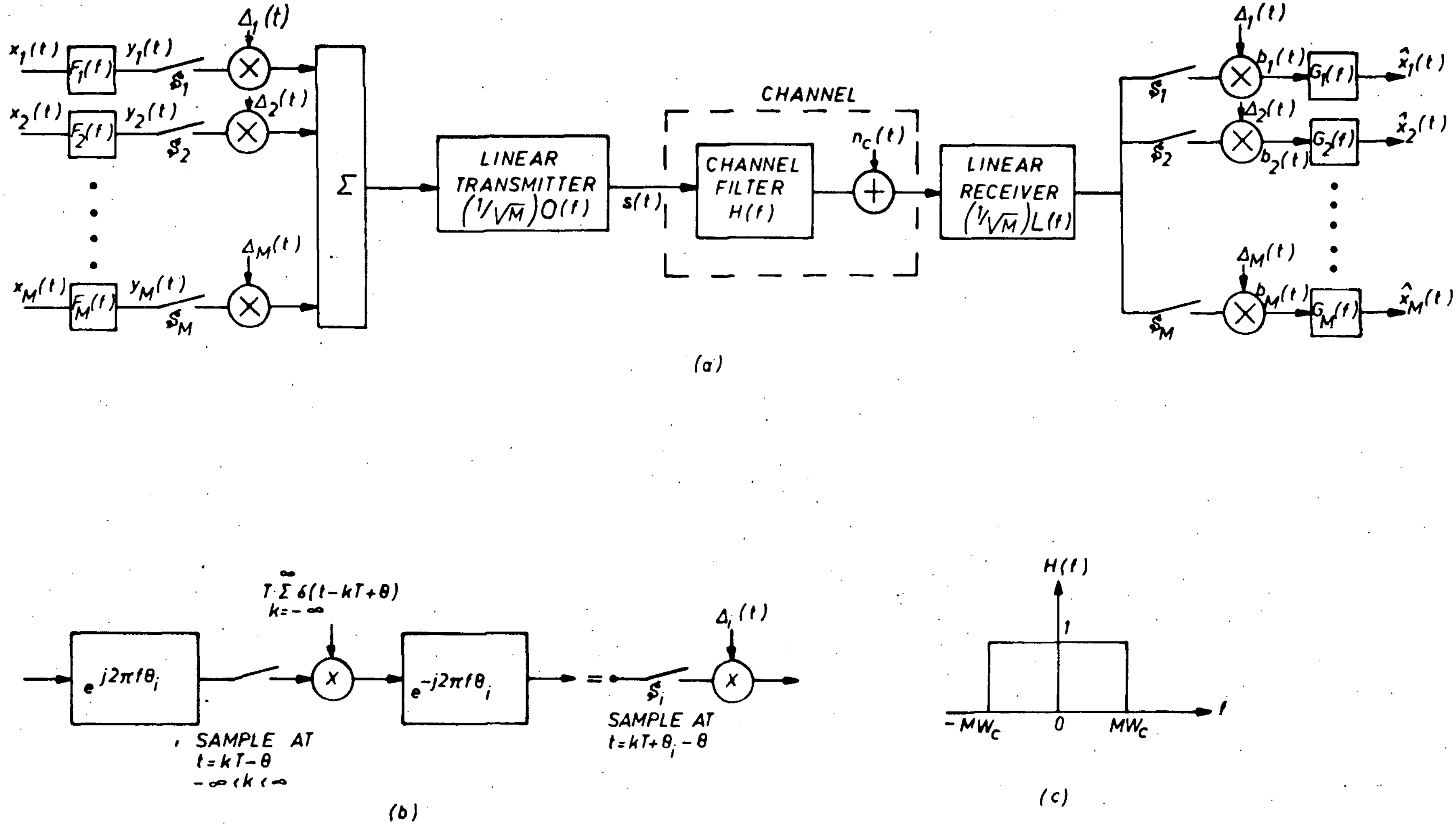

Fig. 3 (a) Multiplexed PAM system. Functions $F_i(f)$, $G_i(f)$, $(i=1,2,\ldots,M)$, $O(f)$, $H(f)$, and $L(f)$ are transfer functions of linear filters. Signal $y_i(t)$ is sampled by sampler $\$_i$ at $t=kT+\theta_i-\theta$, where k is any integer. Impulse train $\Delta_i(t)=T.\sum_{k=-\infty}^{\infty}\delta(t-kT-\theta_i+\theta)$.

(b) Equivalent representation of a sampler.

(c) Channel filter transfer characteristic for Example 2.

$$\phi_{b_i}(t,\tau)=\Delta_i(t)\Delta_i(\tau)\{\int_{-\infty}^{\infty}\int_{-\infty}^{\infty}\ell(\beta_3)\ell(\beta_4)\phi_{n_c}(t-\beta_3,\tau-\beta_4)d\beta_3 d\beta_4$$

$$+\int_{-\infty}^{\infty}\int_{-\infty}^{\infty}o(\beta_3)o(\beta_4)[\sum_{j=1}^{M}\Delta_j(t-\beta_3)\Delta_j(\tau-\beta_4)\phi_{y_j}(t-\beta_3,\tau-\beta_4)d\beta_3 d\beta_4\}$$

Substituting and integrating over t, gives

$$\varepsilon_i=\phi_{z_i}(0)-2\int_{-\infty}^{\infty}\int_{-\infty}^{\infty}\int_{-\infty}^{\infty}g_i(\beta_1)u(\beta_2)a_i(\beta_3)\Delta_i(\beta_2+\theta_i-\theta)\phi_{y_i x_i}(-\beta_2+\theta_i-\theta,\beta_1-\beta_3+\theta_i-\theta)d\beta_1 d\beta_2 d\beta_3$$

$$+\iiiint_{-\infty}^{\infty}g_i(\beta_1)g_i(\beta_2)\ell(\beta_3)\ell(\beta_4)\Delta_i(\beta_1-\beta_2+\theta_i-\theta)\phi_{n_c}(-\beta_3+\theta_i-\theta,\beta_1-\beta_2-\beta_4+\theta_i-\theta)d\beta_1 d\beta_2 d\beta_3 d\beta_4$$

$$+\iiiint_{-\infty}^{\infty}g_i(\beta_1)g_i(\beta_2)o(\beta_3)o(\beta_4)\Delta_i(\beta_1-\beta_2+\theta_i-\theta)\sum_{j=1}^{M}\Delta_j(-\beta_3+\theta_i-\theta)\Delta_j(\beta_1-\beta_2-\beta_3+\theta_i-\theta)$$

$$\phi_{y_j}(-\beta_3+\theta_i-\theta,\beta_1-\beta_2-\beta_3+\theta_i-\theta)d\beta_1 d\beta_2 d\beta_3 d\beta_4$$

Since $x_i(t)$ and $n_c(t)$ are stationary, $\phi_{y_i x_i}(t,\tau)$, $\phi_{n_c}(t,\tau)$ and $\phi_{x_i}(t,\tau)$ depend only on $t-\tau$. Applying Parseval's theorem repeatedly and using $\Phi_{y_i}(f)=|F_i(f)|^2\Phi_{x_i}(f)$ and $\Phi_{y_i x_i}(f)=F_i(f)\Phi_{x_i}(f)$, ε_i can be expressed as

$$\varepsilon_i=\int_{-\infty}^{\infty}|A_i(f)|^2\Phi_{x_i}(f)df+(\frac{1}{M})\int_{-\infty}^{\infty}|G_i(f)|^2\sum_{k=-\infty}^{\infty}|L(f+kf_s)|^2\Phi_{n_c}(f+kf_s)df$$

$$+\int_{-\infty}^{\infty}|G_i(f)|^2\sum_{j=1}^{M}|U_j(f)|^2\sum_{k=-\infty}^{\infty}|F_j(f+kf_s)|^2\Phi_{x_j}(f+kf_s)df-2\int_{-\infty}^{\infty}F_i(f)G_i(f)A_i^*(f)U(f)\Phi_{x_i}(f)df \tag{50a}$$

$$U(f)=\sum_{k=-\infty}^{\infty}O(f+kf_s)H(f+kf_s)L(f+kf_s)/M. \tag{50b}$$

$$U_m(f)=[\sum_{k=-\infty}^{\infty}O(f+kf_s)H(f+kf_s)L(f+kf_s)\exp\{-2j\pi(f+kf_s)(\theta_m-\theta_i)\}]/M \tag{50c}$$

The transmitter power S_T is given by

$$S_T=E\{\frac{1}{T}\int_0^T s^2(t)dt\} \tag{51a}$$

$$=\sum_{i=1}^{M}S_i \tag{51b}$$

where

$$S_i = (1/M)\int_{-\infty}^{\infty} |F_i(f)|^2 \Phi_{x_i}(f) \sum_{k=-\infty}^{\infty} |O(f+kf_s)|^2 df \tag{51c}$$

is the transmitter power associated with the i^{th} signal $x_i(t)$.

The requirement of distortionless channel transmission is often imposed, which means that there is no intersymbol or interchannel distortion at sampling times $t=kT+\theta_i-\theta$ $(i=1,2,\ldots,M)$. Replacement of the samplers in Fig. 3a by their equivalent representations in Fig. 3b[28], followed by application of Smith's [24] results shows that distortionless transmission occurs if and only if

$$(I/M) \sum_{k=-\infty}^{\infty} O(f+kf_s)H(f+kf_s)L(f+kf_s)\exp\{-j2\pi(f+kf_s)(\theta_j-\theta_i)\} = \delta_{ij}\Lambda \tag{52}$$

where Λ is any real constant and $\delta_{ij}=0$ for $i\neq j$ and $\delta_{ij}=1$ for $i=j$. Substitution of (52) into (50a) gives an equation identical to (9), provided the following substitutions are made: $\Phi_x(f)=\Phi_{x_i}(f)$, $F(f)=F_i(f)$, $G(f)=G_i(f)$, $B(f)=\Lambda$, $C(f)=\Lambda^2$, $|W(f)|^2=1$, $\Phi_n(f)=\Phi_{n_c}(f)|L(f)|^2/M$, and $\varepsilon=\varepsilon_i$. The filters $F_i(f)$ and $G_i(f)$ which minimize ε_i subject to the constraint (51c) can now be obtained using the method of Chapter 2, with $P=S_i$ and $|K(f)|^2=|K_i(f)|^2 = |O(f)|^2/M$. In many cases of interest, $\Phi_{x_i}(f)=\Phi_x(f)$ and $S_i=S=S_T/M$, in which case the optimal filters and the resulting ε_i are independent of i.

<u>Example 1</u>:

Let $O(f)=L(f)=H(f)$, where $H(f)$ is as shown in Fig. 3c. Let $\theta_i-\theta_j=(i-j)T/M$, $f_s=2W_c$, $\Phi_{n_c}(f)=N_o/2$, $S_i=S=S_T/M$ and $A_i(f)=1$ for all i. Let

$$\Phi_{x_i}(f) = \Phi_x(f) = \begin{cases} \sigma/2a & f \leq a \\ 0 & f > a \end{cases} \qquad (i=1,2,\ldots,M)$$

The system is distortionless, and (9) and (10) apply with $\Phi_n(f)=N_o/(2M)$ $\forall |f|\leq MW_c$, $A(f)=B(f)=C(f)=|K(f)|^2=|W(f)|^2=1$, $\Phi_{n_s}(f)=N_o/2$, and $P=S$. The optimal F and G are given in Section 3.1.4. If $a < W_c$ then F and G are ideal lowpass filters of bandwidth a, and $\varepsilon/\sigma = (1+S/aN_o)^{-1}$. If $a \geq W_c$ then Ω is not unique but contains any frequency set of total bandwidth $2W_c$ chosen from the set $|f| < a$ in such a way that its elements do not coincide under frequency translation kf_s, where k is any non-zero integer. In this case $\varepsilon/\sigma=(1-W_c/a)+(W_c/a)(1+S/W_cN_o)^{-1}$.

Example 2:

Consider the same distortionless PAM system in Example 1, with $A_i(f)=1$, $S_i=S$ and

$$\Phi_{x_i}(f) = \Phi_x(f) = \sigma a/\pi(f^2+a^2) \qquad (i=1,2,\ldots,M)$$

Sections 2.3 and 3.1.2 show that for optimal pre and postfiltering Ω contains all frequencies $|f| < W$, where $W < f_s/2$. Fig. 4 shows ε/σ vs. S/N_oW_c for various W_c for the optimal pre and postfilter case (O), as well as for the optimal prefilter only case (PR) in Section 3.2.2 and the optimal postfilter only case (PO) in Section 3.2.3. The frequency sets Ω in all three cases are assumed identical to the set determined for the optimal pre and postfilter case. Fig. 5 shows the signal-to-noise ratio

$$\mathrm{SNR} = \int_\Omega \Phi_x(f)df/[\varepsilon - \int_{\bar{\Omega}} \Phi_x(f)df] \tag{53}$$

for each of the above filtering schemes. The difference in both ε and SNR for the three cases is seen to be significant for $W_c/a > 10$.

If the channel noise $n_c(t)$ in Examples 1 and 2 is white Gaussian, then the capacity per message is

$$C=W_c\log_2(1+S/N_oW_c) \tag{54}$$

If $x_i(t)$ is a Gaussian process with $\Phi_{x_i}(f)$ as in Example 2, then the rate distortion function is expressed parametrically in $\emptyset$ as [25]

$$R(\emptyset) = (2a/\ln 2)(\emptyset-\tan^{-1}\emptyset) \tag{55a}$$

$$\varepsilon(\emptyset)/\sigma = 1+(2/\pi)([\emptyset/(1+\emptyset^2)]-\tan^{-1}(\emptyset)) \tag{55b}$$

The optimum performance theoretically obtainable (OPTA) by a communication system with capacity C is obtained when $R(\emptyset)=C$. Using (54) and (55), the OPTA curves shown in Fig. 4 were obtained.

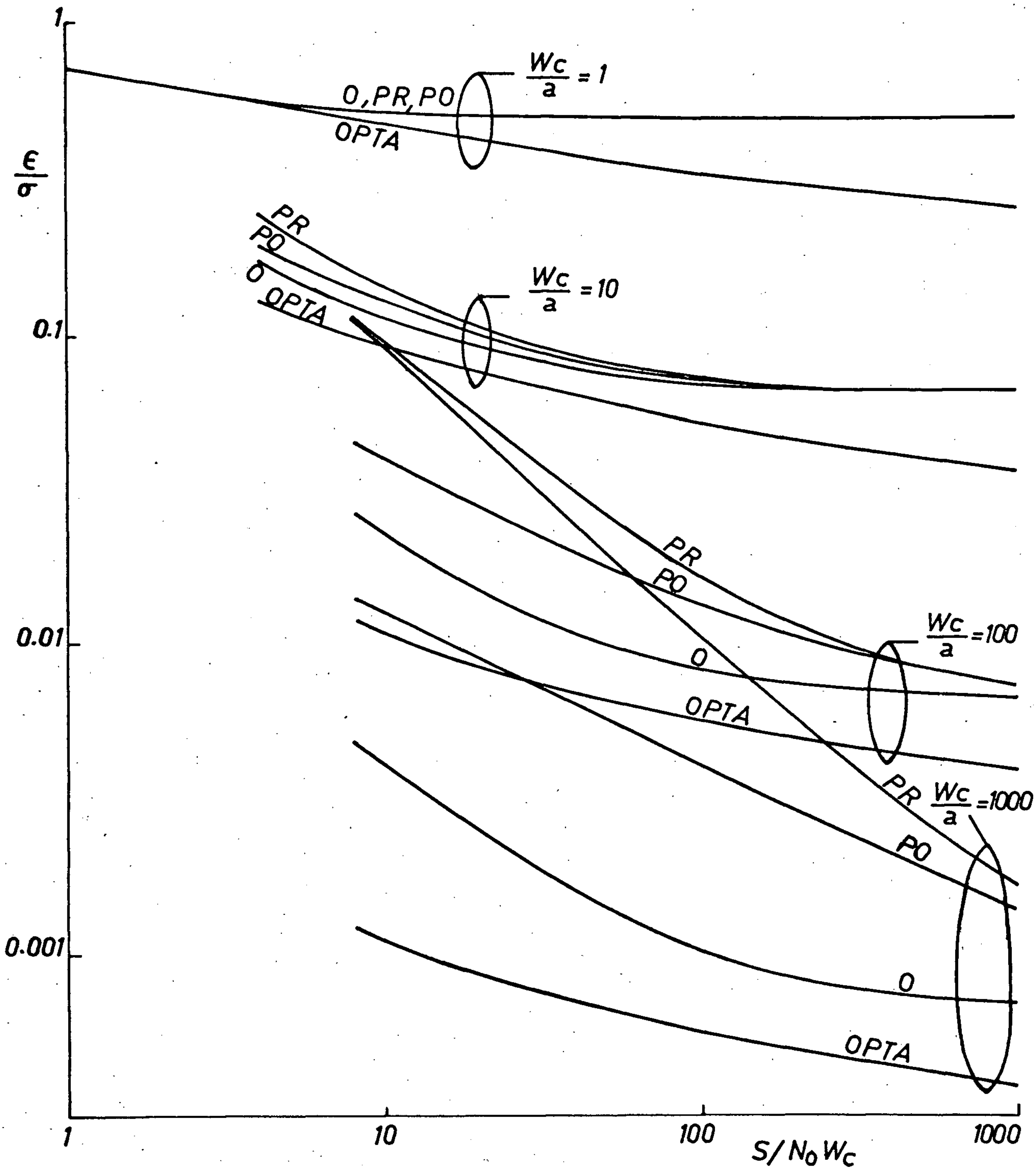

Fig. 4 Normalized error ε/σ versus S/N_oW_c for Example 2. Symbols O, PR, and PO denote optimal filters, optimal prefilter-constant amplitude postfilter, and constant amplitude prefilter-optimal postfilter, respectively. For the curves shown the optimal filter bandwidth $W=W_c$.

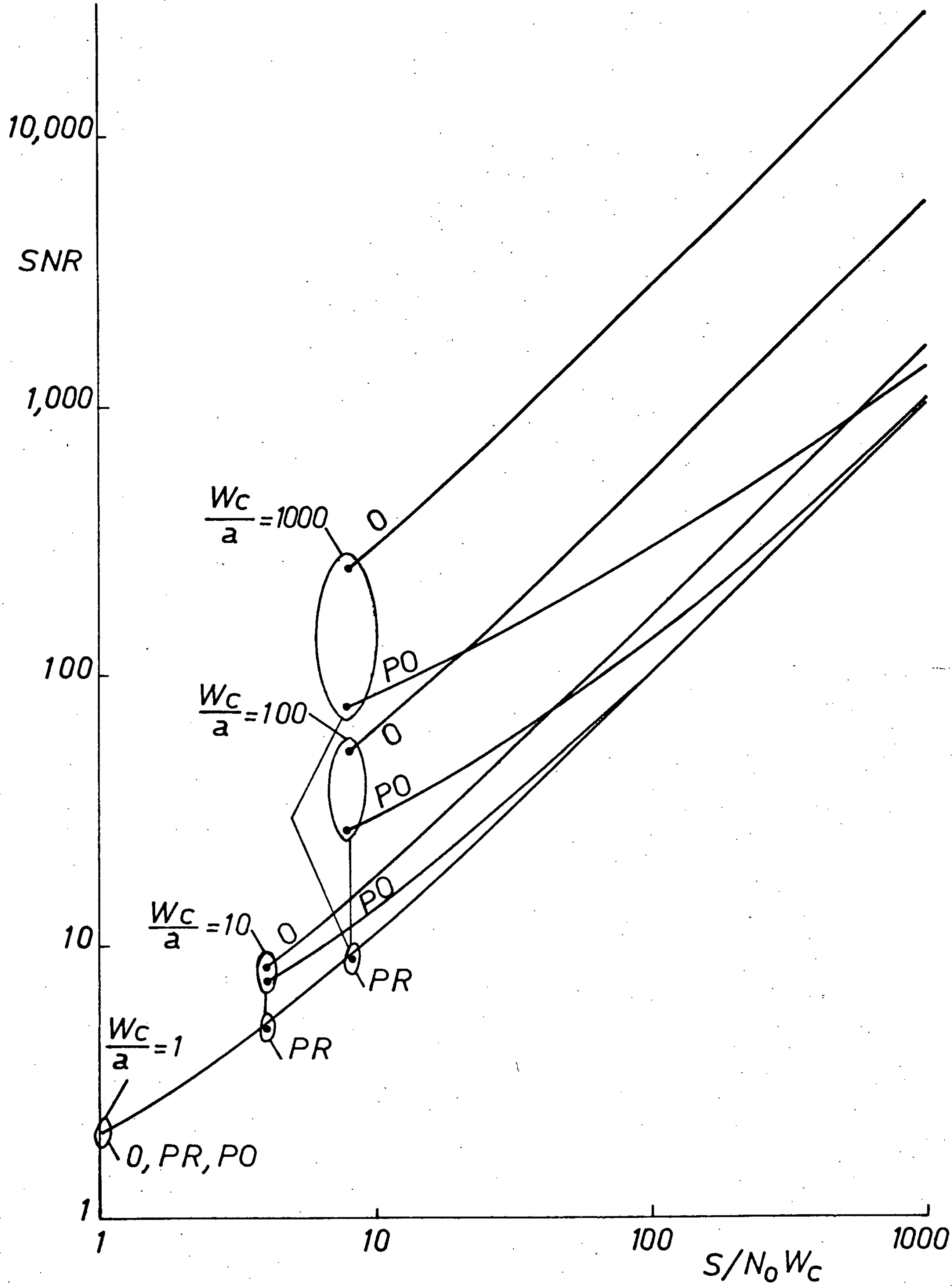

Fig. 5 Signal-to-noise ratio SNR for Example 2. Symbols 0, PR, and PO are defined in the caption of Fig. 4. For the curves shown the optimal $W=W_c$.

For any given C one pair of values of S/N_oW_c and W_c will minimize ε and the resulting ε represents the minimum distortion obtainable by a channel with the corresponding C for the PAM system under consideration. Fig. 10a shows for cases (0) and (PR) the minimum ε/σ and the corresponding W_c/a for Example 2. Fig. 10a can also be regarded as a plot of the minimum C vs ε. In general, ε will exceed that shown in Fig. 10a since the values of S/N_o and W_c for the given channel will not be those which minimize ε for the resulting C.

The analysis relative to Examples 1 and 2 and the results in Figs. 4,5, and 10a also apply when an M-channel single sideband, suppressed-carrier, amplitude modulated (SSB AM/SC) system is used on the channel described in Example 2, provided S is interpreted as the power in the transmitted signal. The analysis also applies to an M-channel double sideband (DSB) AM/SC system provided S again is interpreted as the power in the transmitted signal, except that the bandwidth per message for an DSB AM/SC system is twice that required by an SSB AM/SC system.

4.2 Pulse Code Modulation (PCM)

In this Section the PCM system shown in Fig. 7 is analyzed assuming x(t), and therefore, y(t) is Gaussian, and the mapping of the quantizer output samples v into $\hat{v}$ is by a memoryless digital channel. Correlation funcations are obtained using the Hermite polynomial expansion of the Gaussian probability density function in Section 4.2.1 and the pre and postfiltering problem is examined in Section 4.2.2.

4.2.1 Correlation Functions for Quantized Signals Transmitted Over Discrete Memoryless Channels

Fig. 6a shows a signal y(t) which is sampled, quantized, and trans-

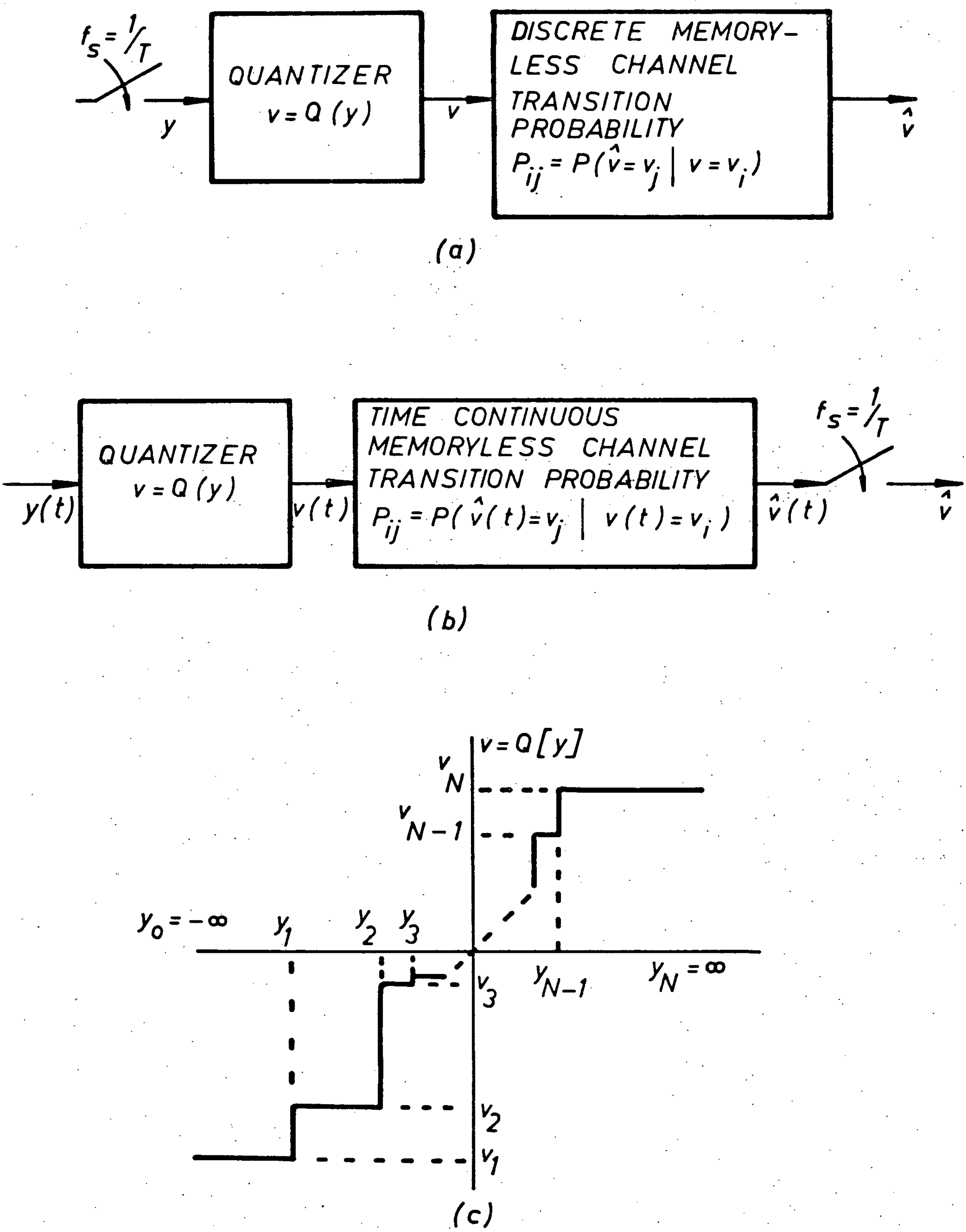

Fig. 6 (a) Quantizer and discrete memoryless channel.
(b) System equivalent to the system shown in Fig. 6a.
(c) Quantizer characteristic.

mitted over a discrete memoryless communication channel. In any realistic system, the sampling operation must be performed before quantization and digital transmission. However, since the quantizer and digital channel are assumed to be memoryless, Fig. 6a can be represented for analysis purposes by the analytically equivalent system of Fig. 6b. In Fig. 6b, let $\phi_{y\hat{v}}(\tau) = E[y(t)\hat{v}(t-\tau)]$ denote the crosscorrelation function of stationary random processes $y(t)$ and $\hat{v}(t)$, $\phi_{\hat{v}}(\tau)$ denote the autocorrelation function of $\hat{v}(t)$, and let $n(t)=\hat{v}(\tau)-y(t)$. Although $\phi_{y\hat{v}}(\tau)$, $\phi_n(\tau)$, and $\phi_{yn}(\tau)$ have been obtained when the channel in Fig. 6 is noiseless [31,33], that is, when

$$P_{ij} = \begin{cases} 1 & i=j \\ 0 & i\neq j \end{cases}$$

the purpose of this Section is to obtain $\phi_{\hat{v}}(\tau)$, $\phi_{y\hat{v}}(\tau)$, $\phi_n(\tau)$, and $\phi_{yn}(\tau)$ when $y(t)$ is a Gaussian process and digital transmission is not error-free.

Let $P(A,B)$ and $P(A/B)$ denote, respectively, the joint probability of events A and B and the probability of event A given B. If $p_y(\alpha,\beta;\tau)$ denotes the second order amplitude probability density of $y(t)$ at times t and $t-\tau$, then

$$\phi_{\hat{v}}(\tau) = E[\hat{v}(t)\hat{v}(t-\tau)]$$

$$= \sum_{i=1}^{N}\sum_{j=1}^{N} v_i v_j \sum_{k=1}^{N}\sum_{m=1}^{N} P[\hat{v}(t)=v_i \,|\, \hat{v}(t-\tau)=v_j,\ v(t)=v_k, v(t-\tau)=v_m]$$

$$P[\hat{v}(t-\tau)=v_j/v(t)=v_k,\ v(t-\tau)=v_m]P[v(t)=v_k,\ v(t-\tau)=v_m]$$

Since[†]

[†]Equation (56) follows from

$$P[\hat{v}(mT)=v_i/v(mT-nT)=v_k]=\begin{cases} P_{ki} & n=0 \\ 0 & n\neq 0 \end{cases}$$

where m and n are any integers, and T is the sampling period of the PCM system shown in Fig. 6a.

$$P[\hat{v}(t)=v_i/v(t-\tau)=v_k] = \begin{cases} P_{ki} & \tau=0 \\ 0 & \tau\neq 0 \end{cases} \tag{56}$$

then

$$\emptyset_{\hat{v}}(\tau) = \sum_{i=1}^{N}\sum_{j=1}^{N} v_i v_j \sum_{k=1}^{N}\sum_{m=1}^{N} P_{ki}P_{mj} \int_{y_{k-1}}^{y_k}\int_{y_{m-1}}^{y_m} p_y(\alpha,\beta;\tau)\, d\alpha d\beta \tag{57}$$

If $y(t)$ is a Gaussian process with mean μ, variance σ^2, autocorrelation function $\emptyset_y(\tau)$ and correlation coefficient $\delta_y(\tau)=[\emptyset_y(\tau)-\mu^2]/\sigma^2$ then [29,30]

$$p_y(\alpha,\beta;\tau)=[\frac{1}{2\pi\sigma^2}][\exp\{-[(\alpha-\mu)^2+(\beta-\mu)^2]/2\sigma^2\}] \sum_{n=0}^{\infty} \frac{\delta_y{}^n(\tau)}{n!} H_n(\frac{\alpha-\mu}{\sigma})H_n(\frac{\beta-\mu}{\sigma}) \tag{58}$$

$$H_n(r) = (-1)^n e^{r^2/2} d^n(e^{-r^2/2})/dr^n \tag{59a}$$

We note here the orthogonality property of the Hermite polynomials $H_n(r)$,

$$\int_{-\infty}^{\infty} \frac{1}{\sqrt{2\pi}} e^{-r^2/2} H_m(r)\, H_n(r)\, dr = \begin{cases} n! & m=n \\ 0 & m\neq n \end{cases} \tag{59b}$$

Substitution of (58) into (57) followed by application of (59b) and $\sum_{i=1}^{N} P_{ki}=1$ yields

$$\emptyset_{\hat{v}}(\tau) = \sigma^2 \sum_{n=0}^{\infty} a_n^2[\delta_y(\tau)]^n \tag{60}$$

where

$$a_0 = (1/\sqrt{2\pi\sigma}) \sum_{i=1}^{N} \frac{v_i}{\sigma} \sum_{k=1}^{N} P_{ki}\int_{y_{k-1}}^{y_k} \exp[-(r-\mu)^2/2\sigma^2]dr$$

$$= E(\hat{v})/\sigma \tag{61a}$$

and, for $n \geq 1$

$$a_n = [(-1)^n/\sqrt{2\pi n!}] \sum_{i=1}^{N} (\frac{v_i-c_n}{\sigma}) \sum_{k=1}^{N} P_{ki}\,\Gamma_n(k) \tag{61b}$$

$$\Gamma_n(k) = \hat{\Phi}^{n-1}[(y_k-\mu)/\sigma]-\hat{\Phi}^{n-1}[(y_{k-1}-\mu)/\sigma] \tag{61c}$$

$$\hat{\Phi}^n(r) = d^n[e^{-r^2/2}]/dr^n \tag{61d}$$

where c_n is any constant.

A similar approach gives

$$\emptyset_{y\hat{v}}(\tau) = E[y(t)\hat{v}(t-\tau)]$$
$$= \sum_{i=1}^{N} \sum_{j=1}^{N} v_i P_{ji} \int_{-\infty}^{\infty} \alpha[\int_{y_{j-1}}^{y_j} p_y(\alpha,\beta;\tau)\, d\beta]\, d\alpha$$
$$= \sigma^2[a_1\delta_y(\tau)+(\mu/\sigma)a_0] \tag{62}$$

Equations (61) and (62) can be used with $n(t)=v(t)-y(t)$, $\delta_y(\tau)=\delta_y(-\tau)$ and $\emptyset_{\hat{v}y}(\tau) = \emptyset_{y\hat{v}}(-\tau)$ to obtain $\emptyset_n(\tau)$ and $\emptyset_{yn}(\tau)$ in Fig. 6 as follows.

$$\emptyset_n(\tau) = \emptyset_{\hat{v}}(\tau) + \emptyset_y(\tau) - \emptyset_{y\hat{v}}(\tau) - \emptyset_{y\hat{v}}(-\tau)$$
$$= \sigma^2[(\mu/\sigma-a_0)^2 + (1-a_1)^2\ \delta_y(\tau) + \sum_{n=2}^{\infty} a_n^2\delta_y{}^n(\tau)] \tag{63}$$

$$\emptyset_{yn}(\tau) = \sigma^2\ [(\mu/\sigma)a_0-(\mu/\sigma)^2]+(a_1-1)\delta_y(\tau) \tag{64}$$

Let $R_u(\tau)=\emptyset_u(\tau)-[E(u)]^2$ and $R_{ux}(\tau)=\emptyset_{ux}(\tau)-E(u)E(x)$, where u and x are any stationary random processes. It follows from (61a) and $E(y)=\mu$ that

$$R_{\hat{v}}(\tau) = \sigma^2 \sum_{n=1}^{\infty} a_n^2\delta_y{}^n(\tau) \tag{65a}$$

$$R_{y\hat{v}}(\tau) = \sigma^2 a_1\delta_y(\tau) \tag{65b}$$

$$R_n(\tau) = \sigma^2[(1-a_1)^2\delta_y(\tau) + \sum_{n=2}^{\infty} a_n^2\delta_y^n(\tau)] \tag{65c}$$

$$R_{yn}(\tau) = \sigma^2(a_1-1)\delta_y(\tau) \tag{65d}$$

In the Appendix, alternative exact expressions, which are sometimes more attractive than the Hermite series expansions, are presented, as well as some useful approximations and bounds for the correlation functions. Also included in the Appendix are the results of this Section applied to the postfiltering problem. It is shown that the effect of crosscorrelation $\emptyset_{yn}(\tau)$ on both the optimal reconstruction postfilter and the reconstruction error is small if the channel is sufficiently good and if the number of levels N in both Max and optimal quantizers is sufficiently large. In general, the same conclusion did not apply for small N or for poor channels.

4.2.2 Pre and Postfiltering in PCM Systems

It follows from the analysis in the previous Section and Appendix A that the PCM system in Fig. 7 can be represented as in Fig. 1. Without loss in generality let $E[x(t)]=E[y(t)]=\mu=0$, then from (61), (63) and (64)

$$\emptyset_{yn}(\tau) = (a_1-1)\emptyset_y(\tau) \tag{66a}$$

$$\emptyset_n(\tau) = P\{a_0^2 + (1-a_1)^2[\emptyset_y(\tau)/P] + \sum_{k=2}^{\infty} a_k^2[\emptyset_y(\tau)/P]^k\} \tag{66b}$$

$$a_n=[(-1)^n\sqrt{2\pi n!}]\sum_{i=1}^{N}\left(\frac{v_i}{\sqrt{P}}\right)\sum_{j=1}^{N} P_{ji}\{\hat{\Phi}^{n-1}[(y_j)/\sqrt{P}]-\hat{\Phi}^{n-1}[y_{j-i})/\sqrt{P}]\} \tag{66c}$$

$$\hat{\Phi}^n(r) = d^n[\exp(-r^2/2)]/dr^n \tag{66d}$$

where P is given by (10) with $|K(f)|^2 = 1$, $\emptyset_y(\tau) = E[y(t)y(t-\tau)]$, $\emptyset_n(\tau) = E[n(t)n(t-\tau)]$ and $\emptyset_{yn}(\tau) = E[y(t)n(t-\tau)]$. Transition probability $P_{ij}=P(\hat{v}=v_j/v=v_i)$ depends on the encoding and decoding scheme as well as on the modulator, demodulator and physical channel. From (66a) it follows that $\hat{B}(f)=a_1-1$. Therefore $B(f)=1+\hat{B}(f)=a_1$ and $C(f)=1+\hat{B}(f)+\hat{B}^*(f)=2a_1-1$.

Although $\Phi_n(f)$ can be obtained by Fourier transforming $\emptyset_n(\tau)$ in (66b) calculation is tedious, particularly when it has tc be performed for several values of T. Ruchkin [34] and Robertson [35] have shown that for

$$P_{ij} = \begin{cases} 1 & i=j \\ 0 & i\neq j \end{cases} \tag{67}$$

$\Phi_{n_s}(f)$ in (16b) is approximately constant for a large class of $\Phi_y(f)$ and all but very coarse quantizing and very small T. One would expect this conclusion to hold for any P_{ij}† in which case $\Phi_{n_s}(f)=T\cdot\emptyset_n(0)$ where

---

† The statement is supported by the results in Appendix A.4 when a Max uniform or nonuniform quantizer is used and P_{ij} is given by (71a).

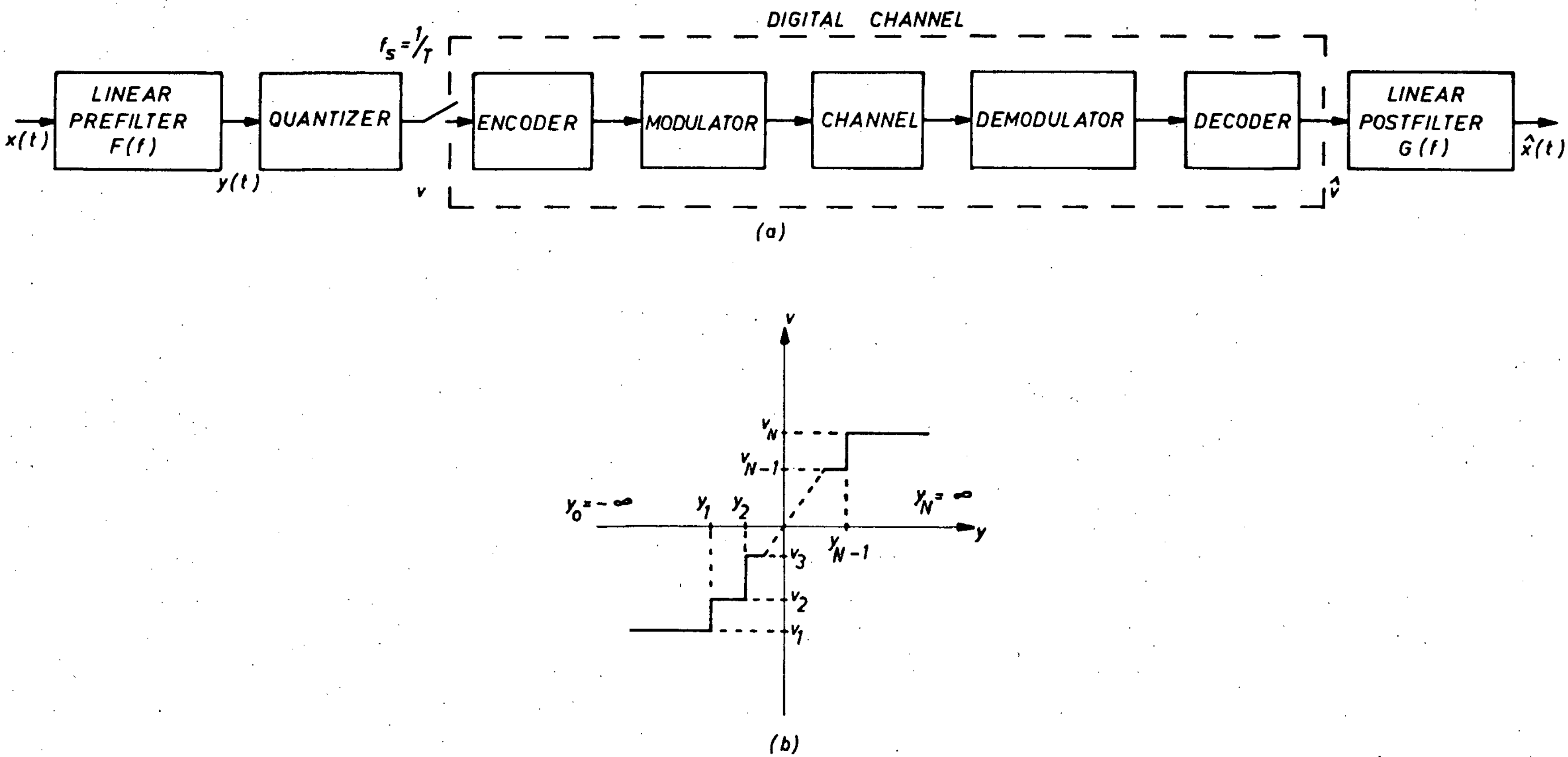

Fig. 7 (a) A PCM system.
(b) Quantizer transfer characteristic.

$$\phi_n(0) = E(n^2)$$

$$= \sum_{i=1}^{N} \sum_{j=1}^{N} P_{ij} \int_{y_{i-1}}^{y_i} (v_j-\alpha)^2 p_y(\alpha)^2 p_y(\alpha) d\alpha \tag{68}$$

and $p_y(\alpha)$ is the amplitude probablity density of $y(t)$. If the quantizer output levels are optimally spaced [36] then

$$v_i = \int_{y_{i-1}}^{y_i} \alpha p_y(\alpha) d\alpha / \int_{y_{i-1}}^{y_i} p_y(\alpha) d\alpha \tag{69}$$

in which case the crosscorrelation between quantization noise and noise resulting from channel transmission errors is zero and

$$\phi_n(0) = \sum_{i=1}^{N} \int_{y_{i-1}}^{y_i} (v_i-\alpha)^2 p_y(\alpha) d\alpha + \sum_{i=1}^{N} \sum_{j=1}^{N} P_{ij} (v_i-v_j)^2 \int_{y_{i-1}}^{y_i} p_y(\alpha) d\alpha \tag{70}$$

The y_i's and v_j's of the quantizer are usually proportional to $\sqrt{P}$, in which case $\Phi_{n_s}(f)$ is proportional to P. It follows that ε in Chapters 2 and 3 is independent of P while $|F|^2$ and $|G|^{-2}$ are proportional to P. In fact, substitution of $\Phi_{n_s}(f)=TP\phi_n(0)$ into (9) where $\phi_n(0)=E(n^2)$ when P=1, followed by replacement of P by $\int_{-\infty}^{\infty} |K(f)F(f)|^2 \Phi_x(f) df$ and subsequent minimization of ε with respect to F and G is an alternative way to obtain the optimal F, G and ε for PCM without use of the power constraint (10).

Example 3:

For the PCM system in Fig. 7 let d be such that $d=\log_2 N$ takes on only integer values, and let

$$P_{ij} = p^{d_{ij}} (1-p)^{d-d_{ij}} \tag{71a}$$

$$p = Q[\sqrt{(2S/N_o f_s d)}] \tag{71b}$$

$$Q(x) = (1/\sqrt{2\pi}) \int_x^\infty e^{-r^2/2} dr \tag{71c}$$

where d_{ij} is the Hamming distance between the binary numbers i and j.

Equation (71a) gives P_{ij} which results when the quantizer output amplitudes are natural binary coded and each digit is then transmitted over a white Guassian channel of bandwidth W_c using optimum demodulation and binary antipodal modulated signals whose average power equals S and whose total energy lies in the frequency band of the channel.

Fig. 8 shows ε/σ vs. S/N_oW_c for optimal pre and postfilters when $\Phi_x(f)$ and the modulator, demodulator, and channel are as in Example 2 with M=1 and $f_s d=2W_c$, in which case P_{ij} is given by (71). Max [37] nonuniform quantizers were used, with d chosen to minimize ε/σ. The effect of a non-optimal d on ε/σ was not critical. For example, with $S/N_oW_c = 10$ and $W_c/a = 1000$, the optimal d=3 yields $\varepsilon/\sigma = .00385$ for the (0) case, as opposed to $\varepsilon/\sigma=.00490$ for the non-optimal value of d=6. Also shown is OPTA as given by (55), and ε/σ for the (PR) and (PO) cases. Fig. 9 shows SNR as given by (53). We note here that a further (slight) improvement in both ε and SNR is possible if the quantizer is chosen to minimize $E(n^2)$ in (68) [38], since Max nonuniform quantizers are optimal if and only if P_{ij} is given by (67). As in the PAM case, one S/N_oW_c, W_c pair minimizes ε for a given value of C in (54). Fig. 10a shows this minimum ε vs. C/a for the (0) and (PR) cases in Example 3. For these two curves and for the curves in Figs. 8 and 9 the optimal filter bandwidth $W=W_c/d$.

Example 4

If $f_s d \le C$, where C is the capacity of the physical channel, then optimal encoding and decoding makes P_{ij} as given by (67)†. Although optimal codes are unrealizable because of their infinite block length, they provide a bound on the performance obtainable using any encoding scheme. The ε and SNR

†For optimal codes d is constrained to assume values for which 2^d is a positive integer.

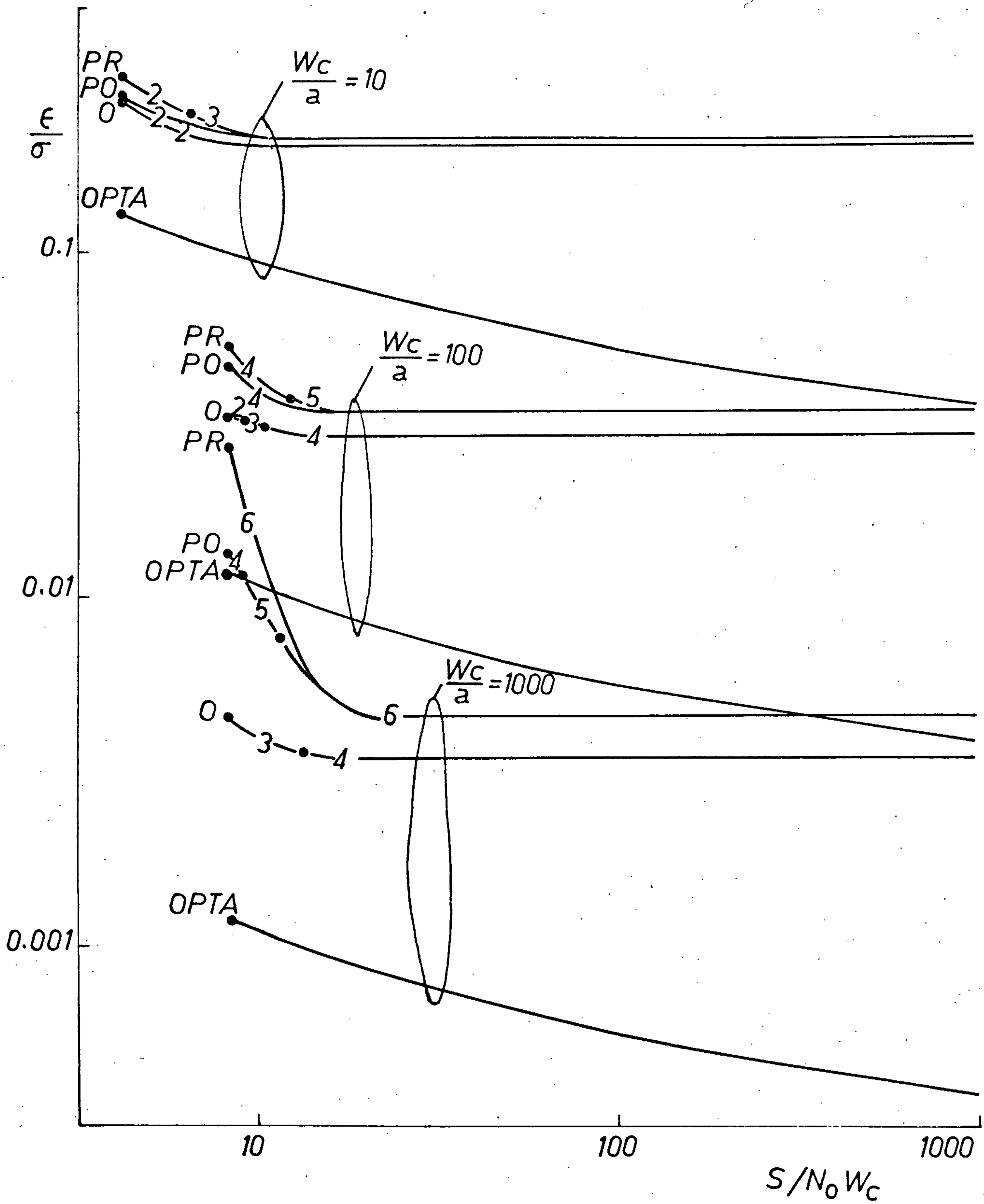

Fig. 8 Normalized error ε/σ versus S/N_oW_c for Example 3. Symbols 0, PR, and PO are defined in the caption of Fig. 4. The number of bits of quantization d which minimizes ε/σ for the given values of W_c/a and S/N_oW_c is shown on the curves. For the curves shown the optimal filter bandwidth $W=W_c/d$.

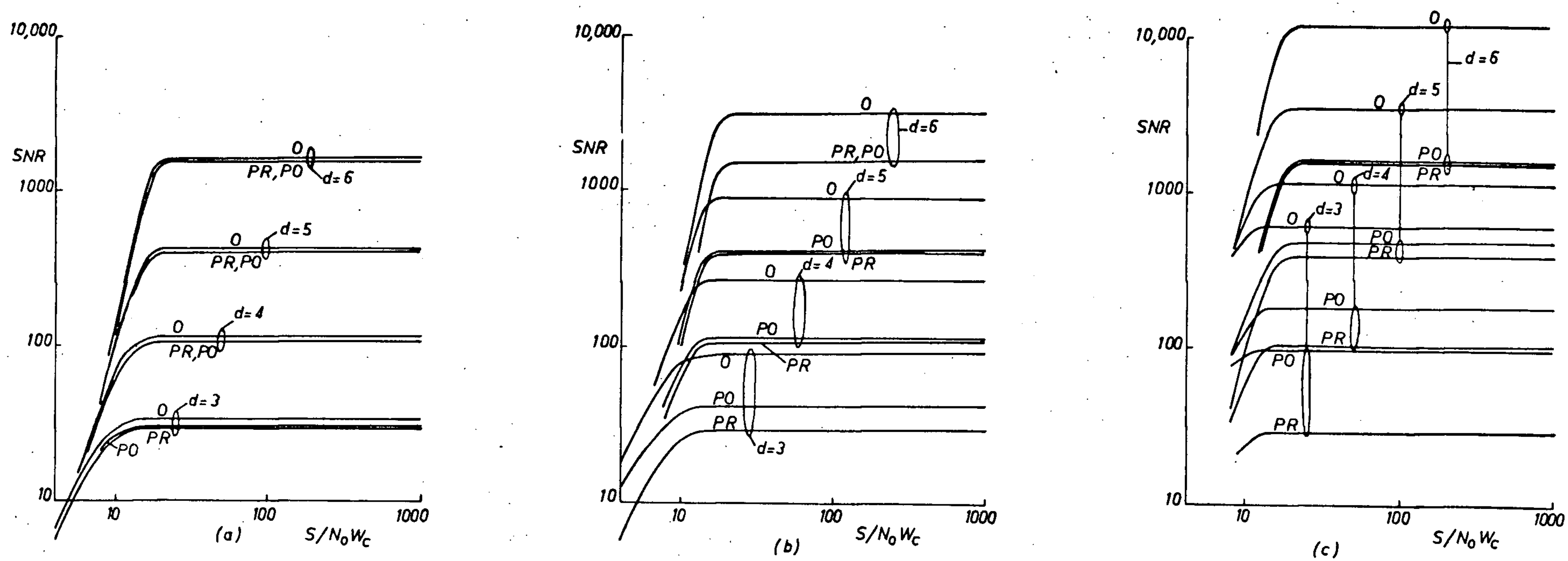

Fig. 9 Signal-to-noise ratio SNR for Example 3. For the curves shown the optimal filter bandwidth $W=W_c/d$.
(a) $W_c/a=10$.
(b) $W_c/a=100$.
(c) $W_c/a=1000$.

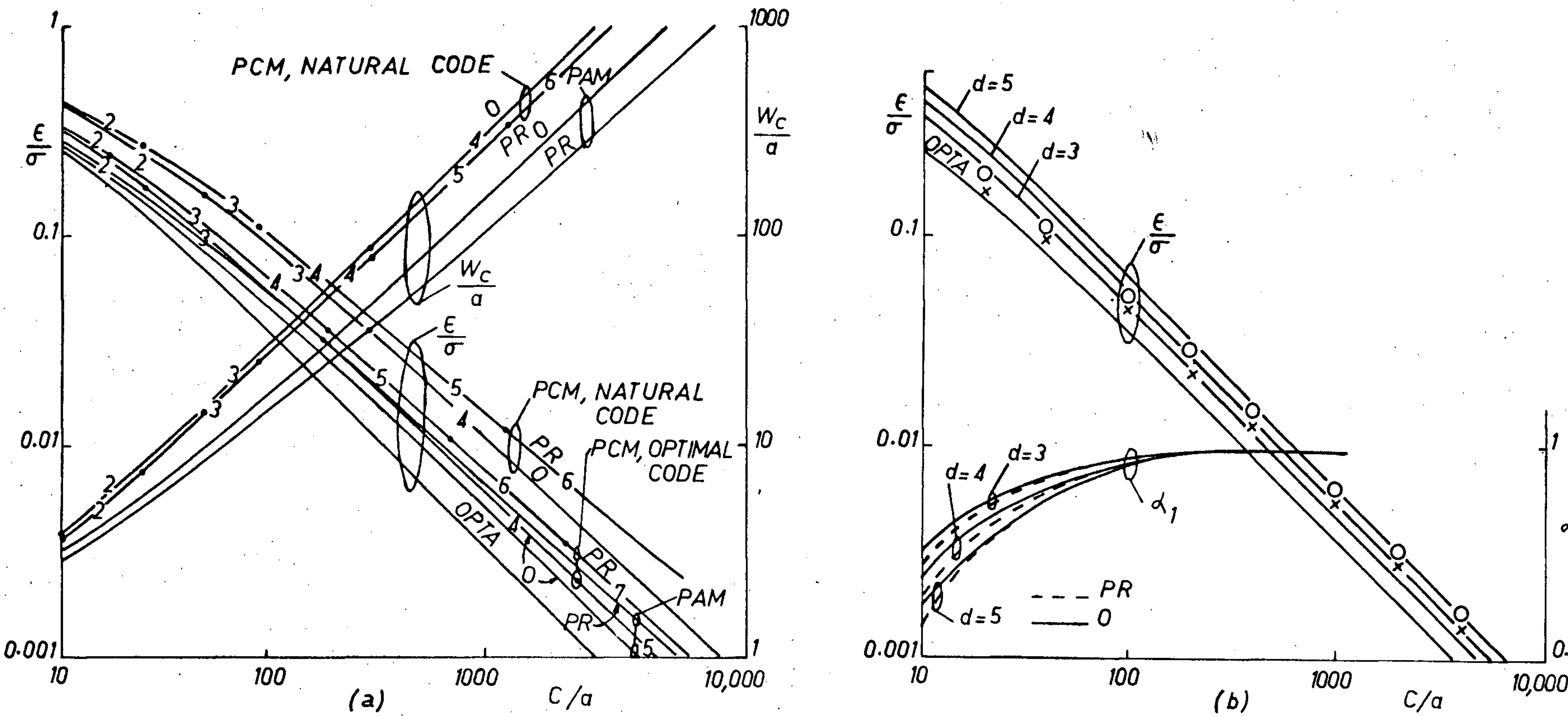

Fig. 10 (a) Normalized minimum error ε/σ for Examples 2,3, and 4 and optimal channel bandwidth W_c/a for Examples 2 and 3. The number of bits of quantization d which minimizes ε/σ are shown. Also shown is the OPTA.
(b) Error ε/σ and optimum feedback coefficient α_1 for DPCM (Example 5). The three filtering schemes, O, PR, and PO, yield identical ε/σ when α_1 is chosen to minimize ε. Indicated for comparison purposes are PAM and PCM results obtained from Fig. 10a: ×-PAM O and o-PCM O, optimal code.

obtained using optimal codes with $f_s d=C$ equals that which results when an analog signal x(t) is prefiltered, sampled and quantized, stored digitally in a memory having no read and write errors at a rate of C bits per second, and later postfiltered.

Let P_{ij} be given by (67), let $f_s d=C$ and let the modulator, demodulator, channel and $\Phi_x(f)$ be as given in Example 2 with M=1, in which case $C=W_c \log_2(1+S/N_o W_c)$. Fig. 10a shows ε/σ and the optimal d vs. C/a for the filters discussed in Section 3.2. Max nonuniform quantizers were used.

When x(t) is non-Gaussian exact theoretical optimization of the system in Fig. 7 is impossible, since the second order amplitude probability density of y(t) at times t and τ cannot be calculated from F(f) and the statistics of x(t). Consequently, $\emptyset_{yn}(\tau)$ and $\Phi_{n_s}(f)$ cannot be calculated exactly and an approach using approximations is required.

4.3 Differential Pulse Code Modulation (DPCM)

A DPCM system is shown in Fig. 11. Input x(t) is prefiltered, sampled and compared with a linear prediction $\hat{y}_k$ of y_k based on its past. The difference e_k between y_k and the predicted value $\hat{y}_k$ is quantized and transmitted over a digital channel. At the receiver a prediction of y_k is also made based on previously received samples and added to the present received sample giving r_k. The sequence $\{r_k\}$ is then postfiltered to yield $\hat{x}(t)$.

If digital transmission is error-free, or if the digital channel represents a digital memory having no read-write errors, then the reconstructed samples $r_k=y_k+q_k$, and the systems in Figs. 11a and 11b yield the same $\hat{x}(t)$. The system in Fig. 11b can be represented as shown in Fig. 1 provided n(t)=q(t) is the noise resulting from quantization of e(t). If one makes the standard assumption valid for $N \geq 8$, [39-42] that the feedback quantization noise is small in comparison with e(t) then

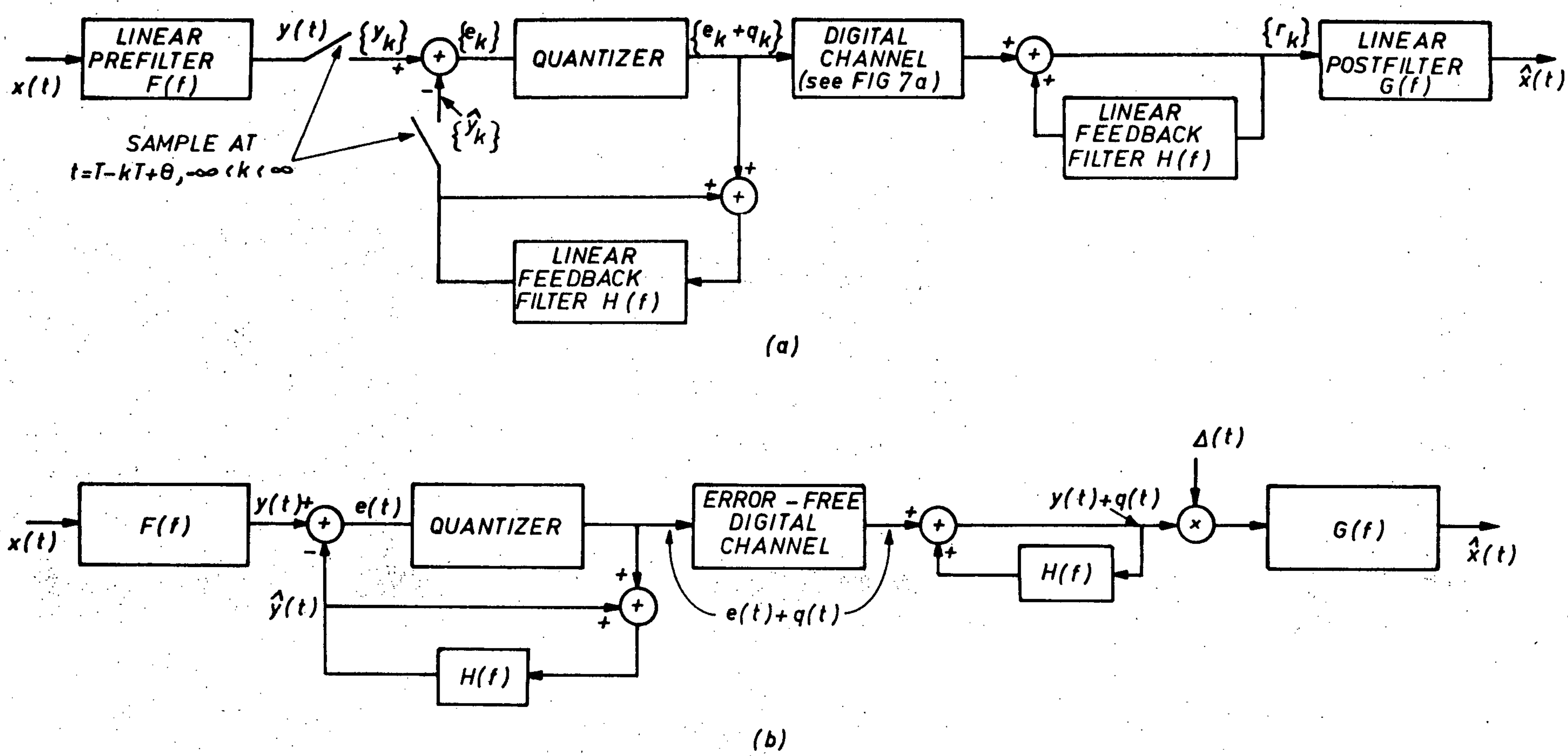

Fig. 11 (a) A DPCM system.
(b) An equivalent system to Fig. 11a when the digital channel is noiseless.
Impulse train $\Delta(t)=T.\sum_{k=-\infty}^{\infty}\delta(t-kT+\theta)$.

$$E[e^2] = \int_{-\infty}^{\infty} |1-H(f)|^2 \; |F(f)|^2 \Phi_x(f)df$$

Assuming that the spectrum of the sampled quantization noise is flat, $\Phi_{n_s}(f) = T\emptyset_n(0)$ where $\emptyset_n(0)$ is given by (68) with $p_e(\alpha)$ replacing $p_y(\alpha)$.

If x(t) is Gaussian, then y(t) and e(t) are Gaussian, provided the feedback quantization noise is neglected. From (66) it follows that $\Phi_{eq}(f) = (a_1-1)\Phi_e(f)$, from which one obtains $\Phi_{yn}(f)=(a_1-1)[1-H(f)]^*|F(f)|^2\Phi_x(f)$ where a_1 is obtained from (66c) with P_{ij} defined by (67) and $P = E[e^2]$. Thus, $\hat{B}(f)=(a_1-1)[1-H(f)]^*$.

The input and output of the linear filters H(f) in Fig. 11a are signals sampled every T seconds. It follows that for any realizable H(f) no loss in generality results if $H(f) = \sum_{k=1}^{L} \alpha_k e^{-j2\pi kfT}$ where L is any positive integer; if $\alpha_k=0(k=1,2,\ldots,L)$ then a PCM system results. With this H(f) and x(t) Gaussian the analysis in Chapters 2 and 3 applies with $|W(f)|^2=1$,

$$|K(f)| = \left|1 - \sum_{k=1}^{L} \alpha_k e^{-j2\pi kfT}\right| \tag{72a}$$

$$B(f) = 1 + (a_1-1)[1 - \sum_{k=1}^{L} \alpha_k \; e^{j2\pi kfT}] \tag{72b}$$

$$C(f) = 1 + 2(a_1-1)[1 - \sum_{k=1}^{L} \alpha_k \cos 2\pi kfT] \tag{72c}$$

provided C(f)>0. Functions K, B and C are periodic in 1/T as required in Chapter 2. We note here that the paragraph which immediately preceeds Example 3 in Section 4.2 also applies here.

Example 5

For the DPCM system described above, let the channel capacity $C=f_s d$ and the modulator, demodulator, channel and $\Phi_x(f)$ be as given in Example 2 with M=1, in which case $C=W_c \log_2(1+S/N_o W_c)$. If the prefilter is an ideal low-pass filter with cutoff frequency $W=f_s/d>>a$, then $\{y_k\}$ approaches a first-order

Markov sequence and the linear prediction of y_k which minimizes $E[q_k^2]$ is obtained by considering the most recent available sample y_{k-1} [39]. Based on this fact, it is anticipated that using one sample of feedback (L=1) to minimize ε will be almost as good as using many samples, in which case $|K(f)|$ B(f), and C(f) are given by (72) with L=1. In order to ensure that C(f)>0, one must restrict $|\alpha_1| < 1$ and the quantizer characteristic such that $a_1 > 0.75$. Let the quantizer be Max nonuniform [37]; then the restriction $a_1 > 0.75$ is satisfied for $d \geq 2$. Sections 2.3 and 3.1.2 show that the optimal pre and postfilter Ω_o contains all frequencies $|f| < W$ where $W \leq f_s/2$. Fig. 10b shows ε/σ vs. C/a for the three filtering schemes, 0, PR and PO when d=3,4 and 5. Also shown is the value of α_1 which minimizes ε for the designated C/a for the 0 and PR cases. For the curves shown the optimal filter bandwidth is $W=f_s/2d$. The fact that ε/σ vs. C/a is the same for all three filtering schemes indicates that whatever redundancy reduction is not done by the prefilters will be done by H(f), provided α_1 is optimized. Note that the smaller d the closer is ε/σ to OPTA. The reason for this behaviour is that for a fixed C, T decreases as d decreases, with the result that $\hat{y}_k$ becomes a more accurate prediction of y_k and ε/σ decreases. Curves of ε/σ vs. C/a for d=2 and d=1 are not shown because the validity of the assumption that the feedback quantization noise is small in comparison with e(t) becomes doubtful.

When x(t) in Fig. 11 is non-Gaussian the above analysis is not necessarily applicable, in which case an approach using approximations is required for optimization . When the digital channel is noisy, an approach to optimization using approximations is also necessary even when x(t) is Gaussian.

4.4 System Comparisons

Fig. 10a shows the advantage of optimal encoding relative to that of PCM natural coding when S/N_oW_c and W_c are such that, for natural coding, ε is minimized for a given capacity C. This advantage is even more pronounced when S/N_oW_c and W_c are not chosen to minimize ε for natural coding. For given filters of bandwidth W the differences (not shown) in SNR for the two types of coding are more pronounced than are the differences in ε.

The differences in ε for PCM and DPCM are evident from Fig. 10b. It follows from (53) that for any given d and filter pair of bandwidth W the advantage in DPCM over PCM with respect to SNR is even more pronounced than is the advantage with respect to ε. The difference in SNR between PCM and DPCM appears elsewhere for ideal lowpass filters [40].

Comparison of Fig. 4 with Fig. 8 shows that when S/N_oW_c is small and W_c is large, PCM tends to yield lower values of ε than does PAM, while the converse is true when S/N_oW_c is large and W_c is small. Fig. 10a shows that for all values of C/a shown the best obtainable performance for PAM is superior to that for PCM for both the 0 and PR cases. Fig. 10b shows the best PAM to be superior to optimum DPCM only for $C/a \lesssim 100$.

Finally, we note that when x(t) and the channel are as described in Example 2 with M=1, ε obtainable using optimal filters, optimal quantization and optimal encoding is approximately twice OPTA for PCM and 1.3 times OPTA for DPCM with d=3. A further (slight) decrease in ε for optimal coded PCM and DPCM is possible if the quantizer outputs are entropy† coded prior to being optimally channel-encoded [40,41].

---

†Entropy coding is the same as Huffman coding or Shannon-Fano coding.

5. COMPUTER SIMULATION OF PRE AND POSTFILTERING IN PAM, PCM, AND DPCM SPEECH COMMUNICATION SYSTEMS

5.1 Introduction

The purpose of the following Chapters is to relate the rather general theoretical study of the previous Chapters to the practical design of speech communication systems. At this time it is not possible to formulate a mathematically tractable evaluation criterion for speech that agrees completely with the subjective judgments made by human auditors. It is the lack of such a desirable mathematical criterion that necessitates subjective measurements before more conclusions regarding the possible benefits of pre and postfiltering in speech communication systems can be reached.

In the following Chapters, various pre and postfiltering schemes for PAM, PCM, and DPCM communication systems are simulated and subjectively evaluated when the input signal is speech. Because of the empirical nature of the problem, the filtering schemes described in the previous Chapters are not strictly adhered to, but are incorporated into the simulation with practical modifications.

The filtering schemes considered are the unweighted ($W(f)=1\ \forall f$ in Fig. 1) weak noise filtering scheme and the optimal prefilter-constant amplitude postfilter scheme. Weak noise filters are used instead of optimal pre and postfilters since weak noise filters yield virtually the same performance as optimal filters whenever $P/\int_{\Omega}[|K(f)|^2\Phi_{n_s}(f)/C(f)]\,df \gg 1$ (see Section 3.2.1) and have the practical advantage that the filter transfer characteristics are essentially dependent only on the relative spectra of the input signal and the noise. The optimal prefilter-constant amplitude postfilter scheme (see Section 3.2.2) is considered since under certain practical assumptions the filters are lowpass. As lowpass filters are commonly employed in speech communication systems, this scheme will serve as a useful comparison for the weak noise filtering scheme.

In Section 5.2, the assumptions and restrictions imposed in the investigation are tabulated. Also included is a Table giving the filter characteristics used in the simulation of the PAM, PCM, and DPCM systems. Section 5.3 is devoted to a brief explanation of the digital simulation facilities. Both hardware and software are discussed.

In Chapter 6, the subjective testing method is explained and the subjective results interpreted. Included is a heuristic explanation for the subjective behaviour of lowpass and weak noise filtering schemes used in PAM, PCM, and DPCM communication systems. Finally, a few concluding remarks are presented, including the feasibility of using a frequency weighted mean-integral-squared error criterion as an objective measure of speech quality and the possibilities of using weak noise filters for PCM television systems.

5.2 Assumptions and Restrictions

The following assumptions and restrictions are used in the investigation:

1) No intersymbol or interchannel distortion is assumed in the PAM system shown in Fig. 3.
2) Error-free transmission is assumed in the digital channel of the PCM and DPCM systems shown in Figs. 7 and 11, respectively.
3) The PCM and DPCM quantizers are assumed to have nonuniform steps conforming to the μ=100 logarithmic nonlinearity of Smith [45]. Smith has shown that such a quantizer characteristic has the

practical advantage that when the quantizer input signal is speech the signal-to-quantization noise ratio is relatively insensitive to talker volumes. Logarithmic (μ=100) quantizers with 1,2,...7 bits of quantization are simulated.

4) The quantizer overload voltage is set at 4 times the RMS value of the quantizer input signal. Published results [46] show that for a wide class of filters the instantaneous amplitude of filtered speech has less than a 1 percent probability of exceeding 4X the RMS value, and subjective tests have confirmed that a 1 percent probability of peak clipping is virtually undetectable [47]. For DPCM the RMS value is evaluated by neglecting the quantizer in the feedback loop.

5) Previous-sample feedback is used in the DPCM simulation. Therefore, from (72a), $|K(f)| = |1 - \alpha_1 e^{-j2\pi fT}|$. The prediction coefficient α_1 is set to the normalized autocorrelation function of the prefiltered speech evaluated at the sampling period T [39-41].

6) The additive noise in the PAM systems and the quantization noise in the PCM and DPCM systems are assumed to be uncorrelated with the signal. Hence, B(f) = C(f) = 1. In addition, the sampled quantization noise spectrum $\Phi_{n_s}(f) = \sum_{k=-\infty}^{\infty} \Phi_n(f+kf_s)$ is assumed to be constant for all frequency f. Since the systems are simulated on a digital computer and are not operated in real-time, A(f) is arbitrarily set to unity for all f. If real-time operation was performed, A(f) would be the transfer function of the system time-delay.

7) The systems tested are assumed to be of sufficiently high quality

so that the frequency set Ω, over which the prefilter and post-filter transfer functions are non-zero, is given by

$$\Omega = \left\{ \begin{array}{l} f{:}f = q + kf_s \text{ where } q\varepsilon\ [-\frac{1}{2} f_s, \frac{1}{2} f_s] \text{ and } k\varepsilon I_{q_o}. \\ \text{Integer set } I_{q_o} \text{ is defined by (24).} \end{array} \right\} \quad (73)$$

In most cases of interest, Ω will be equal to the optimal set Ω_o derived in Section 2.3.

8) On the basis of assumptions 5), 6), and 7), and the results of Sections 3.1.3 and 3.2.1, prefilter and postfilter characteristics are presented in Table 5.1 for PAM, PCM, and DPCM.

9) From assumption 5), α_1 is adjusted in the DPCM weak noise filter simulations so

$$\alpha_1 = \frac{\int_{-\infty}^{\infty} |F(f)|^2\ \Phi_x(f) e^{-j2\pi fT} df}{\int_{-\infty}^{\infty} |F(f)|^2\ \Phi_x(f) df}$$

where $|F(f)|^2 = \sqrt{\Phi_x(f)}/|1-\alpha_1 e^{-j2\pi fT}|$ is given in Table 5.1.

10) Bandpass filtering, if required, is achieved by concatenating highpass filters (HPF) and lowpass filters (LPF). The HPF has an attenuation of 45 dB or more at 1/1.07 X the 3 dB cut-off frequency and the LPF has an attenuation of 45 dB or more at 1.07 X the 3 dB cut-off (see Fig. 12). Frequency set Ω is physically realized by setting the 3 db cut-off frequencies of the HPF at $1.07f_\ell$ and those of the LPF at $f_u/1.07$, where f_ℓ and f_u are the lower and upper cut-off frequencies of the frequency bands comprising Ω. Such frequency scaling is expected to render negligible the distortion caused by aliasing.

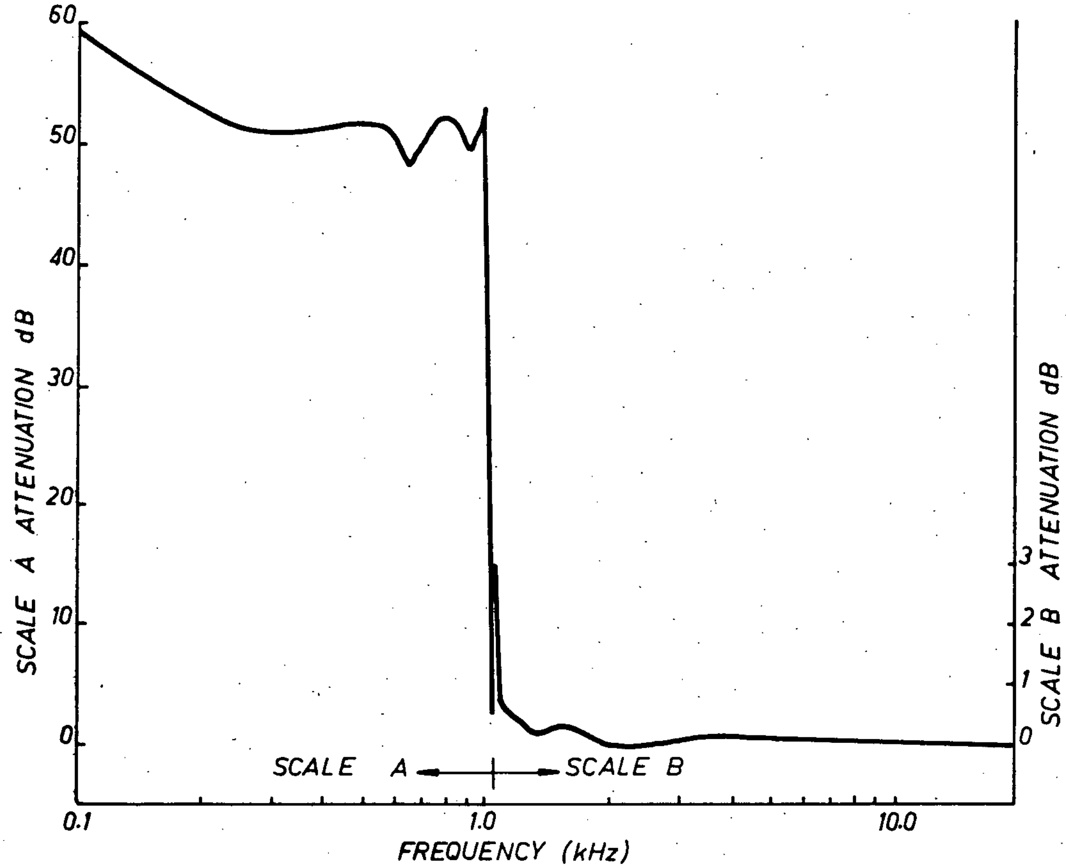

(a)

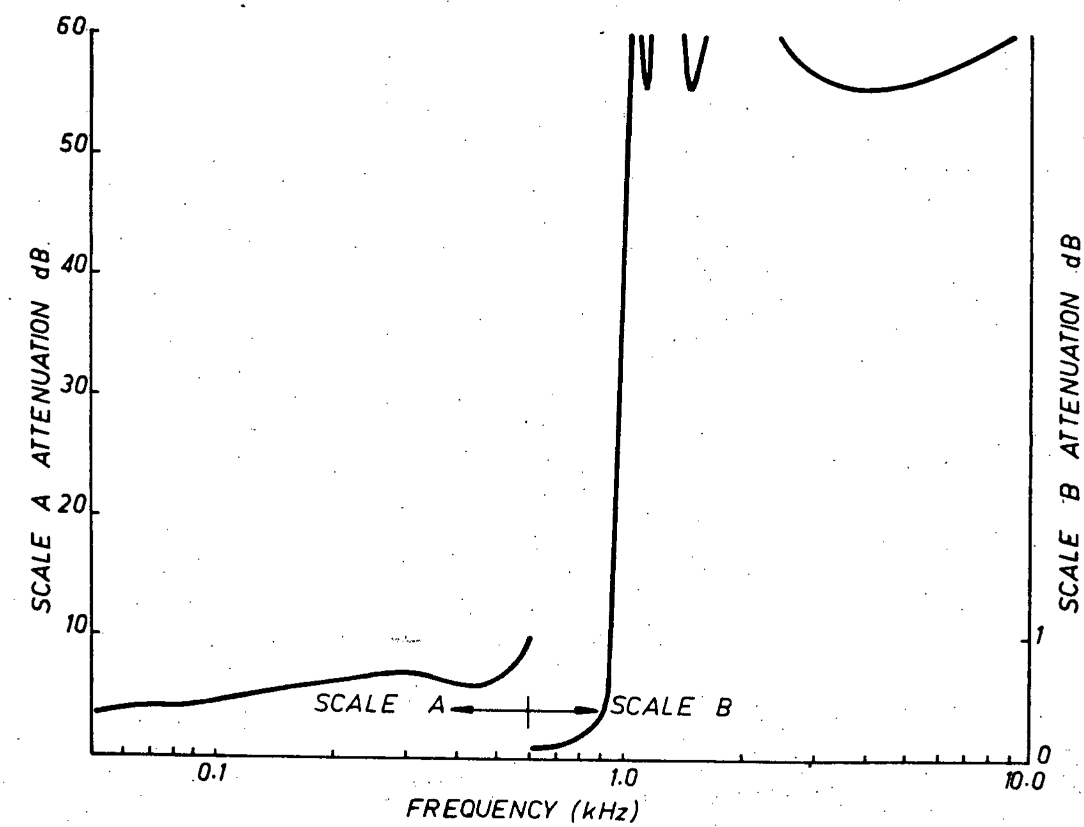

(b)

Fig. 12 Typical frequency response.
(a) Highpass filter.
(b) Lowpass filter.

		PAM	PCM	DPCM
Unweighted	$\lvert F(f)\rvert^2$	$\sqrt{\Phi_{\bar{n}_s}(f)/\Phi_x(f)}$	$\sqrt{1/\Phi_x(f)}$	$\sqrt{1/\Phi_x(f)}/\lvert 1-\alpha_1 e^{-j2\pi fT}\rvert$
Weak Noise	G(f)	1/F(f)	1/F(f)	1/F(f)
Filters	Ω	from (73) with A(f)=W(f)=1	from (73) with A(f)=W(f)=1	from (73) with A(f)=W(f)=1
Optimal Prefilter-	$\lvert F(f)\rvert^2$	1	1	1
Constant Amplitude	G(f)	1/F(f)	1/F(f)	1/F(f)
Postfilter	Ω	from (73) with A(f)=W(f)=1	from (73) with A(f)=W(f)=1	from (73) with A(f)=W(f)=1

Table 5.1 Prefilter and Postfilter Characteristics used in the Computer Simulation

5.3 Digital Computer Simulation

Application of digital simulation to the subjective study of speech communication systems has been described by previous investigators [48-51]. It was demonstrated that savings in time and money could be achieved through the elimination of extensive hardware construction. Additional benefits include ease and flexibility in modifying system parameters, exact reproduction of data (stored on digital tape), and precise control of the simulated system. In this Section, hardware and programming requirements peculiar to this simulation are discussed.

The key to the simulations considered here is found in the realization of the pre and postfilters as analog bandpass filters in series with digital filters. Some of the advantages of using digital filters include very predictable stable performance of arbitrarily high precision and great ease in changing filter response [52,53]. The equivalent realizations are shown in Fig. 13.

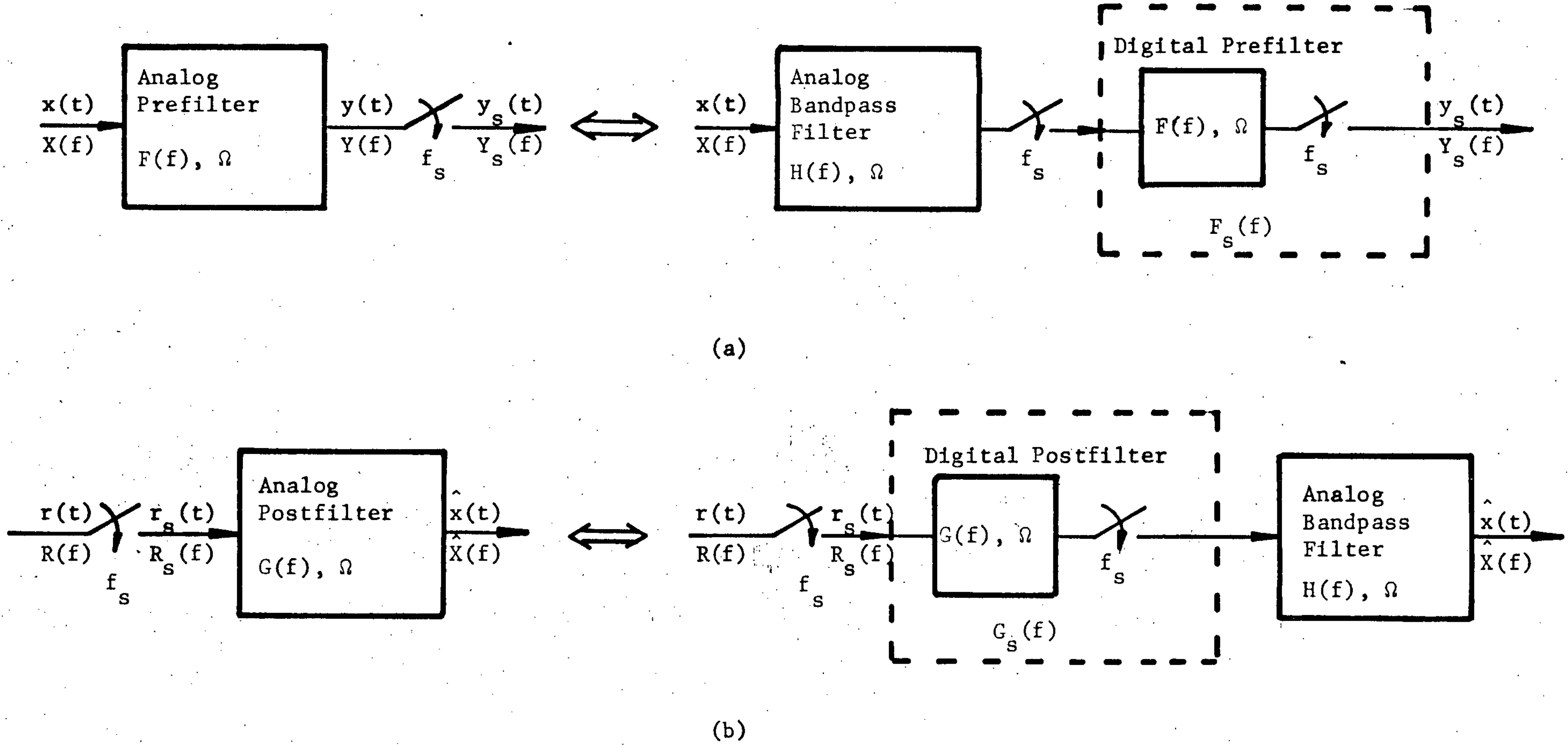

Fig. 13 Equivalent realization.
(a) Prefilter.
(b) Postfilter.

The passbands occupied by the filters are denoted as set Ω and are constrained such that there is no overlapping of passbands when translated by integer multiples of the sampling frequency (no aliasing). If $U_s(f)=[U(f)]_s=\sum_{k=-\infty}^{\infty} U(f+kf_s)$, then

$$Y_s(f)=[F(f)X(f)]_s \equiv F_s(f)[H(f)X(f)]_s \tag{74a}$$

and

$$\hat{X}(f)=G(f)R_s(f) \equiv H(f)G_s(f)R_s(f) \tag{74b}$$

Equivalence relation (74a) follows from the fact that $[F(f)X(f)]_s = [F(f)H(f)X(f)]_s = F_s(f)[H(f)X(f)]_s$ and (74b), from $G(f) = H(f)G_s(f)$.

5.3.1 Digital Recording and Playback System

A block diagram of the digital recording system used in the simulation is shown in Fig. 14a. The analog signal is filtered into passbands which prevent aliasing for a given sampling rate (see (73) and assumption 10) in Section 4.2) and then sampled-and-held for analog-to-digital conversion. The analog-to-digital converter (ADC) codes each sample into 10 bits and transfers it to the buffer and control unit (BCU). Noise introduced by the conversion process is ignored since its level is sufficiently low to be masked out by the noise introduced in the simulations.

The buffer consists of two blocks, each capable of storing 508 ten-bit characters. The blocks are utilized in a double-buffered manner so that data is being written out of one block onto tape while at the same time data is being read into the other block from the ADC. The sequence of operations is that when a block becomes full, the tape transport is started and writing commences. After the block is written the tape transport is stopped to await filling of the other block. The procedure is repeated until an end-of-file (EOF) pulse is encountered on the BCU.

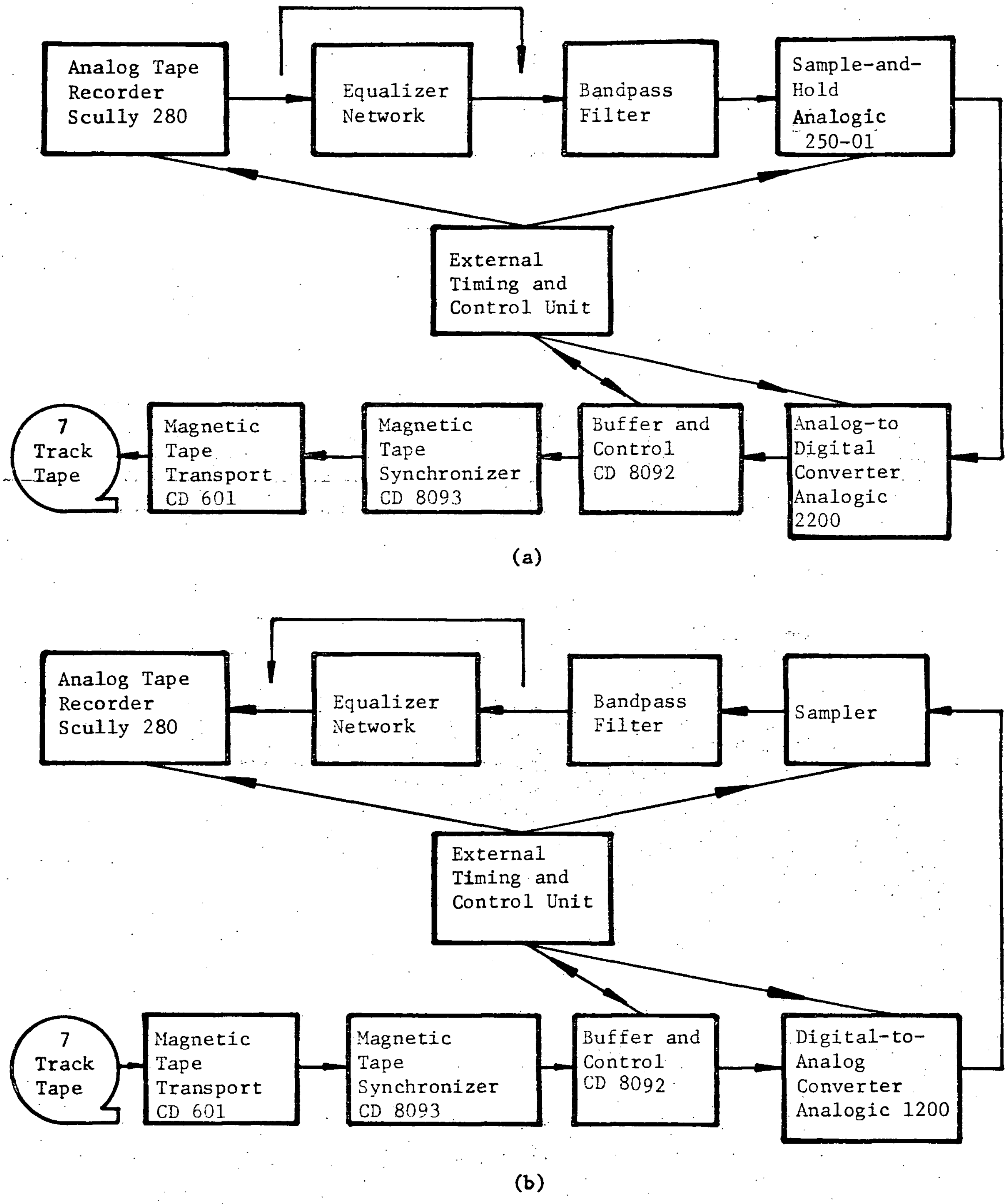

Fig. 14 Block diagram.
(a) Digital Recording System.
(b) Digital Playback System.

The tape synchronizer furnishes timing and control pulses to insure that the data are written on digital tape in proper format. Since the CD 601 is a 7 track tape drive, the five most significant bits of each sample are written in one tape byte and the remaining five least significant bits in the following byte. The sixth tape track is used to identify the most or least significant byte and the seventh track is reserved for a parity check bit. The tape speed and density are set at 37.5 inches/second and 556 bytes/inch, respectively.

Due to the relatively long memory cycle time of the CD 8092 (approximately 4 μsec), the maximum sampling rate is approximately 6500 samples per second. Speech experiments [41,42] have shown that such a limit imposes a constraint on the quality of speech that can be analyzed. Since a maximum sampling rate of 12 kHz is required for the simulation, the analog signal was recorded on the Scully 280 at 15 inches/second and played back at 7.5 inches/second when a sampling rate of greater than 6.5 kHz is required. This effectively doubles the actual sampling rate. To compensate mismatching of record and playback equalizers resulting from the difference in record and playback tape speeds, an external equalizer is used to smooth out the tape recorder frequency response.

The external timing and control unit (ETCU) starts and stops the analog tape recorder, supplies command pulses to the sample-and-hold (SH) and ADC, and EOF pulses to the BCU. Timing is under control of a Wavetek Model 111 signal generator whose frequency is adjusted to the desired sampling rate. Prior to digital recording, the analog tape is positioned so that the playback head on the tape recorder coincide with a visual mark on the tape. The mark is placed far enough ahead of the pre-recorded analog signal to allow the tape recorder to come up to full speed before the signal passes over the playback head. Once the analog tape is positioned, the tape recorder is started manually by operating a push button on the ETCU. Digital recording is delayed until the analog tape recorder reaches full speed. At the end of the delay, command pulses are automatically supplied to the SH and ADC to trigger analog-to-digital conversion. After a predetermined span of time corresponding to the length of the analog sample, an EOF pulse is automatically supplied to the BCU to terminate digital recording and a pulse applied to the analog tape recorder to stop playback.

Analog reconstruction of the digital samples is accomplished by the digital playback system shown in Fig. 14b. The filter passbands are the same as those used during digital recording. The ratio of sampling period to sampling interval is constrained to be greater than 10 in order to approximate the characteristics of impulse sampling. If the desired sampling rate exceeds 6.5 kHz, the actual sampling rate is set at one-half this value and the analog signal recorded at 7.5 inches/second and played back at 15 inches/second. The external equalizer is supplied to compensate mismatching of the tape recorder's internal record and playback equalizers.

Prior to digital playback, the 7 track digital tape is blocked into physical records consisting of 508 data samples and and EOF mark written to signify the end of the file. The blocks are separated by an interrecord gap of 0.75 inches to allow stopping and starting of the tape transport. The sequence of operation is initiated by loading the BCU with the first two data blocks read from digital tape. The analog tape recorder is then started manually by depressing a push button on the ETCU. After a sufficient time delay to allow the tape recorder to reach full speed, command pulses are supplied at the sampling rate to the BCU, digital-to-analog converter (DAC), and sampler to trigger the conversion of digital samples from the buffer into analog samples. Each time a buffer block is emptied, the tape transport is started and another data block is read from tape. When an EOF mark is encountered on tape, the entire buffer is emptied and an EOF pulse sent to the ETCU. The ETCU then stops the analog tape recorder.

5.3.2 Simulation Program

The PAM, PCM, and DPCM communication systems are simulated on a IBM System/360 Model 67 data processing system. Since the binary tape produced by the digital recording system is written in format which cannot be accessed directly by FORTRAN input/output statements, a preliminary conversion stage is required. A FORTRAN-callable subroutine in assembly language reads the 7 track tape and returns to the calling program a fixed-point number representing the decimal equivalent of the binary number that was written onto digital tape. The calling program blocks the data into physical records each containing 768 data samples, and writes the data onto 9 track tape using an unformatted WRITE statement. The 9 track tape is then used as the input tape for the simulation program written entirely in FORTRAN IV.

The communication systems simulated on the IBM/360 are shown in Fig. 15. Noise data previously recorded onto digital tape from a Grason-Stradler Model 4550 noise generator connected to a lowpass filter with cut-off frequency set at half the sampling rate is used to form the noise sequence $\{n_k\}$ in the PAM system of Fig. 15a. Multiplying the sequence by a scale factor gives the desired channel signal-to-noise ratio, S/N_oW_c, at the postfilter input. Signal power S is the prefilter output power and N_oW_c is the noise power. The logarithmic quantizers and linear predictor used in the PCM and DPCM simulations shown in Figs. 15b and c are designed in accordance with assumptions 3) to 5) of Section 5.2. Mapping of the quantizer

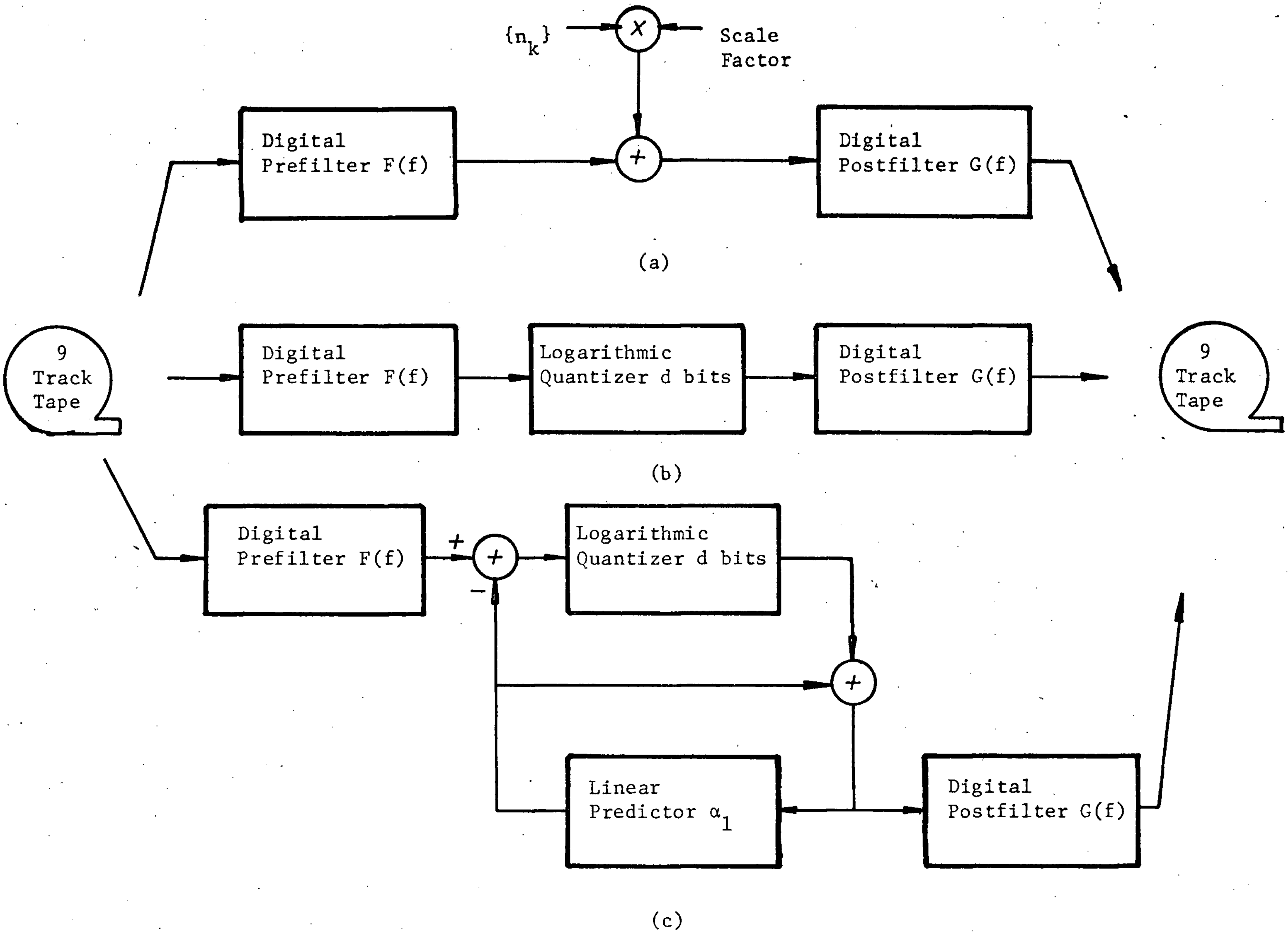

Fig. 15 Simulated communication systems.
(a) PAM.
(b) PCM.
(c) Previous-sample feedback DPCM.

input samples into the 2^d possible output levels is performed by a d-step successive approximation procedure.

Extensive literature has been published on the design of digital filters [53-57]. In this thesis, the method proposed by Helms [57] is followed for designing the digital pre and postfilters shown in Fig. 15. In the method, convolution of the desired frequency response with the Dolph-Chebyshev function is used to achieve nonrecursive (transversal) digital filters with the following desirable properties:

1) The desired frequency response can be specified numerically, graphically, or analytically.
2) The method allows nonrecursive filters to be designed to a specific resolution, defined as the bandwidth of the transitions between discontinuities in the desired frequency response, and to a specific ripple, defined as the maximum deviation from the desired frequency response for frequencies outside the transition regions.
3) The method tends to produce relatively good resolution for a given ripple and for a given number of coefficients used in specifying the impulse response on the nonrecursive filter.
4) The nonrecursive filter is easily implemented by using the fast convolution application of the fast Fourier transform [53,57-59].

The above method is applied to the design of nonrecursive filters which simulate the pre and postfilters specified in Table 5.1. Exception to the Table is made by modifying the frequency set Ω so for any band contained in Ω, the lower and upper cut-off frequencies, f_ℓ and f_u, are scaled to $1.07f_\ell$ and $f_u/1.07$, respectively. The scaled values correspond to the 3 dB cut-off frequencies used in the analog bandpass filters during digital recording (see assumption (10) in Section 5.2). Specifications used in the design were ripple equal to 0.1 percent and number of coefficients equal to 256. This resulted in a resolution of $(1.46/256)f_s \log_{10}(Q/.001)$ where f_s is the sampling rate and Q is the number of discontinuities in the desired frequency response. Implementation of the nonrecursive filters so designed is by the select-saving method of fast convolution [57,58].

Extensive literature on power spectra estimation has also been published [60-62]. The method used here for the estimation of power spectra follows closely that proposed by Welch [62]. The method involves sectioning the time series, taking modified periodograms of these sections, and averaging these modified periodograms. Dolph-Chebyshev window coefficients [57] and non-overlapping segments consisting of 256 samples each are used in the calculation of the modified periodograms. The autocorrelation function is estimated by computing the inverse Fourier transform of the power spectrum.

Computation of discrete Fourier transforms (DFT's) and inverse DFT's (IDFT's) in the above design, implementation, and estimation methods is performed using Cooley's FORTRAN IV subroutine [63] based on the fast Fourier transform (FFT) algorithm [59,61,64]. The FFT allows computationally efficient design and implementation of nonrecursive digital pre and postfilters, and provides computationally efficient estimation of power spectra and autocorrelation functions.

6. SUBJECTIVE EVALUATION OF PRE AND POSTFILTERS IN PAM, PCM, AND DPCM SPEECH COMMUNICATION SYSTEMS

6.1 Introduction

During the design, development, and testing of speech communication systems, there is a need for evaluation and for an optimization criterion. In the past, intelligibility has been utilized as the main criterion for the subjective evaluation of speech communication systems. However, since the intelligibility of speech output signals from modern communication systems is close to 100 percent, intelligibility alone as a measure of speech quality cannot suffice as a design criterion.

The concept of speech quality encompasses the total auditory impression of speech on a listener and not just its intelligibility aspect. Speech quality includes additional factors such as loudness, naturalness, clarity, speaker identifiability, timbre and rhythmic character, amplitude or time distortions, and many others. In general, quantitative evaluation of all these factors may be difficult or impossible. However, if certain assumptions on the psychological dimensions which characterize speech quality are made, speech quality can be described on the unidimensional scale, preference [65]. Preference as a parameter of speech quality is the attitude of a listener towards a speech signal when he compares it with a second speech signal and is, therefore, a relative measure of quality. The aspect of preference becomes dominant with respect to over-all speech quality when the following conditions are fulfilled, which is often true in many practical cases:

a) The intelligibility of speech is high.

b) The level of the speech signals is presented at optimum loudness, which is defined as the speech level at which a listener prefers to hear speech.

c) The recognizability of the speaker is of minor interest to the listener.

A method of subjective preference testing is described in Section 6.2 and the results of the subjective evaluation using the method is discussed in Sections 6.3 and 6.4.

6.2 Subjective Test Method

The subjective test method utilized in this study is similar to the isopreference method proposed by numerous investigators [65-68]. In the method, preference is evaluated by a forced pair-comparison test, and the results shown as isopreference (equal preference) contours on a sampling rate versus channel signal-to-noise ratio, or number of quantization bits, diagram. The quality rating assigned to each isopreference contour is the signal-to-noise ratio of a degraded speech signal which is subjectively equivalent to the reference signal associated with the isopreference contour [69]. An alternative quality scale obtained by the subjective estimate method [70] is also presented.

6.2.1 Speech Material, Equipment, Listeners, and Further Details on System Simulation

The speech material used throughout the study consists of the two sentences, "Joe took father's shoe bench out. She was waiting at my lawn". These sentences contain most of the phonemes found in English and have a power spectrum typical of conversational speech [71]. The sentences, spoken by a 31 year old male university professor with a Western Canadian accent, were recorded on a single-track Scully 280 tape recorder at 15 ips using an

AKG D-200E low impedance, cardioid microphone. The recording was performed in an Industrial Acoustics Company Model 1205-A quiet room. Additional speech material was not considered due to the prohibited amount of data processing involved.

Statistics on the spoken sentences were obtained using the digital simulation facilities described in Section 5.3. The effective bandwidth of the digitized spoken sentences was limited to 6 kHz. This was accomplished by reducing the Scully tape recorder to 7.5 ips, lowpass filtering at 3 kHz, and sampling at 6 kHz. Fig. 16a shows the amplitude probability density of the speech samples normalized relative to their RMS value. Also shown for comparison are the Laplacian distribution [45] and the Gamma distribution [72], which are often used as speech models. In Fig. 16b, the relative power spectrum of the digitized speech is presented. The method used for the power spectrum estimation has been described in Section 5.3.2. Also shown for comparison purposes is a relative speech spectrum from Benson and Hirsh [71]. Their spectrum represents the long-time average spectra of 90-second samples of technical and news material for five male speakers. Although the sentences used in this study represent only approximately 5 seconds of speech in real-time, Fig. 16 shows there is close enough agreement with published results to provide a representative sample which is typical of conversational speech.

Speech samples for the listening tests were obtained by:

a) digitally recording the analog recorder sentences (see Fig. 14a)

b) digitally simulating PCM, PCM, or DPCM communication systems (see Fig. 15), and

c) analog recording the processed sentences (see Fig. 14b).

Since the original speech signal is approximately lowpass with power density spectrum shown in Fig. 16b, the passband for the pre and post-

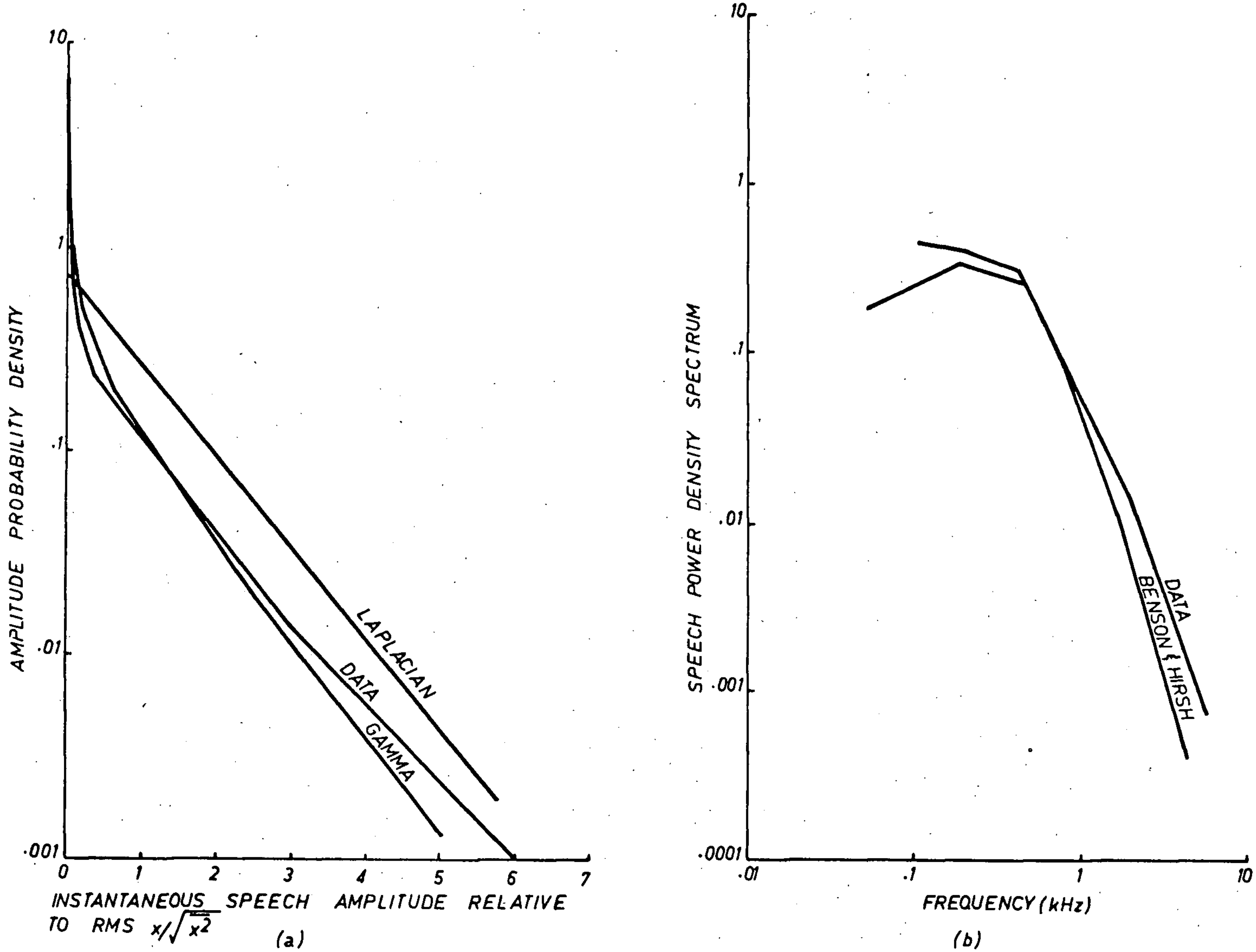

Fig. 16 (a) Normalized amplitude probability density of speech. Symmetrical average of positive and negative data.
(b) Power density spectrum of speech.

filters given in Table 5.1 is $\tilde{\Omega} \triangleq \{f: |f| < \frac{1}{2} f_s\}$, where f_s is the sampling frequency. (See Section 3.1.2 for definition of lowpass signal.) For such a frequency set Ω, the analog filters used in the digital recording and playback systems are lowpass with passband less then half the sampling rate (see Fig. 13). Furthermore, the digital filters used in the optimal prefilter-constant amplitude postfilter scheme are lowpass digital filters.

In step c), loudness was controlled by monitoring the record amplifier output of the Scully analog tape recorder, and adjusting the record level so the recorded speech samples sounded equally loud. It was shown that close agreement exists between the listeners' and the experimenter's judgment of equal loudness. Analog tapes for the listening tests were made by splicing the speech samples into the desired format.

All listening tests were conducted in a quiet room using Sharpe HA-10-MK II stereo headphones. External volume controls were provided with each headphone. Prior to each listening session, a pair of speech samples was played in order to allow the listeners to adjust their volume controls. During the course of the listening session the listeners were not allowed to readjust their loudness levels. The listeners were 17 male graduate students and staff members whose ages ranged from 21 to 41 years. The mean age was slightly over 25 years, and all except one listener was under 28 years. Only 16 of the 17 listeners were used on any one listening test. All listeners showed no hearing abnormalities and all had little or no previous experience in listening tests.

6.2.2 Determination of Isopreference Contours

Isopreference contours connecting points of equal subjective quality on a sampling rate versus channel signal-to-noise ratio plane are presented in Fig. 17 for PAM systems. Contours shown in Fig. 17a are for lowpass pre and postfilters (LPF) and Fig. 17b are for weak noise pre and postfilters (WNF). Similar isopreference contours on sampling rate versus number of quantization bits planes are presented in Figs. 18 and 19 for PCM and DPCM systems, respectively. Also shown are curves of constant channel capacity.

The isopreference contours were obtained from pair-comparison tests. For each of the 6 planes shown in Figs. 17, 18, and 19, a random sequence of approximately 96 pairs of speech samples were heard by each listener. Three listening sessions with 4 test runs per sessions were conducted during the course of a week.

A test run consisted of 48 paired comparisons and lasted about 15 minutes. After each test run, a rest period of approximately 5 minutes followed. No systematic variation of test results was detected due to listener fatigue in sessions of this duration. Prior to each listening session, the listeners read the following instructions.

> In this listening test you will hear pairs of speech signals. Each pair is separated by a 5 second silent interval. After listening to a pair, indicate in the appropriate column which speech signal of the pair you would prefer to hear. If both speech signals sound equally good, make an arbitrary choice. The first speech signal of each pair is designated as "A", and the second, as "B". The speech material used throughout the tests consists of the two sentences, "Joe took father's shoe bench out. She was waiting at my lawn".

Approximately 5 seconds were required to hear each speech signal and a 1 second interval separated each speech signal in the pair.

As an example of how the points in Figs. 17, 18, and 19 were ob-

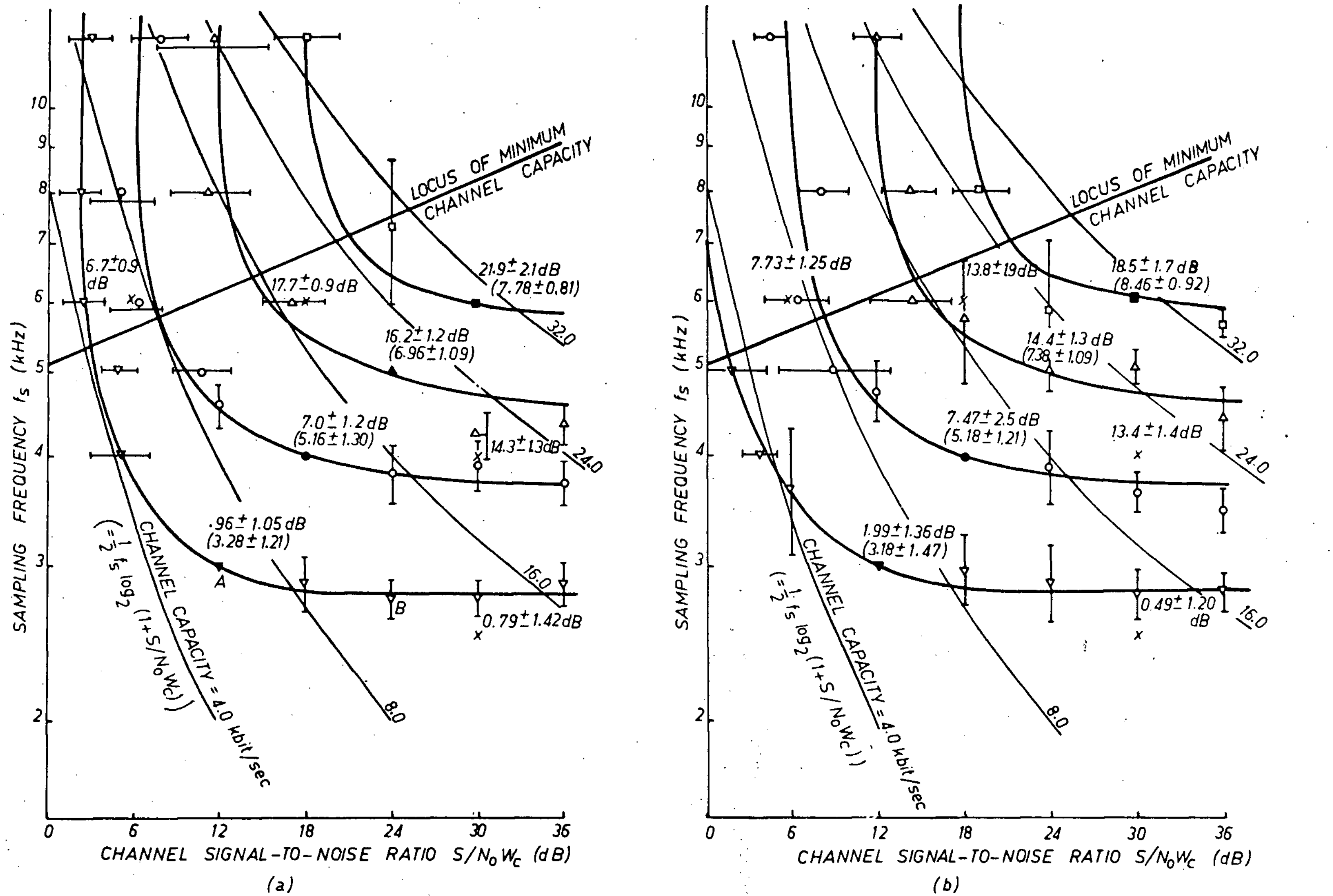

Fig. 17 PAM isopreference contours. Plus and minus standard deviations of each experimental point are denoted by the bar through the point. Reference points associated with each isopreference contour are drawn solid. $(S/N)_{subj}$ values are given in dB and Sc values are enclosed in brackets. The bandwidth of the pre and postfilter equals $f_s/2$.
(a) Lowpass filtering scheme (LPF).
(b) Weak noise filtering scheme (WNF).

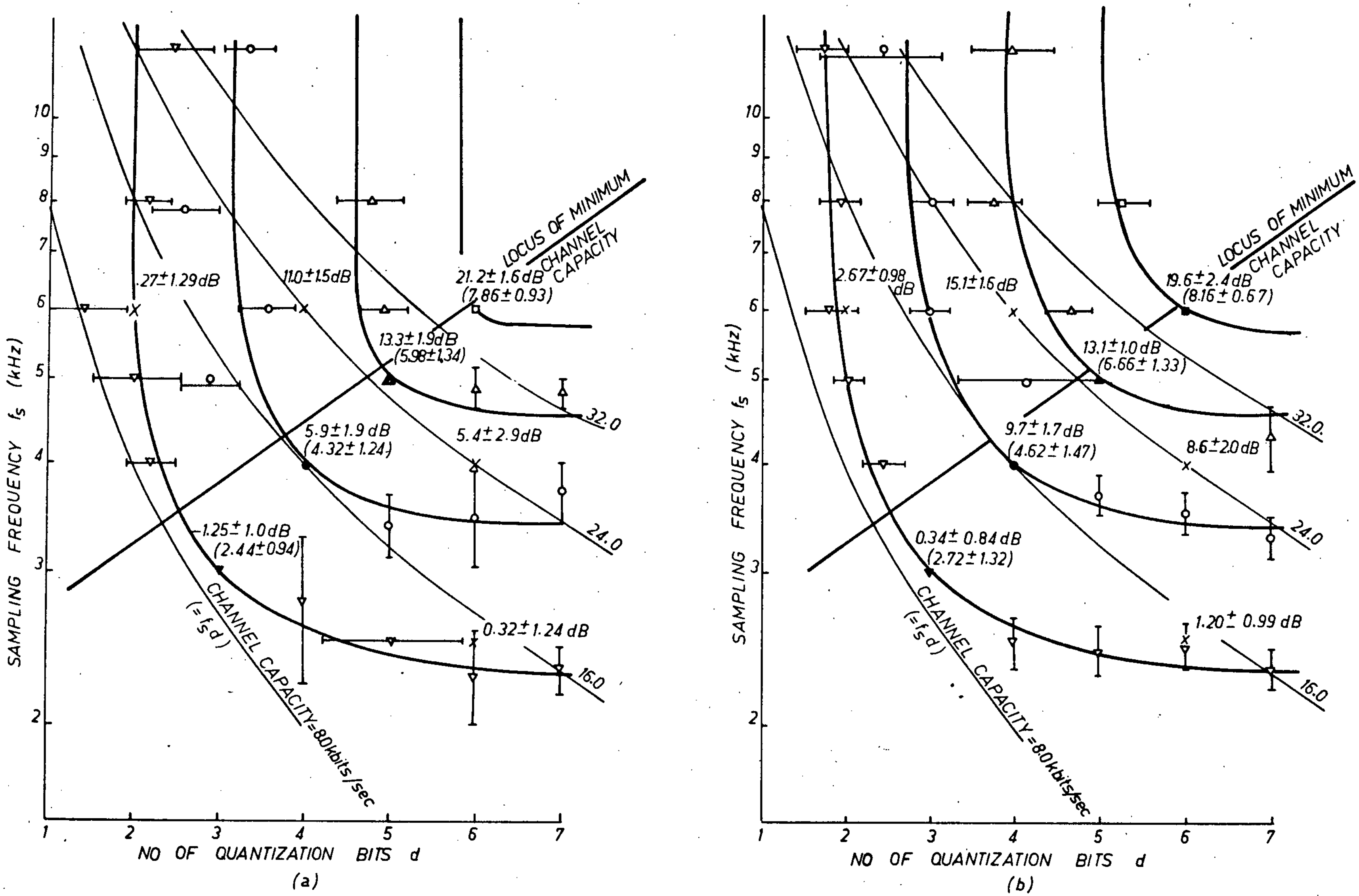

Fig. 18 PCM isopreference contours. See Fig. 17 caption for further comments.
(a) LPF.
(b) WNF.

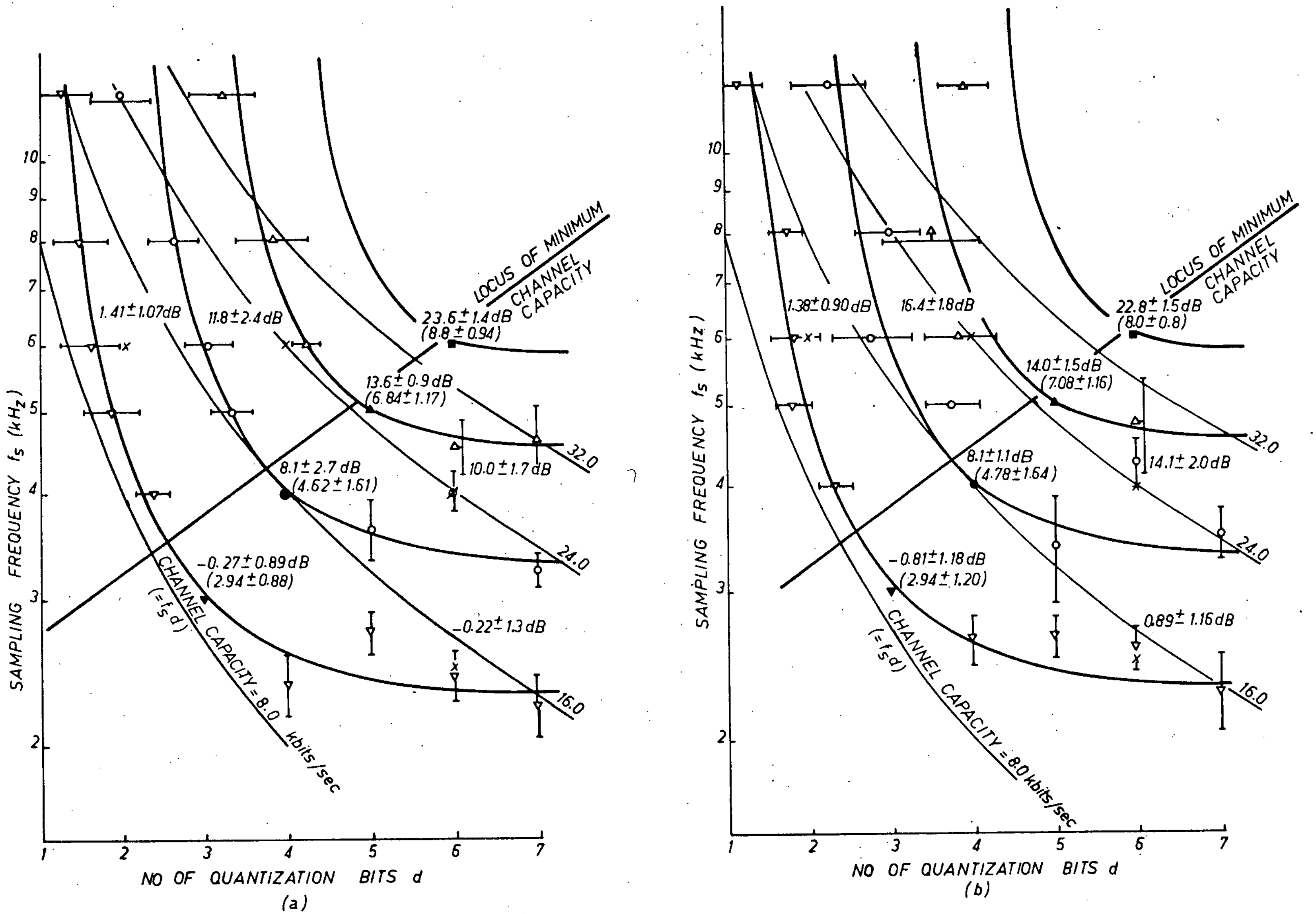

Fig. 19 DPCM isopreference contours. See Fig. 17 caption for further comments.
(a) LPF.
(b) WNF.

tained, consider points A and B in Fig. 17a. PAM LPF speech samples having f_s and S/N_oW_c values of point A were paired with four different PAM LPF samples having a S/N_oW_c of 24 dB, but different values of f_s. The ordinate of Fig. 20a shows the percentage of listeners who preferred A to the sample for which f_s was as defined by the abscissa. The range in f_s was chosen large enough so that the preference judgments would vary from 0 to 100 percent. From the psychometric curve drawn through the experimental points, the 50 percent point (2.76) was obtained. The corresponding abscissa value in Fig. 20a defines point B in Fig. 17a.

All other points hear the isopreference contour passing through reference point A were obtained by comparing speech samples corresponding to point A with other samples. The expected shape of the isopreference contour determined whether f_s or S/N_oW_c was constant for the samples being compared with those of point A. Other isopreference contours in Fig. 17a were obtained by an identical procedure, although a different reference point was used for each contour. The reference points are drawn solid in Fig. 17a. When it was expected that f_s was the main determinant of speech quality, S/N_oW_c was held constant and f_s varied, as in Fig. 20a. Thus, S/N_oW_c was held constant in the lower right region of each f_s-S/N_oW_c plane in Fig. 17, while f_s was held constant in the upper left region. Similarly, isopreference contours on f_s-d planes were obtained in Figs. 18 and 19 for PCM and DPCM systems.

In plotting all psychometric curves, it was found that normal distribution curves fitted all data points. For this reason, the proportion p_i of the listeners preferring the speech sample corresponding to the reference point was converted to unit normal deviates y_i, and a weighted least squares technique was used to fit a straight line to the data points. All p_i values of 0.00 and 1.00 were changed to 0.01 and 0.99, respectively, before conversion to y_i. The weight ω_i attached to each deviate y_i was given by

$$\omega_i = N_i e^{-y_i^2}/2\pi p_i(1-p_i)$$

where N_i is the number of judgments on which y_i is based. In our case $N_i=16$ for all i. The weight ω_i, which is proportional to the Muller-Urban weight, equals the reciprocal of the variance associated with y_i [73,74]. Fig. 20b shows the psychometric curve in Fig. 20a plotted in unit normal deviates. An indication of the goodness of fit of the straight line y=ax+b (y being the unit normal deviate and x being either f_s, S/N_oW_c, or d) to the data points was obtained by calculating $\gamma^2=\langle(a-a_1)^2\rangle/\sigma^2(a)$, where $\sigma^2(a)$ is the statistical deviation expected in a, and $\langle(a-a_1)^2\rangle$ is the mean squared error between the true coefficient a_1 and the fitted coefficient a[75]†. A value of γ significantly larger than unity implies that the function used in the least squares fit is incorrect††. For the psychometric curve in Fig. 20b, $\gamma=0.12$. For all psychometric curves used to obtain the isopreference points shown in Figs. 17, 18, and 19, $\gamma<1.96$.

The slope of the line in Fig. 20b equals $1/\sigma$, where σ is the standard deviation of the normal distribution curve fitted to the points. The standard deviation σ_I of the isopreference point is given by Culler's formula [73]

$$\sigma_I = \sigma/\left(\sum_{i=1}^{N} \omega_i p_i\right)^{1/2}$$

where N is the number of points fitted. The plus and minus standard deviation associated with each isopreference point is indicated in Fig. 17, 18, and 19.

---

†Alternatively, $\gamma^2=\langle(b-b_1)^2\rangle/\sigma^2(b)$, where b_1 is the true coefficient.

††If a (b) is normally distributed with mean a_1 (b_1) and variance $\sigma^2(a)$ ($\sigma^2(b)$), then γ^2 has a chi-squared distribution with one degree of freedom [76]. For a 95 percent confidence limit, the critical value of χ^2 is $\chi_c^2=3.84$, and the critical value of γ is $\gamma_c=\chi_c=1.96$.

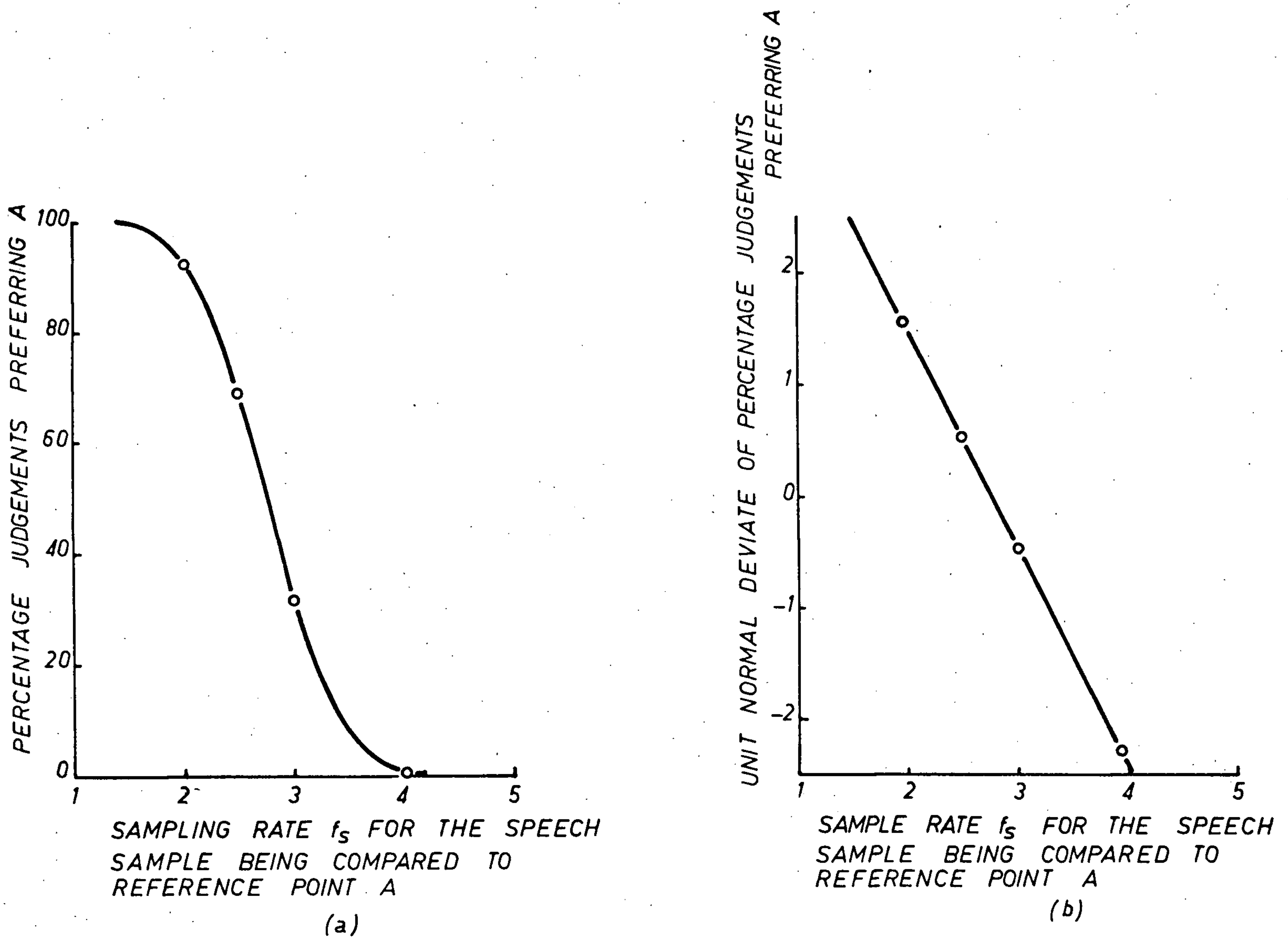

Fig. 20 Psychometric curve for obtaining isopreference point B in Fig. 17a.
Reference point is point A in Fig. 17a.
(a) Ordinate in linear preference units.
(b) Ordinate in unit normal deviates.

The isopreference curves, which are based on visual fits to the data points, were drawn close to points of small variance and were constrained to have the same general shape as the neighboring curves.

6.2.3 Scaling Isopreference Contours

It has been implied in the previous sub-Section that transitivity exists along an isopreference contour. That is, all speech communication systems defined by points on an isopreference contour will be equal in preference when compared directly with each other. Furthermore, if transitivity is assumed among planes defined by Figs. 17, 18, and 19, then scale values could be assigned to the isopreference contours that would identify and rank order them [66].

One method of selecting a set of numbers for a preference scale is to use an easily measurable physical characteristic of a family of continuously degradable standard reference signals. In this study, a family of reference signals which is easily generated by digital means and has a uniquely defined signal-to-noise (S/N) ratio is utilized. Such a family is defined by [69]

$$r_\alpha(t_k) = (1+\alpha^2)^{-1/2}\ [s(t_k) + \alpha \cdot n(t_k)]$$

where $n(t_k)=\varepsilon(t_k)\cdot s(t_k)$ is a noise process derived by multipling signal samples $s(t_k)$ by a zero mean discrete stochastic process $\varepsilon(t_k)= \pm 1$, which is uncorrelated with signal $s(t_k)$ and whose samples form a sequence of uncorrelated random variables. Parameter α determines the S/N ratio of $r_\alpha(t_k)$, that is, $S/N=\alpha^{-2}$. The scaling task is to determine in pair-comparison tests which of a one-parameter family of reference signals $r_\alpha(t_k)$ with different S/N ratios is equivalent in preference to the test speech signal. The S/N ratio of the isopreference reference signal is then attributed to the test signal as its subjective signal-to-noise ratio $(S/N)_{subj}$.

In the subjective evaluation, signal samples $s(t_k)$ are obtained by digitally recording "Joe....lawn". Lowpass filtering with an effective bandwidth of 4 kHz and sampling at an effective rate of 8 kHz were used. This is approximately the rate used in the Bell System voice frequency PCM system, T1 Carrier System [77]. Simulation of reference signals $r_\alpha(t_k)$ with α so varied that S/N= -9, -6, -3, 0, 3,...33 dB is performed in the IBM 360/67 computer using a pseudo-random number generator [78] to generate discrete samples $\varepsilon(t_k)$. Speech samples for pair-comparison tests are obtained using the digital playback system described previously.

In the listening tests, speech samples representing the simulated communication systems to be scaled are paired with the reference signals to form a random sequence. The listeners, test instructions, and psychometric method are identical to those used previously in Section 6.2.2. Two weeks separated these tests from the listening tests for determining isopreference contours. Two listening sessions were conducted during the course of a week. In the first session, 3 test runs consisting of 60 paired comparisons each were presented. In the second session, another 3 tests runs consisting of 60 paired comparisons were presented, along with an extra test run. This fourth run consisted of 48 pairs and was conducted to obtain an alternative quality scale. Further details are presented in the latter part of the Section.

The $(S/N)_{subj}$ and standard deviation of various points are indicated in Figs. 17, 18, and 19 in units of dB. Since transitivity is assumed, each isopreference contour is assigned the $(S/N)_{subj}$ value equal to the value of its reference point (the point drawn solid). Points designated by an "X" were used as a simple check on transitivity. The deviation in $(S/N)_{subj}$ values between the "X" point and the adjacent isopreference contours can be used as a measure to which the transitivity criterion is met. Taking into account the standard deviation associated with the $(S/N)_{subj}$ values, the results show approximately the correct rank ordering.

An alternative procedure, which is based on the subjective estimate method [70] and similar in principle to the category-judgment method [68,70] commonly used in the over-all rating of telephone systems, is presented for obtaining a quality scale. The procedure is divided into two phases, familiarization and evaluation. In the familiarization phase, a point of reference for listeners' responses is established by presenting a pair of reference signals which are representative of the extreme points on the quality scale. This is commonly known as "anchoring". A subjective scale value of 0 is assigned to speech samples which are just unintelligible and a value of 10 is assigned to 6 kHz lowpass speech samples. Since the evaluation test was the fourth test run in the final listening session for determining subjective S/N ratios, it was not deemed necessary to orient the listeners to the range of qualities to be encountered in the evaluation phase. Prior to the evaluation test the listeners heard a sample representative of the upper anchor point, 6 kHz lowpassed speech, and was told the samples heard in the first 3 test runs were representative of the speech samples to be evaluated. In an effort to provide a lower anchor, it was suggested to the listeners that some of the samples heard in the previous test runs could quite possibly be assigned 0 scale values. The experimenter was referring specifically to the standard reference signals having S/N ratios of -9 and -6 dB.

In the evaluation phase, the test samples to be scaled were paired with the 6 kHz lowpass reference samples and presented to the listeners in a random sequence. Each test sample was evaluated twice by the 16 listeners; once when the pair consists of test sample followed by reference sample, and once when the pair order is reversed. Reference samples were interspersed so as to refresh the listeners of the standard of reference. Prior to the evaluation test, the listeners read the following instructions.

> In this listening test you will hear pairs of speech signals. Each pair is separated by a 5 second silent interval. If a speech signal which is JUST UNINTELLIGIBLE has a scale value of 0, and one of the speech signal of the pair ("A" or "B") has a scale value of 10, how would you rate the other speech signal of the pair on an equal half-interval scale, that is, 0,0,5,1.0,...,9.5,10? The speech signal which has a scale value of 10 is indicated by the number "10" in column "A" or "B", depending on whether the first or the second speech signal of the pair has the scale value of 10. Indicate your scale value in the appropriate blank space provided. The speech material used throughout the test consists of the two sentences,
> "Joe took father's shoe bench out. She was waiting at my lawn".

The scale values Sc of each test sample was obtained by averaging the 32 ratings of the 16 listeners. The standard deviation was also computed. The scale value and standard deviation of the reference points associated with each isopreference contour are shown in Figs. 17, 18, and 19. These values are enclosed in brackets to distinguish them from their corresponding $(S/N)_{subj}$ values.

6.3 Further Results and Discussion of Subjective Evaluation

Inspection of each of the planes defined in Figs. 17, 18, and 19 shows that points on the isopreference contours which are representative of the communication systems requiring the least channel capacity for a given speech quality lie approximately along a straight line. Lines of minimum channel capacity are fitted to these points by visual examination.

In Fig. 21, subjective ratings for the PAM LPF and WNF, PCM LPF and WNF, and DPCM LPF and WNF isopreference contours shown in Figs. 17, 18, and 19, respectively, are plotted versus their associated minimum channel capacity, defined as the point of intersection of the locus of minimum channel capacity with the isopreference contour. Subjective scale $(S/N)_{subj}$ is used in Fig. 21a, and Sc is used in Fig. 21b. Some of the data points have been slightly displaced horizontally in order to represent the plus and minus standard deviation of the point. Their actual abscissa values are designated by "X"'s on the curves fitted to the points. If there is only one "X" in a cluster of data points, then all points have a common abscissa value. One curve is drawn through the PAM LPF and PAM WNF points since the points are not sufficiently separable in view of their overlapping standard deviations. Similarly, only one curve is fitted to the PCM LPF, PCM WNF, DPCM LPF, and DPCM WNF points. In Fig. 21a, the points were fitted by straight lines, whereas in Fig. 21b, the points were approximated by normal distribution curves. In relation to the range of subjective scale values spanned by the points in Fig. 21, note the appreciably larger standard deviations associated with the points in Fig. 21b when compared with those of Fig. 21a. This is to be expected since the subjective estimate method is very strongly influenced by the variety and variability of the listeners. Furthermore, comparison of the PAM curve and the PCM-DPCM curve shows that over the quality range tested, PAM communication systems operating with f_s and S/N_oW_c values defined by the loci of minimum channel capacity in Fig. 17 achieve a given speech quality at a capacity which is less than that achieved by PCM and DPCM systems operating with f_s and d values defined by the loci of minimum channel capacity in Figs. 18 and 19.

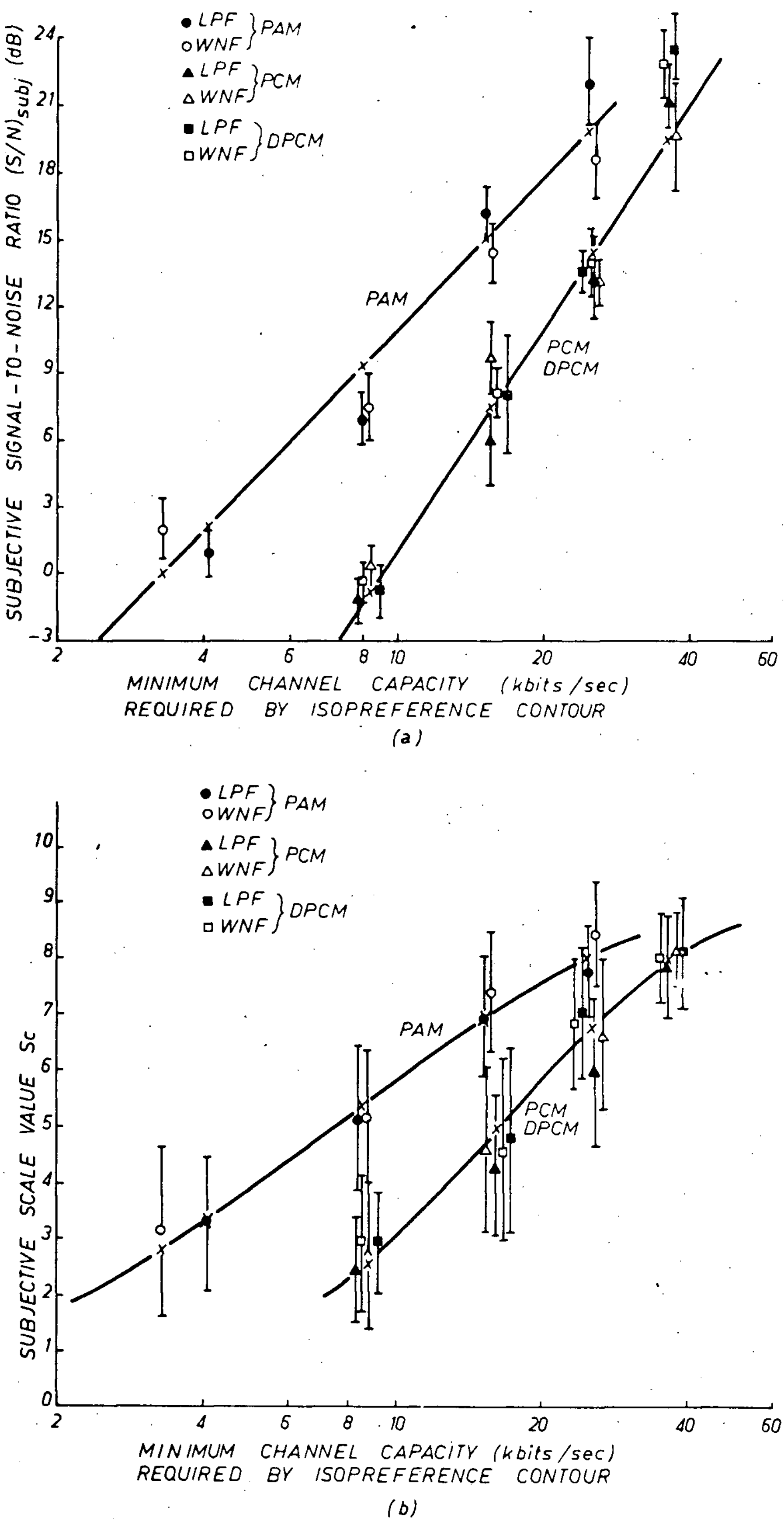

Fig. 21 Quality rating os isopreference contours shown in Fig. 17, 18, and 19 versus their corresponding minimum channel capacity.
(a) Subjective scale in $(S/N)_{subj}$.
(b) Subjective scale in Sc.

The relation between $(S/N)_{subj}$ and Sc is given in Fig. 22. This was obtained by plotting $(S/N)_{subj}$ versus Sc for each reference point (points drawn solid) shown in Figs. 17, 18, and 19. As expected by eliminating the common axis, channel capacity, in Figs. 21a and 21b, the normal distribution curve also fits the points.

For purposes of comparison, the isopreference contours shown in Figs. 17a and 17b are redrawn in Fig. 23a, and those in Figs. 18a, 18b, 19a, and 19b are redrawn in Fig. 23b. The $(S/N)_{subj}$ and Sc values attached to the isopreference contours are obtained from Fig. 21 and represent values which were derived by smoothing the original ratings of the isopreference contours of Figs. 17, 18, and 19. These values are given by the ordinates of the "X" points in Fig. 21. Also redrawn are the curves of constant channel capacity and the lines of minimum channel capacity.

All isopreference contours in Fig. 23 display the same general behaviour. As S/N_oW_c (d) increases along a line of constant f_s, a region is reached in which continued increase in S/N_oW_c (d) does not yield any significant improvement in quality. In this region, quality is limited by speech bandwidth. Similarly, as f_s is increased along a line of constant S/N_oW_c (d), a region is reached in which further increase in f_s results in little improvement in speech quality. In this region, transmission (quantization) noise limits quality.

Comparison of LPF and WNF isopreference contours shows that only in the noise-limited region does weak noise filters have any effect on subjective performance. An explanation follows. For a given f_s weak noise filters and lowpass filters have identical passbands; so when speech bandwidth is the main factor limiting quality, LPF and WNF isopreference contours converge. In the filter passband, however, weak noise filters have frequency character-

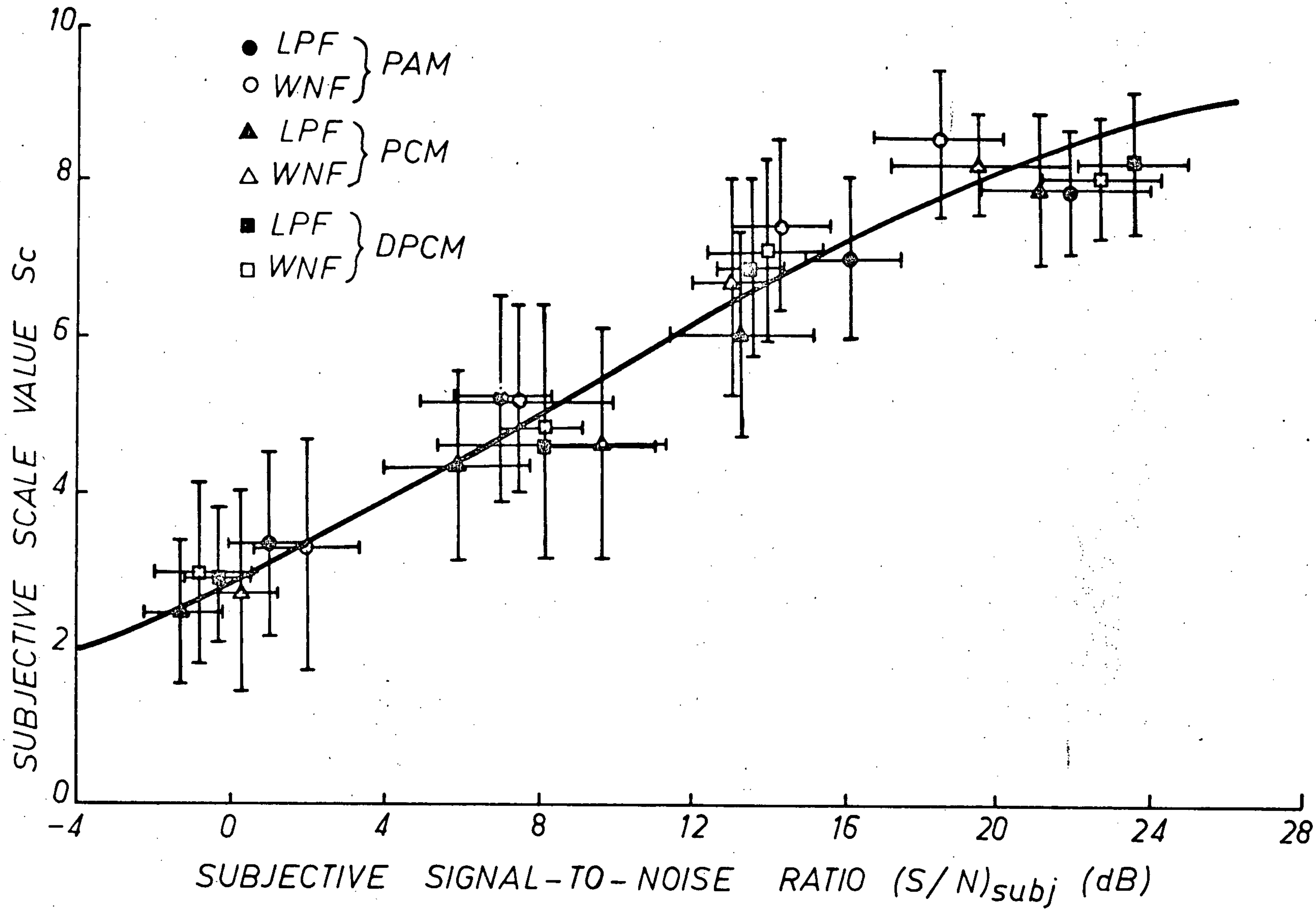

Fig. 22 Relation between scale value Sc and subjective signal-to-noise ratio $(S/N)_{subj}$.

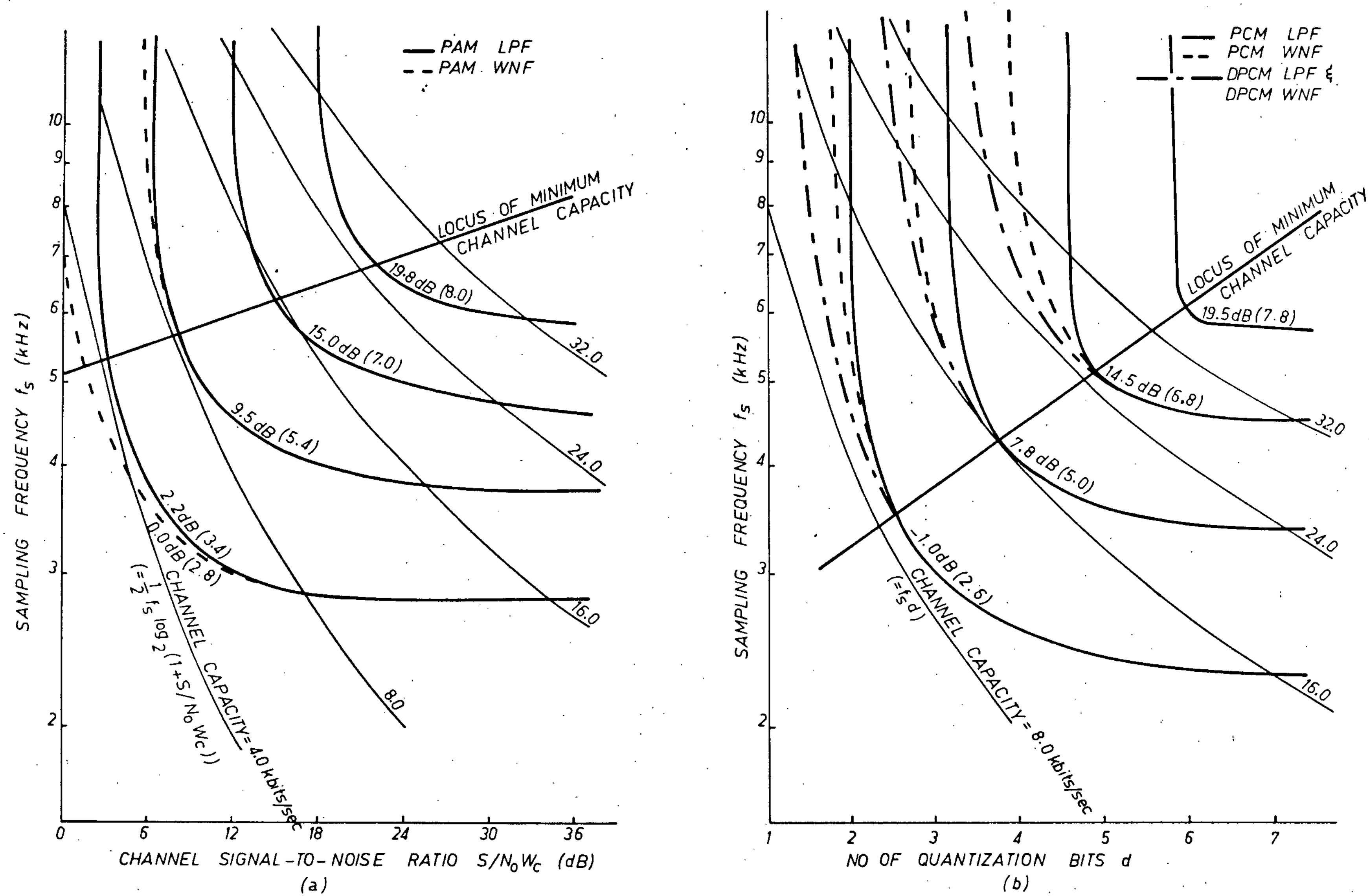

Fig. 23 Isopreference contours with quality ratings derived from the curves fitted to the raw data in Fig. 21. $(S/N)_{subj}$ values are in dB and Sc values are enclosed in brackets.
(a) PAM.
(b) PCM and DPCM.

istics which are "best" suited to minimize noise. Hence, when inband noise is the main factor limiting speech quality, weak noise filters may improve the subjective preformance of the communication system. The improvement, if any, is shown in the upward roll-off sections of the isopreference contours. The roll-off in WNF contours is less steep in comparison to LPF contours.

The subjective performance of PAM communication systems is shown in Fig. 23a. Over the range of f_s and S/N_oW_c considered, the improvement in speech quality afforded by the use of weak noise pre and postfilters is negligible in comparison to the performance achieved by lowpass filters. This can be seen by comparing the isopreference contours of the two filtering schemes. Note that the high quality PAM LPF and PAM WNF contours are identical in shape and rating, whereas, only a slight discrepancy exists between low quality PAM LPF and PAM WNF contours.

In Fig. 23b, the subjective performance of PCM and DPCM systems is shown. In the region below and to the right of the locus of minimum channel capacity, PCM LPF, PCM WNF, DPCM LPF, and DPCM WNF isopreference contours are identical both in form and subjective rating. In this region where speech bandwidth limits quality, speech quality is essentially independent of the type of communication system (PCM or DPCM) and of the choice of filtering scheme (LPF or WNF), but only essentially dependent on the system bandwidth. This follows from the fact that the differential aspect of DPCM and the spectral-shaping of WNF only affect the inband distortion and not the out-of-band distortion which arises from bandlimiting. Furthermore, if PCM and DPCM systems are operated along the locus of minimum channel capacity, then the channel capacity required by each system to achieve a given speech quality is identical for PCM LPF, PCM WNF, DPCM LPF, and DPCM WNF systems (also see Fig. 21). The DPCM LPF and DPCM WNF contours are also identical in form and subjective rating. Weak noise filters, on the otherhand, can improve the subjective performance of PCM systems in the region which is above and to the left of the line of minimum channel capacity. Comparison of PCM LPF and PCM WNF contours shows that in this region weak noise filters may reduce by almost one bit the number of quantization bits required to achieve a given speech quality. This bit reduction with respect to PCM LPF systems, however, is less than that achieved by DPCM systems.

In retrospect, a heuristic explanation for the relative subjective behaviour of WNF systems with respect to LPF systems can be postulated from the objective results of Chapter 4. Let the speech signal, defined by the statistics given in Fig. 16, be approximated by a stationary Gaussian signal with first-order Butterworth spectrum

$$\Phi_x(f) = \sigma a/[\pi(f^2 + a^2)] \tag{74}$$

where a = 600 Hz. If the input speech signal to the LPF and WNF systems simulated in Chapter 5 is assumed to have these statistical properties, then the objective results for the PR (optimal prefilter-constant amplitude postfilter) and the 0 (optimal pre and postfilters) systems discussed in Chapter 4 are indicative of the objective performance that could be achieved by LPF and WNF speech communication systems.

Fig. 5 shows the inband signal-to-noise ratio (SNR) defined by equation (53) for PAM PR and PAM 0 systems. The objective advantage gained by using optimal pre and postfilters can be expressed in terms of the signal-to-noise improvement factor SNRIF, which is simply the ratio of SNR achieved using 0 filters over the SNR achieved using PR filters. Note from Fig. 5 that SNRIF is an increasing function of W_c/a. The maximum W_c/a considered in the subjective investigation of PAM is $W_c/a]_{max} = f_s]_{max}/2a = 12000/(2 \cdot 600) = 10$.

Fig. 5 shows that for $W_c/a \leq 10$, the SNRIF ≤ 1.6. Since such a relatively small improvement in SNR can be achieved by WNF systems, only slight subjective differences are expected between PAM LPF and PAM WNF systems. Examination of the isopreference contours shown in Fig. 23a suggests that such is the case.

In Fig. 9, the SNR for PCM systems are presented. Although digital channel errors are taken into consideration in the analysis, system performance approaches the error-free case when S/N_oW_c becomes large and exceeds the threshold point on the SNR curve. Fig. 9 shows that for error-free transmission, the difference in inband signal-to-noise ratio SNR between the PR and 0 curves is small when $W_c/a \cong 10$. However, if the W_c/a of the PCM system is increased to 100, the SNRIF ≤ 3. The exact value is dependent on the number of quantization bits d used in the PCM system. For the systems simulated here, values of $W_c/a = f_s d/2a$ ranging up to 70 is used. Interpolating the results shown in Fig. 9, values of SNRIF up to approximately 2 would apply in the simulation. Based on these objective results, subjective performances of PCM LPF and PCM WNF are expected to be moderately different. Fig. 23b shows the PCM LPF and PCM WNF isopreference contours. Note the moderately large deviation between the LPF and WNF contours in the upper left region of the f_s-d plane.

In Fig. 10b, ε/σ is shown for DPCM. The over-all distortion ε/σ, due to inband noise and filtering error, for both PR and 0 systems are the same which indicates that whatever redundancy reduction is not done by the prefilter will be done by the differential aspect of the DPCM system. Hence, the subjective performance for DPCM LPF system is expected to be the same as for the DPCM WNF system. Fig. 23b shows that such is the case.

Since digital computer simulations of PAM and suppressed-carrier, amplitude modulation (AM/SC) systems are identical, the subjective results for PAM can also apply to AM/SC. Sampling rate f_s must be interpreted as twice the bandwidth W_b of the baseband speech signal and S, as the average transmitted power. For single sideband (SSB) AM/SC, $W_c = W_b$, whereas for double sideband (DSB) AM/SC, $W_c = 2W_b$. Hence, in Figs. 17 and 23, f_s must be replaced by $2W_b$, and the values for the constant channel capacity curves must be left unchanged for SSB AM/SC, but doubled for DSB AM/SC. Also in Fig. 21, the abscissa must be scaled by a factor of 2 when the PAM curves are used to represent DSB AM/SC subjective performance.

6.4 Concluding Remarks

6.4.1 Summary and Comparison with Previous Works

Results of the present evaluation show the effects of two filtering schemes, namely, lowpass filtering (LPF) and weak noise filtering (WNF), on speech quality in PAM, PCM, and DPCM communication systems. Subjective effects of sampling rate f_s and channel signal-to-noise ratio S/N_oW_c in PAM systems, and subjective effects of sampling rate and number of quantization bits d in PCM and DPCM systems are also considered in addition to the effects of filtering. It was observed that no significant subjective differences exist between PAM LPF and PAM WNF systems for all f_s and S/N_oW_c considered in the simulation. Also, no significant differences exist between DPCM LPF and DPCM WNF systems. For PCM LPF and PCM WNF, however, significant differences in subjective performance can exist. It was shown that such subjective behaviours can be heuristically explained using the objective results of Chapter 4.

A measure of confidence in the subjective results can be obtained by plotting the subjective signal-to-noise ratio $(S/N)_{subj}$ or the scale value Sc of all isopreference contours shown in Fig. 23 versus their corresponding saturating f_s values. If all points lie approximately on the fitted curve irregardless of whether the points are representative of PAM LPF, PAM WNF, PCM LPF, PCM WNF, DPCM LPF, or DPCM WNF systems, then the credibility of the subjective results is suggested. This follows from the fact that when the isopreference contours in Fig. 23 saturate horizontally, the type of communication system (PAM, PCM or DPCM) and the choice of filtering scheme (LPF or WNF) are irrelevant factors in determining speech quality. In this saturation region, speech quality is, in effect, solely dependent on the bandwidth of the system (equal to $\frac{1}{2}f_s$). Fig. 24 shows $(S/N)_{subj}$ and Sc versus the saturating f_s. Examination reveals that all points lie close to the fitted curve, thereby implying the credibility of the subjective results. The saturating f_s values used in Fig. 24 correspond to the ordinate values of the isopreference contours in Fig. 23 when a S/N_oW_c abscissa value of 36 dB is used for PAM, and when a d abscissa value of 7 bits is used for PCM and DPCM. At these abscissa values the isopreference contours are approximately flat.

PAM (actually AM/SC) LPF, PCM LPF, and DPCM LPF speech systems have been considered in previous subjective investigations [41,42]. In the previous works, it was suggested that DPCM LPF systems were unconditionally superior to PCM LPF systems. The present work, shows that DPCM LPF systems, properly designed, will always be at least as good as PCM LPF systems, and that under certain conditions DPCM LPF systems may be superior to PCM LPF systems. When PCM LPF and DPCM LPF systems are compared with regards to minimum channel capacity required to achieve a certain speech quality, PCM LPF and DPCM LPF appear to be subjectively equivalent (see Figs. 21 and 23b). On the otherhand, when the systems are operated "nonoptimally", that is, off the line of minimum channel capacity, DPCM LPF systems may yield better

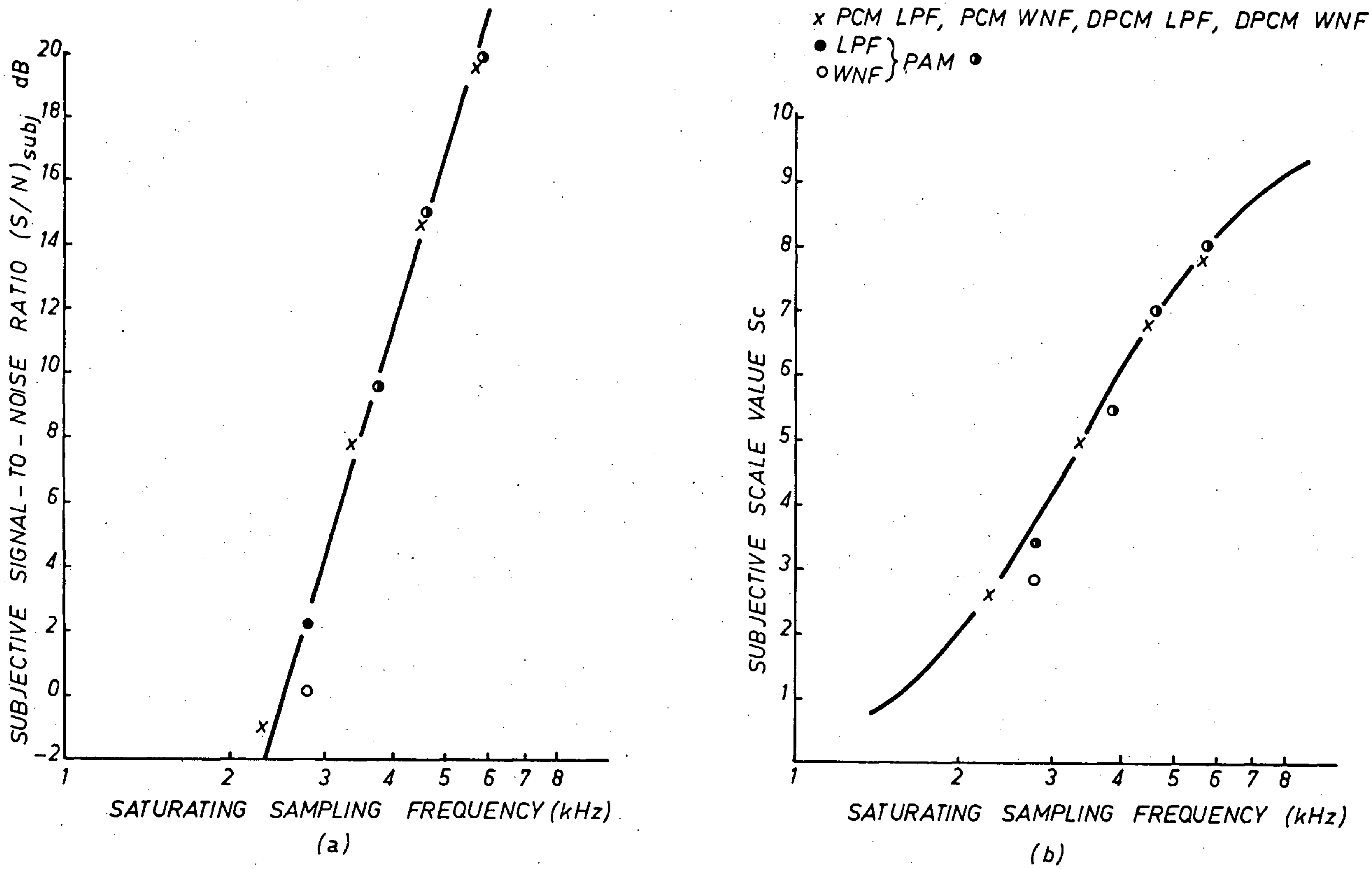

Fig. 24 Quality rating of isopreference contours versus the isopreference contour saturating values of sampling rate f_s.
(a) Subjective scale in $(S/N)_{subj}$.
(b) Subjective scale in Sc.

performance. In particular, for systems operating in the upper left region of the f_s-d plane shown in Fig. 23b, DPCM LPF systems require a lower channel capacity to achieve a certain quality than do PCM LPF systems. There is agreement with previous work [42] that SSB AM/SC LPF systems can be superior to both PCM LPF and DPCM LPF systems when the channel capacity required by the systems is low, say less than 40 kbits/sec. This can be seen in Fig. 21.

Since the speech material and subjective testing methods used in the investigations are similar, the discrepancy may be attributed partly to the variety and variability of the listeners, and partly to the differences in equipment and methods used in generating the speech samples. In the present investigation, a better microphone was used to record the original speech sample; a better analog tape recorder was used to record the play the speech samples; and finally, better headphones were used in the listening tests. Furthermore, a digital computer was used to simulate the various communication systems considered in this study, whereas previous investigations were performed in real-time using hardware models of the AM, PCM, and DPCM systems. The problems of drift, sensitivity, and component tolerances inherent in hardware models, but eliminated in digital computer simulation, introduce additional inband noise to the existing inband quantization noise which is designed into PCM LPF and DPCM LPF systems. This additional noise prolongs the saturating effect of inband noise on speech quality and partially nullifies the predominant effect of bandwidth on speech quality in the bandwidth-limited saturation region of the isopreference contours. Furthermore, the added presence of inband noise on speech quality has the tendency to make DPCM LPF systems appear unconditionally superior to PCM LPF systems since the inband noise reduction capability of DPCM LPF systems has greater influence over a larger portion of the isopreference contour. Comparison of the PCM LPF and DPCM LPF isopreference contours in Fig. 23 with previous work [41] shows that the isopreference contours obtained previously saturate from inadequate speech bandwidth much less abruptly than those of the present investigation. This suggests the presence of unwanted inband noise in the previous work, and suggests uncertainty in the previously reached conclusion that PCM LPF systems are unconditionally superior to PCM LPF systems.

6.4.2 Subjective Weighting Function for Speech

Extensive subjective testing was mandatory in this investigation because an objective measure of over-all speech quality from physical parameters of the communication systems was not available. It is tempting, therefore, to try to find a mathematically tractable evaluation criterion for speech which is based on physically measurable quantities of the speech communication system alone, and which nevertheless agrees with subjective measurements. One such objective measure is the frequency weighted mean-integral-squared error criterion (see Fig.1)

$$\mathrm{WMSE} = \int_{-\infty}^{\infty} \Phi_e(f)\,|W(f)|^2\, df \tag{75}$$

where $\Phi_e(f)$ is the power density spectrum of the error signal, and weighting function $W(f)$ represents the relative sensitivity of human auditors to error at that frequency. The underlying basis behind (75) is the tacit assumption that the subjective effect of the error signal is additive in power. The feasibility of the WMSE criterion has been demonstrated in the design of PCM noise-feedback systems for still monochrome television pictures [23].

Since all communication systems which are represented by points on an isopreference contour are subjectively equivalent, an objective measure of speech quality must yield the same figure of merit for all systems on the contour. Furthermore, the figure of merit should increase as isopreference contours of increasing quality are considered. When the objective measure is the WMSE criterion, weighting function W(f) must be chosen such that the WMSE is constant along an isopreference contour, and the WMSE must increase as isopreference contours of higher quality are considered. The physical parameters that were varied to obtain the isopreference contours in the PAM systems were sampling rate f_s and channel signal-to-noise ratio S/N_oW_c. In PCM and DPCM systems, the parameters were f_s and number of quantization bits d. Since the passband of the pre and postfilters is a function of f_s and since transmission noise and quantization noise are functions of S/N_oW_c and d, respectively, the planes defining the isopreference contours may be interpreted as planes of out-of-band filtering error versus inband noise. Therefore, an indication of the relative importance of out-of-band filtering error and inband noise on speech quality can be obtained from the isopreference contours shown in Fig. 23. Over part of the contour (horizontal), filtering error is the main determinant on speech quality, and over the other part (vertical), inband noise is the main determinant.

In an attempt to satisfy the constant WMSE condition over the entire isopreference contour, let $\Phi_e(f)$ include out-of-band, as well as inband error. Therefore, W(f) must not only take into consideration subjective effects of inband noise, but also speech bandwidth. However, because of the saturating effect of filtering error and of inband noise on speech quality, the only solution for W(f) is the trivial one, W(f)=0 for all frequency f. The trivial solution suggests that the subjective effect of filtering error and inband noise is not additive, and indicates the inadequacy of the WMSE criterion as an objective measure of speech quality.

The trivial solution can be seen by considering the PAM LPF isopreference contours shown in Fig. 23a. Note that as S/N_oW_c is increased beyond approximately 18 dB, the lower quality isopreference contour remains constant at $f_s \cong 2.8$ kHz. If A and B are any two different points in this saturating portion of the contour, then $W(f)$ must satisfy

$$\int_{-\infty}^{\infty} \Phi_{\tilde{e}A}(f)\,|W(f)|^2\,df = \int_{-\infty}^{\infty} \Phi_{\tilde{e}B}(f)\,|W(f)|^2\,df \tag{76}$$

where $\Phi_{\tilde{e}A}(f)$ and $\Phi_{eB}(f)$ are the error spectra associated with PAM LPF systems represented by points A and B, respectively. Since the cutoff frequencies of the lowpass filters are $W_b=\frac{1}{2}f_s=1.4$ kHz, and since additive white Gaussian noise comprises the inband noise

$$\Phi_{eA}(f) = \begin{cases} \Phi_x(f) & , |f| \geq W_b \quad \text{filtering error} \\ y_A & , |f| < W_b \quad \text{inband noise} \end{cases} \tag{77a}$$

$$\Phi_{eB}(f) = \begin{cases} \Phi_x(f) & , |f| \geq W_b \quad \text{filtering error} \\ y_B & , |f| < W_b \quad \text{inband noise} \end{cases} \tag{77b}$$

Substituting (77) into (76) yields

$$y_A \int_{-W_b}^{W_b} |W(f)|^2\,df = y_B \int_{-W_b}^{W_b} |W(f)|^2\,df \tag{78}$$

However, since points A and B represents PAM systems with different $S/N_oW_c, y_A \neq y_B$. Hence, the only solution to (78) is $W(f)=0, |f|<W_b$. Solution $W(f)=0$ for all f follows by application of the same arguments to isopreference contours of higher quality. Note that for these contours, f_s saturates at higher values, thereby yielding higher values of W_b.

6.4.3 Application to Television Signals

Computer simulations and subjective evaluation of pre and postfilters in PAM, PCM, and DPCM speech communication systems have demonstrated the usefulness of the analytical results in Chapter 4 in interpreting the relative subjective behaviour of communication systems. The signal-to-noise ratio improvement factor SNRIF, which is simply the ratio of SNR's for systems using optimal pre and postfilters (0) and systems using optimal prefilter-constant amplitude postfilter (PR), was shown to be a reasonable indicator of the relative subjective advantage which may be gained by using optimal pre and postfilters. For a SNRIF value close to unity, small differences in speech quality was observed between communication systems using WNF and systems using LPF. Values of SNRIF appreciably greater than unity implies that the subjective advantage to be gained in using weak noise filters may be significant.

Picture quality, like speech quality, cannot be judged by an objective measure alone. However, by analogy with the speech problem, an indication of the relative subjective performance between video systems using WNF and systems using LPF can be obtained from the analytical results of Chapter 4. The envelopes for the power spectral density of Picturephone† (PP) signals and standard broadcast television (BCTV) signals have approximately first-order Butterworth spectra (73) with corner frequencies at 15 kHz and 49 kHz, respectively [79]. In addition, PP signals are normally bandlimited to 375 kHz, and BCTV signals are approximately bandlimited to 4.5 mHz. Hence, for PP signals transmitted by PAM systems, $W_c/a]_{PP}=375/15=26$ and from interpolation of the results shown in Fig. 5, SNRIF$\cong$2. For such a value of SNRIF, only a moderate improvement in picture quality is expected from PAM systems which use weak noise filters to pre and postfilter Picturephone signals. For BCTV the parameter $W_c/a]_{BCTV}=4500/49\cong 90$, and from Fig. 5, SNRIF$\cong$5. Such a

---

†Picturephone® is a low bandwidth television system of the Bell System.

large value of SNRIF implies that a large subjective advantage can be gained by using WNF to pre and postfilter BCTV signals for PAM transmission. In PCM systems, $W_c/a]_{PP}$=375d/15=26d and $W_c/a]_{BCTV}$=4500d/49≅90d where d is the number of quantization bits used in the PCM video communication system. For typical values of d, approximately 4 to 8, PP SNRIF≅4, and BCTV SNRIF≅10. These values suggest that a large subjective advantage is possible by filtering PCM video signals with WNF. On the other hand, because of the efficient redundancy reduction aspect of DPCM systems, no improvement in picture quality is expected from DPCM video systems using WNF instead of LPF.

In general, SNRIF values for systems transmitting video signals are significantly larger than the corresponding values for systems transmitting speech signals. This suggests greater advantages can be achieved using weak noise filters for video signals than for speech signals. However, due to the obvious differences in subjective nature of the two signals, final judgement about the use of weak noise filters in PAM, PCM, and DPCM video communication systems must be based on subjective viewing tests[†].

[†]The author is aware that some subjective results for PCM and DPCM television systems exist in the literature [20,21,23]. However, in all these investigations the sampling rate, and hence, the bandwidth of the system was fixed. Since this is an important physical parameter, the subjective effects of sampling rate, as well as noise (transmission and/or quantization) in optimal pre and postfiltering of television systems should be considered.

7. CONCLUSIONS

Pre and postfilters which minimize the frequency weighted mean-integral-squared error in noisy sampled systems have been considered. In the analysis, no restrictions are imposed on the input signal spectrum and the noise spectrum, and negligible cross-correlation between the signal and noise is not assumed. An algorithm for determining the jointly optimal pre and postfilters is presented, and the validity of the algorithm proved. The principal conclusion to be drawn from the algorithm is that the jointly optimal pre and postfilters are bandlimited to a frequency set of total measure less than or equal to the sampling frequency, of which no two points coincide under integer multiple translations of the sampling frequency. An important practical consequence of this conclusion is that the optimal pre and postfilters can be synthesized by combinations of analog bandpass and digital spectral-shaping filters.

Several suboptimal pre and postfiltering schemes have been investigated. One scheme that was studied results when the magnitude of the prefilter transfer function is constrained to have a constant amplitude in the passband and the postfilter chosen to minimize the mean-squared error of the system. Another suboptimal scheme occurs when the postfilter transfer function is constrained to have a constant magnitude in the passband and the prefilter optimized. A third suboptimal scheme, designated as weak noise filtering, was also investigated. Weak noise filters yield virtually the same performance as jointly optimal pre and postfilters in many cases of interest and have the practical advantage that their filter transfer characteristics are dependent only on the input signal spectrum and the relative spectrum of the noise.

Applications of the optimization algorithm to PAM, PCM, and DPCM communication systems have been considered. A M-channel time-multiplexed PAM system with no intersymbol or interchannel distortion in the channel is analyzed. In the PCM analysis, digital channel errors are included, and correlation functions for quantized signals transmitted over discrete memoryless channels are derived and shown to be a necessary part of the filter optimization. In the DPCM analysis, error-free digital transmission is assumed and the cross-correlation between signal and quantization noise is taken into consideration.

Performance characteristics, showing mean-squared error and inband signal-to-noise ratio versus channel signal-to-noise ratio, are determined explicitly for optimal pre and postfiltered PAM and PCM systems with first-order Butterworth input spectrum. These characteristics are compared with the performance characteristics achieved by PAM and PCM systems which use suboptimal filtering schemes and with the optimal performance theoretically attainable. Performance characteristics, showing mean-squared error versus channel capacity, are also determined for PAM, PCM, and DPCM systems when the system parameters are optimized to yield the least mean-squared error for a given channel capacity. Examination of the performance characteristics show that significant reduction in mean-squared error and significant improvement in inband signal-to-noise ratio are possible for PAM and PCM systems which use optimal pre and postfilters in place of the more conventional lowpass pre and postfilters. For DPCM systems which use jointly optimal filters, however, negligible reduction in mean-squared error was observed. This suggests that whatever redundancy reduction is not done by the prefilter will be done by the differential aspect of the DPCM system.

Because of the subjective nature of speech, the effect of pre and postfiltering in PAM, PCM, and DPCM communication systems for speech transmission is studied by simulation methods and evaluated with subjective tests. Weak noise pre and postfilters (WNF), which yield virtually the same performance as optimal pre and postfilters, are considered in the subjective evaluation as well as lowpass pre and postfilters (LPF). The digital simulation fascilities and the subjective testing methods are described, and the subjective results interpreted.

As a direct result of the isopreference test method utilized in the subjective investigation, isopreference contours showing the subjective effects of LPF and WNF on a sampling frequency f_s versus channel signal-to-noise ratio S/N_oW_c diagram are obtained for PAM speech communication systems. For PCM and DPCM systems, the isopreference contours for the two filtering schemes are obtained on a f_s versus number of bits of quantization d diagram. It was observed that all isopreference contours could be separated into two distinct saturation regions. In one saturation region, quality is limited by speech bandwidth and in the other, inband noise limits quality.

Examination of the LPF and WNF isopreference contours for PAM, PCM, and DPCM systems shows that only in the noise-limited region do weak noise filters have any effect on subjective performance. It was observed that no significant subjective differences exist between PAM LPF and PAM WNF systems and between DPCM LPF and DPCM WNF systems. For PCM systems, however, significant improvement in subjective performance could be achieved by using WNF in place of LPF. In the noise-limited saturation region of the isopreference contour, PCM systems which use WNF reduce by almost one bit the number of quantization bits required to achieve a given speech quality. This bit reduction with respect to PCM LPF systems is still less than that achieved by DPCM systems.

Along each PAM isopreference contour, one combination of f_s and

S/N_oW_c yields the least channel capacity that is required by a PAM system in order to achieve the speech quality associated with the contour. Similarly, along each PCM or DPCM isopreference contour, one combination of f_s and d yields the least channel capacity required by the PCM or DPCM system in order to achieve the speech quality associated with the contour. Comparison of the minimum channel capacities required by PAM, PCM and DPCM systems in order to achieve a given speech quality, shows that the minimum channel capacities required by both PAM LPF and PAM WNF systems are equivalent, and that the minimum channel capacities required by all PCM LPF, PCM WNF, DPCM LPF, and DPCM WNF systems are equivalent. Therefore, when system parameters in PAM, PCM, and DPCM systems are chosen to minimize the channel capacity required to achieve a specific speech quality, there is no subjective advantage in using weak noise filters in place of lowpass filters, and no subjective advantage in using DPCM systems in place of PCM systems.

Although particular application to speech communication systems is considered in this investigation, application of pre and postfiltering in video communication systems is also worthy of consideration. The usefulness of the objective measure, signal-to-noise ratio improvement factor SNRIF, has been demonstrated in the interpretation of the relative subjective behaviour of PAM, PCM, and DPCM systems which use LPF and WNF. Since, in general, the SNRIF for video communication systems is significantly larger than the SNRIF for speech communication systems, greater improvement in performance is expected in using weak noise filters in place of lowpass filters for video signals. However, ultimate judgement on the use of weak noise filters in PAM, PCM, and DPCM video communication systems must be based on subjective viewing tests.

APPENDIX CORRELATION FUNCTIONS AND RECONSTRUCTION ERROR FOR QUANTIZED GAUSSIAN SIGNALS TRANSMITTED OVER DISCRETE MEMORYLESS CHANNELS

The purpose of this Appendix is to present alternative exact expressions, and some useful approximations and bounds for the correlation functions discussed in Section 4.2.1, and to show how $\emptyset_n(\tau)$ and $\emptyset_{yn}(\tau)$ affect the mean-squared error which results when the received samples $\hat{v}$ in Fig. 6 are operated on by any linear time-invariant filter to yield an output $\hat{x}(t)$ which approximates any linear time-invariant operation on x(t). For sufficiently good channels, the cross-correlation between the quantizer input signal and the quantization plus channel noise is shown to have little effect on both the optimal reconstruction filter and the reconstruction error when the number of levels N in Max nonuniform and uniform quantizers is sufficiently large. This same conclusion does not apply, in general, for small N or for poor channels.

A.1 Exact Expressions for Correlation Functions

In this section, alternative exact expressions for $\emptyset_{\hat{v}}(\tau)$ and $\emptyset_{y\hat{v}}(\tau)$ are presented. Substituting (58) into (57) yields the following equations, in which $\delta=\delta_y(\tau)$,

$$\emptyset_{\hat{v}}(\tau) = \sum_{i=1}^{N} \sum_{j=1}^{N} \frac{y_i y_j}{2\sqrt{2\pi}} \sum_{k=1}^{N} \sum_{m=1}^{N} P_{ki} P_{mj} \int_{x_{k-1}}^{x_k} \{ \frac{1}{\sigma} \exp[-\frac{(\alpha-\mu)^2}{2\sigma^2}] \} \{\mathrm{erf}[\frac{(x_m-\mu)-\delta(\alpha-\mu)}{\sqrt{2\sigma^2(1-\delta^2)}}] - \mathrm{erf}[\frac{(x_{m-1}-\mu)-\delta(\alpha-\mu)}{\sqrt{2\sigma^2(1-\delta^2)}}] \}d\alpha \qquad \text{(A.1a)}$$

where

$$\mathrm{erf}(x) = (2/\sqrt{\pi}) \int_{o}^{x} e^{-r^2}\, dr \qquad \text{(A.1b)}$$

Equation (A.1) can be simplified as follows

$$\emptyset_{\hat{v}}(\tau) = \sum_{i=1}^{N} \sum_{k=1}^{N} \frac{y_i P_{ki}}{\sqrt{2\pi}} \int_{(x_{k-1}-\mu)/\sigma}^{(x_k-\mu)/\sigma} \Psi(\delta,\eta)\ \exp(-\frac{\eta^2}{2})d\eta \tag{A.2a}$$

where

$$\Psi(\delta,\eta) = \sum_{j=1}^{N} \sum_{m=1}^{N} \frac{y_j P_{mj}}{2} \{\mathrm{erf}[\frac{(x_m-\mu)/\sigma - \delta\eta}{\sqrt{2(1-\delta^2)}}] - \mathrm{erf}\ [\frac{(x_{m-1}-\mu)/\sigma - \delta\eta}{\sqrt{2(1-\delta^2)}}]\} \tag{A.2b}$$

Equation (A.2) for $\emptyset_{\hat{v}}(\tau)$ reduces to the result obtained by Kellogg [22] when $\mu=0$, $\sigma^2=1$, and the digital channel in Fig. 6 is noiseless. Similarly, from (62) we obtain the following alternative expression for $\emptyset_{y\hat{v}}(\tau)$.

$$\emptyset_{y\hat{v}}(\tau) = (\sigma/\sqrt{2\pi}) \int_{-\infty}^{\infty} \eta\Psi(\delta,\eta)\ \exp(-\eta^2/2)d\eta \tag{A.3}$$

Functions $\emptyset_{y\hat{v}}(\tau)$ and $\emptyset_{yn}(\tau)$ are easily computed using the series expansion since a_o and a_1 are the only coefficients involved. Whether the series representations (60,63) or the direct expressions (A.1,A.2) should be used to evaluate $\emptyset_{\hat{v}}(\tau)$ and $\emptyset_n(\tau)$ depends on the number of terms in the series required to yield sufficiently good approximations to the desired functions. When a large number of terms are needed, direct calculation may be more efficient.

A.2 Approximation and Bounds

Some useful approximations and bounds are now derived. It follows from (65) that

$$|R_{\hat{v}}(\tau)/\sigma^2 - \sum_{n=1}^{M} a_n^2\ \delta_y^n(\tau)| \leq |\delta_y^{M+1}(\tau)| \sum_{n=M+1}^{\infty} a_n^2 \tag{A.4a}$$

$$|R_n(\tau)/\sigma^2 - (1-a_1)^2\delta_y(\tau) - \sum_{n=2}^{M} a_n^2\ \delta_y^n(\tau)| \leq |\delta_y^{M+1}(\tau)| \sum_{n=M+1}^{\infty} a_n^2 \tag{A.4b}$$

Division of (A.4a) by $R_{\hat{v}}(0)/\sigma^2$ and (A.4b) by $R_n(0)/\sigma^2$ yields bounds relative to $R_{\hat{v}}(0)$ and $R_n(0)$ on the error which results when the first M terms of the series are used to approximate $R_{\hat{v}}(\tau)$ and $R_n(\tau)$.

In many practical situations the following equations apply for all $0 \leq k \leq N$, $1 \leq i \leq N$ and $1 \leq j \leq N$.

$$(y_k-\mu) = -(y_{N-k}-\mu) \tag{A.5a}$$

$$P_{ji} = P_{N+1-j\,,\,N+1-i} \tag{A.5b}$$

$$v_i-c = -(v_{N+1-i}-c) \tag{A.5c}$$

From (A.5c) it follows that constant c is given by the following equation, which holds for all $1 \leq i \leq N$.

$$c = (v_i + v_{N+1-i})/2 \tag{A.5d}$$

Equations (A.5a) and (A.5c) hold for virtually all practical quantization schemes. Equation (A.5b) applies when the quantizer output levels are transmitted over a discrete memoryless channel using a natural binary code. When (A.5a) applies, it follows from (61c) and (61d) that

$$\Gamma_n(k) = (-1)^n\,\Gamma_n(N+1-k) \quad 1 \leq k \leq N \tag{A.6}$$

Substitution of (A.5) and (A.6) into (61b) shows that

$$a_n = \begin{cases} 0 & \text{n even, positive} \\ (-2\sqrt{2\pi n!})\left(\sum_{i=1}^{L}\sum_{k=1}^{L}\left(\frac{y_i-c}{\sigma}\right)(P_{ki}-P_{k,N+1-i})\Gamma_{n-1}(k)\right. & \text{n odd, positive} \end{cases} \tag{A.7a}$$

where

$$L = \begin{cases} N/2 & \text{N even} \\ (N-1)/2 & \text{N odd} \end{cases} \tag{A.7b}$$

Substitution of (A.5) into (61a) yields, after some algebra, the following equation for a_0,

$$a_0 = c/\sigma \tag{A.7c}$$

It follows that when $a_n=0$ for n even and positive, inequality $R_{\hat{v}}(\tau)/\sigma^2 | \geq | \delta_y^M(\tau) | \sum_{n=1}^{M} a_n^2$ holds. Dividing (A.4a) by the inequality yields for $M \geq 1$,

$$|R_{\hat{v}}(\tau)/\sigma^2 - \sum_{n=1}^{M} a_n^2 \, \delta_y^n(\tau)| / |R_{\hat{v}}(\tau)/\sigma^2| \leq |\delta_y(\tau)| \, B_{\hat{v}}(M) \qquad (A.8a)$$

$$B_{\hat{v}}(M) = \sum_{n=M+1}^{\infty} a_n^2 \Big/ \sum_{n=1}^{M} a_n^2 \qquad (A.8b)$$

where from (65a)

$$\sum_{n=M+1}^{\infty} a_n^2 = R_{\hat{v}}(0)/\sigma^2 - \sum_{n=1}^{M} a_n^2 \qquad (A.8c)$$

Similarly, for $M \geq 2$

$$|R_n(\tau)/\sigma^2 - (1-a_1)^2\delta_y(\tau) - \sum_{n=2}^{M} a_n^2 \, \delta_y^n(\tau)| / |R_n(\tau)/\sigma^2| \leq |\delta_y(\tau)| B_n(M) \qquad (A.9a)$$

$$B_n(M) = \sum_{n=M+1}^{\infty} a_n^2 / [(1-a_1)^2 + \sum_{n=2}^{M} a_n^2] \qquad (A.9b)$$

Note $B_{\hat{v}}(i) = B_{\hat{v}}(i+1)$ and $B_n(i) = B_n(i+1)$ for all positive even integers i. The bounds in (A.8) and (A.9) are attractive because they give approximation errors relative to $R_{\hat{v}}(\tau)$ and $R_n(\tau)$.

A.3 Optimal Postfiltering of Quantized Signals Transmitted over Discrete Memoryless Channels

Although much work has been done on the reconstruction of sampled signals [8,9], channel errors and correlation between signal and noise were assumed negligible. In this Section of the Appendix, the effect of $\phi_n(\tau)$ and $\phi_{yn}(\tau)$ on the mean-squared error which results when the received samples $\hat{v}$ are operated on by a linear time-invariant postfilter is considered.

Let the samples $\hat{v}$ in Fig. 6 be multiplied by the impulse train

$\Delta(t) = T.\sum_{k=-\infty}^{\infty} \delta(t-kT+\theta)$ where $\delta(t)$ is the unit impulse, and let the resulting signal be filtered by a linear time-invariant filter having impulse response $g(t)$ (see Fig. A.1). Let $z(t) = a(t)\otimes y(t)$ be the desired output signal, where $a(t)$ is any real time function with Fourier transform $A(f)$, and let $n(t)=\hat{v}(t)-y(t)$.

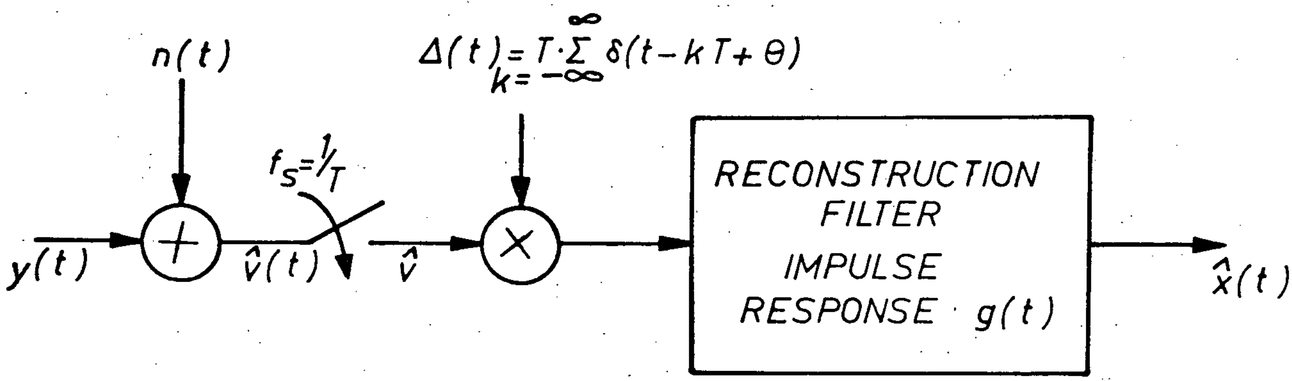

Fig. A.1 Reconstruction system. Signal $\hat{v}(t)$ is sampled at $t=kT-\theta$.

If $\Phi_y(f)$, $\Phi_n(f)$ and $\Phi_{yn}(f)$ are the Fourier transforms of $\phi_y(\tau)$, $\phi_n(\tau)$ and $\phi_{yn}(\tau)$, respectively, then mean-integral-squared error

$$\varepsilon = E\{\frac{1}{T}\int_o^T [z(t)-\hat{x}(t)]^2 dt\}$$

$$= \int_{-\infty}^{\infty} [|A(f)|^2 \Phi_y(f)+|G(f)|^2 \sum_{k=-\infty}^{\infty} \Phi_y(f+kf_s)-2A(f)G^*(f)\Phi_y(f)]df$$

$$+\int_{-\infty}^{\infty} |G(f)|^2\Phi_{n_s}(f)df + 2\int_{-\infty}^{\infty} \{-[A(f)G^*(f)\Phi_{yn}(f)-|G(f)|^2 \sum_{k=-\infty}^{\infty} \Phi_{yn}(f+kf_s)]\}df \tag{A.10}$$

where

$$\Phi_{n_s}(f) = \sum_{k=-\infty}^{\infty} \Phi_n(f+kf_s) \tag{A.11}$$

and * denotes complex conjugate.

The first term in (A.10) represents error which results from the postfilter's inability to make $\varepsilon=0$ even when $n(t)=0$. The second term results from quantization plus channel noise, while the third term results from the interaction of $y(t)$ with $n(t)$. When $y(t)$ is a Gaussian process and $\mu=0$ or $a_o=\mu/\sigma$, then, from (64) $\Phi_{yn}(f)=(a_1-1)\Phi_y(f)$ and the contribution of the last term relative to that of the second term is

$$\rho=2[1-a_1]\frac{\int_{-\infty}^{\infty} G^*(f)[A(f)-G(f)]\Phi_y(f)df-\int_{-\infty}^{\infty}|G(f)|^2\sum_{\substack{k=-\infty\\k\neq 0}}^{\infty}\Phi_y(f+kf_s)df}{\int_{-\infty}^{\infty}|G(f)|^2\Phi_{n_s}(f)df} \tag{A.12}$$

In many cases of interest $y(t)$ is bandlimited in the sense that if $\Phi_y(f)\neq 0$ then $\Phi_y(f+kf_s)=0$ for any non-zero integer k. If $G(f)$ is bandlimited in the same way then the second integral in the numerator of (A.12) equals zero. If, in addition, $A(f)=G(f)$ for all f for which $\Phi_y(f)\neq 0$ then $\rho=0$ and

$$\varepsilon = \int_{-\infty}^{\infty} |G(f)|^2\ \Phi_{n_s}(f)df$$

If $y(t)$ is Gaussian with $\mu=0$ or $a_o=\mu/\sigma$ and if $G(f)$ is chosen to minimize ε then [25,26]

$$G(f) = a_1A(f)\Phi_y(f)/[(2a_1-1)\sum_{k=-\infty}^{\infty}\Phi_y(f+kf_s) + \Phi_{n_s}(f)] \tag{A.13a}$$

If $G(f)$ is chosen to minimize the first two integrals in (A.10) and $G(f)$ is given by (A.13a) with $a_1=1$, that is

$$G(f) = A(f)\Phi_y(f)/[\sum_{k=-\infty}^{\infty}\Phi_y(f+kf_s) + \Phi_{n_s}(f)] \tag{A.13b}$$

Substituting (A.13b) into (A.12) yields

$$\rho = 2(1-a_1) \tag{A.14}$$

From (A.12), (A.13), and (A.14) it follows that if $2(1-a_1)$ is sufficiently small then the crosscorrelation between y(t) and n(t) can be neglected in calculating both ε and the optimal G(f).

Although $\Phi_{n_s}(f)$ can be obtained from (A.11) and $\Phi_n(f)$ from (63), calculation is tedious, particularly when it has to be performed for several quantizers and several values of T. Ruchkin [34] and Robertson [35] have shown that with P_{ij} given by (67), $\Phi_{n_s}(f)$ is approximately constant for a large class of $\Phi_y(f)$ with all but very coarse quantizing and very small T. One could expect this conclusion to hold reasonably well for any P_{ij}†, in which case $\Phi_{n_s}(f)=T\cdot\phi_n(0)$ where

$$\begin{aligned}\phi_n(0) &= E[n^2] \\ &= \sum_{i=1}^{N}\sum_{j=1}^{N} P_{ij} \int_{y_{i-1}}^{y_i} (v_j-\alpha)^2\, p_y(\alpha)d\end{aligned} \tag{A.16}$$

and $p_y(\alpha)$ is the amplitude probability density of y(t).

A.4 An Example

Let

$$P_{ij} = p^{d_{ij}}(1-p)^{d-d_{ij}} \tag{A.17}$$

where N is constrained to make $d = \log_2 N$ an integer, and where d_{ij} is the Hamming distance between quantizer output levels i and j. Equation (A.17) results when the quantizer output levels are natural binary coded and transmitted over a discrete memoryless channel having bit error probability p.

---

†The following example supports this statement, since the a_n's are not strongly dependent on P_{ij} when $N \geq 4$.

Tables A.1 and A.2 and Fig. A.2 describe the behaviour of $a_n (1 \leq n \leq 9)$, $2(1-a_1)$, $\phi_n(0)$, $B_{\hat{v}}(1)$ and $B_{\hat{v}}(3)$ when Max [37] uniform and nonuniform quantizers are used. Max quantizers minimize $\phi_n(0) = E(n^2)$ for any given N when p = 0, and make E(n) = 0 and $a_n = 0$ for n even, since (A.5) is satisfied. From Tables A.1 and A.2 one see that $a_1^{\,2} >> a_n^{\,2}$ for $N \geq 4$, and that for any N and p most of the magnitudes of $(1-a_1)$, a_3, a_5, a_7, and a_9 are of approximately the same order, as one would expect for noise whose bandwidth is considerably larger than that of signal y(t). Fig. A.2a suggests that $2(1-a_1)$ decreases as p decreases and N increases.

As P_{ij} approaches the values in (67) each coefficient a_n continuously approaches the value which results when P_{ij} is given by (67), and both the nonuniform and uniform quantizers which minimize $E(n^2)$ converge, respectively, to uniform and nonuniform Max quantizers [38]. It follows from (A.12-A.14) and Fig. A.2a that for any redundant or non-redundant coding scheme with optimum nonuniform or optimum uniform quantization, the cross-correlation of y with n has little effect on both ε and the optimal G(f) if N is sufficiently large and if the channel is sufficiently good. The previous statement is not true in general. For example, let G(f) minimize ε on the assumption that $\phi_{yn}(\tau) = 0$. Then with a Max quantizer for which N=2 and a natural binary code with p = 0.1, (A.14) shows that the last integral in (A.10) is almost as large as the second integral, since $a_1 = .5094$ and $\rho = .98$.

Tables A.1 and A.2 show that $\phi_n(0)$ increases with p for any fixed value of N, and that a finite non-zero value of N minimized $\phi_n(0)$ for each p > 0, an effect noted and explained elsewhere [38].

Figs. A.2b and A.2c show $B_{\hat{v}}(1)$ and $B_{\hat{v}}(3)$ vs. N and p. Not shown is $B_{\hat{v}}(M)$ for $M \geq 5$, whose behaviour was found to be virtually identical to $B_{\hat{v}}(3)$ for all values of $N \geq 1$ and $p \geq 0.01$.

p	0.0					0.001				
$\log_2 N$	1	2	3	4	5	1	2	3	4	5
a_1	.6367	.8823	.9654	.9905	.9977	.6354	.8806	.9636	.9887	.9959
a_3	-.2599	-.1552	-.0611	-.0196	-.0056	-.2594	-.1549	-.0611	-.0198	-.0058
a_5	.1744	.0108	-.0311	-.0197	-.0079	.1740	.0108	-.0310	-.0197	-.0079
a_7	-.1345	.0362	.0243	.0002	-.0041	-.1343	.0361	.0242	.0003	-.0040
a_9	.1110	-.0485	-.0044	.0083	.0027	.1108	-.0484	-.0044	.0082	.0026
$\emptyset_n(0)$	.3634	.1175	.0345	.0095	.0025	.3659	.1225	.0415	.0178	.0119
$2(1-a_1)$	.7266	.2354	.0691	.0190	.0047	.7291	.2389	.0728	.0227	.0081

p	0.01					0.1				
$\log_2 N$	1	2	3	4	5	1	2	3	4	5
a_1	.6240	.8647	.9469	.9724	.9802	.5094	.7058	.7780	.8051	.8167
a_3	-.2547	-.1521	-.0611	-.0210	-.0074	-.2079	-.1242	-.0574	-.0291	-.0188
a_5	.1709	.0106	-.0299	-.0193	-.0082	.1395	.0087	-.0212	-.0154	-.0097
a_7	-.1318	-.0354	.0238	.0009	-.0030	-.1076	.0289	.0199	.0058	.0044
a_9	.1088	-.0476	-.0047	.0072	.0017	.0888	-.0388	-.0067	-.0003	-.0047
$\emptyset_n(0)$	.3888	.1670	.1034	.0926	.0956	.6181	.6002	.6981	.8071	.8949
$2(1-a_1)$	.7520	.2707	.1062	.0552	.0396	.9813	.5883	.4440	.3898	.3667

Table A.1 Max Nonuniform Quantizer

p	0.0					0.001				
$\log_2 N$	1	2	3	4	5	1	2	3	4	5
a_1	.6367	.8812	.9626	.9885	.9965	.6354	.8794	.9606	.9865	.9945
a_3	-.2599	-.1639	-.0800	-.0342	-.0134	-.2594	-.1635	-.0799	-.0341	-.0134
a_5	.1744	.0220	-.0245	-.0261	-.0166	.1740	.0219	-.0245	-.0260	-.0166
a_7	-.1345	.0241	.0280	.0097	-.0011	-.1343	.0240	.0279	.0097	-.0011
a_9	.1110	-.0362	-.0131	.0043	.0064	.1108	-.0362	-.0131	.0043	.0064
$\emptyset_n(0)$	.3634	.1188	.0374	.0115	.0035	.3659	.1238	.0446	.0211	.0156
$2(1-a_1)$	.7266	.2377	.0749	.0231	.0070	.7291	.2412	.0787	.0270	.0110

p	0.01					0.1				
$\log_2 N$	1	2	3	4	5	1	2	3	4	5
a_1	.6240	.8635	.9433	.9687	.9766	.5094	.7049	.7700	.7908	.7972
a_3	-.2547	-.1606	-.0784	-.0335	-.0132	-.2079	-.1311	-.0640	-.0274	-.0107
a_5	.1709	.0215	-.0241	-.0256	-.0163	.1395	.0176	-.0196	-.0209	-.0133
a_7	-.1318	.0236	.0274	.0095	-.0011	-.1076	.0193	.0224	.0078	.0069
a_9	.1088	-.0355	-.0129	.0042	.0063	.0888	-.0290	-.0105	.0035	.0051
$\emptyset_n(0)$	.3888	.1683	.1092	.1065	.1233	.6181	.6002	.7250	.9106	1.129
$2(1-a_1)$	.7520	.2729	.1134	.0626	.0469	.9813	.5901	.4599	.4185	.4056

Table A.2 Max Uniform Quantizer

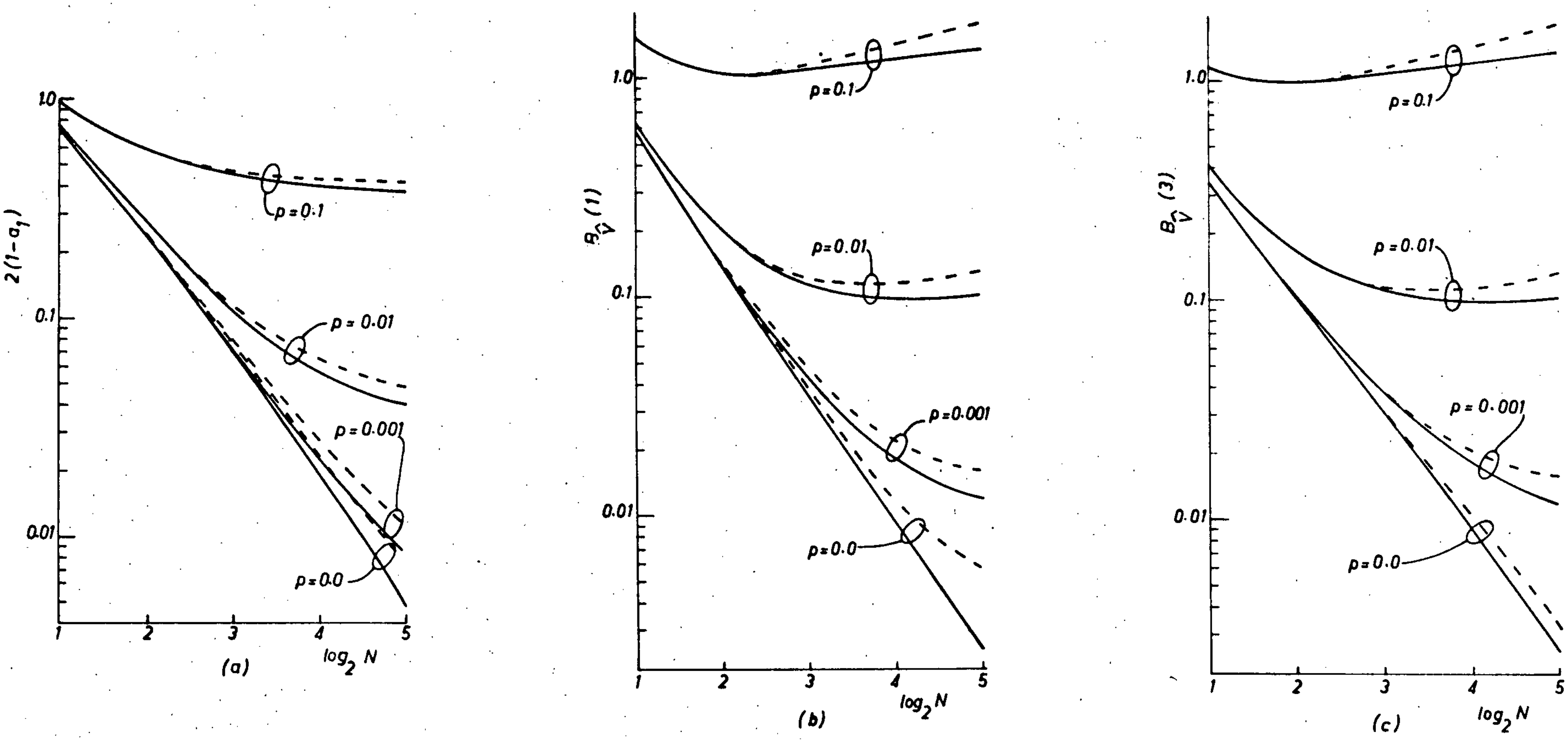

Fig. A.2 Functions $2(1-a_1)$, $B_{\hat{v}}(1)$, and $B_{\hat{v}}(3)$ versus $\log_2 N$ and p when y(t) is a stationary Gaussian process. The solid curves apply to Max nonuniform quantizers and the dotted curves apply to Max uniform quantizers.
(a) Ordinate is $2(1-a_1)$.
(b) Ordinate is $B_{\hat{v}}(1)$.
(c) Ordinate is $B_{\hat{v}}(3)$.

REFERENCES

1. J.R. Ragazzini and G.F. Franklin, Sampled-Data Control Systems. New York: McGraw-Hill Book Co., 1958.

2. S.S.L. Chang, Synthesis of Optimum Control Systems. New York: McGraw-Hill Book Co., 1961.

3. B.C. Kuo, Analysis and Synthesis of Sampled-Data Control Systems. Englewood Cliffs, N.J.: Prentice-Hall, 1963.

4. W.K. Linvill and J.M. Salzer, "Analysis of control systems involving digital computers", Proc. IRE, vol. 41, pp. 901-906, July 1953.

5. J.M. Salzer, "Frequency analysis of digital computers operating in real time", Proc. IRE, vol. 42, pp. 457-466, February 1954.

6. N. Wiener, The Extrapolation, Interpolation, and Smoothing of Stationary Time Series with Engineering Applications. New York: J. Wiley and Sons, 1949.

7. R.M. Stewart, "Statistical design and evaluation of filters for the restoration of sampled data", Proc. IRE, vol. 44, pp. 253-257, February 1956.

8. D.S. Ruchkin, "Linear reconstruction of sampled signals", IRE Trans. Communication Systems, vol. CS-9, pp. 350-355, December 1951.

9. J. Katzenelson, "On errors introduced by combined sampling and quantizing", IRE Trans. Automatic Control, vol. AC-7, pp. 58-68, April 1962.

10. J.P. Costas, "Coding with linear systems", Proc. IRE, vol. 40, pp. 1101-1103, September 1952.

11. B.S. Tsybakov, "Linear information coding", Radio Engineering and Electronic Physics, vol. 7, pp. 22-33, January 1962.

12. T. Berger and D.W. Tufts, "Optimum pulse amplitude modulation part I: Transmitter-receiver design and bounds from information theory", IEEE

Trans. Information Theory, vol. IT-13, pp. 196-208, April 1967.

13. R.W. Chang and S.L. Freeny, "Hybrid digital transmission systems - Part I: Joint optimization of analog and digital repeaters", Bell Sys. Tech. J., vol. 47, pp. 1663-1686, October 1968.

14. H.M. Robbins, "An extension of Wiener filter theory to partly sampled systems", IRE Trans. Circuit Theory, vol. CT-6, pp. 362-370, December 1959.

15. P.M. DeRusso, "Optimum linear filtering of signals prior to sampling", AIEE Trans., vol. 79, pt. II, pp. 549-555, January 1961.

16. W.M. Brown, "Optimum prefiltering of sampled data", IRE Trans. Information Theory, vol. IT-7, pp. 269-270, October 1961.

17. J.J. Spilker, Jr., "Theoretical bounds on the performance of sampled data communication systems", IRE Trans. Circuit Theory, vol. CT-7, pp. 335-341, September 1960.

18. L.M. Goodman and P.R. Drouilhet, Jr., "Asymtotically optimum pre-emphasis and de-emphasis networks for sampling and quantizing", Proc. IEEE, vol. 54, pp. 795-796, May 1966.

19. E.G. Kimme and F.F. Kuo, "Synthesis of optimal filters for a feedback quantization system", IEEE Trans. Circuit Theory, vol. CT-10, pp. 405-413, September 1963.

20. R.A. Bruce, "Optimum pre-emphasis and de-emphasis networks for transmission of television by PCM", IEEE Trans. Communication Technology, vol. COM-12, pp. 91-96, September 1964.

21. R.C. Brainard and J.C. Candy, "Direct-feedback coders: Design and performance with television signals", Proc. IEEE, vol. 37, pp. 776-786, May 1969.

22. W.C. Kellogg, "Information Rates on sampling and quantization", IEEE Trans. Information Theory, vol. IT-13, pp. 506-511, July 1967.

23. R.C. Brainard, "Subjective evaluation of PCM noise feedback coder for television", Proc. IEEE, vol. 55, pp. 346-353, March 1967.

24. I.M. Gelfand and S.V. Fomin, Calculus of Variations. Englewood Cliffs, N.J.: Prentice-Hall, 1963.

25. Y.W. Lee, Statistical Theory of Communication. New York: J. Wiley and Sons, 1960, ch. 14.

26. H.L. Van Trees, Detection, Estimation, and Modulation Theory. New York: J. Wiley and Sons, 1968, ch. 6.

27. C.J. Boardman and H.L. Van Trees, "Optimum angle modulation", IEEE Trans. Communication Technology, vol. COM-13, pp. 452-469, December 1965.

28. J.T. Tou, Digital and Sampled-Data Control Systems. McGraw-Hill Book Co., New York, 1959, pp. 281-308.

29. J.W. Smith, "A unified view of synchronous data transmission system design", Bell Sys. Tech. J., vol. 47, pp. 273-300, March 1968.

30. T.J. Goblick, "Theoretical limitations on the transmission of data from analog sources", IEEE Trans. Information Theory, vol. IT-11, pp. 558-567, October 1965.

31. J.J. Bussang, "Crosscorrelation function of amplitude-distorted Gaussian signals", MIT Electronics Research Lab., Mass., Tech. Rept. 216, March 1952.

32. J.D. Bruce, "Correlation functions of quantized Gaussian signals", MIT Electronics Research Lab., Cambridge, Mass., Quart. Progress Rept. 76, pp. 192-198, January 1965.

33. A.I. Velichkin, "Correlation function and spectral density of a quantized process", Telecommunications and Radio Engineering, vol. 17, pp. 70-77, July 1962.

34. D.S. Ruchkin, "Optimal reconstruction of sampled and quantized stochastic

signals", D. Eng. dissertation, Yale University, New Haven, Conn., 1960.

35. G.H. Robertson, "Computer study of quantized output spectra", Bell Sys. Tech. J., vol. 48, pp. 2391-2403, September 1969.

36. R.E. Totty and G.C. Clark, "Reconstruction error in waveform transmission", IEEE Trans. Information Theory, vol. IT-13, pp. 336-338, April 1967.

37. J. Max, "Quantizing for minimum distortion", IRE Trans. Information Theory, vol. IT-6, pp. 7-12, March 1960.

38. A.J. Kurtenback and P.A. Wintz, "Quantizing for noise channels", IEEE Trans. Communication Technology, vol. COM-17, pp. 291-302, April 1969.

39. J.B. O'Neal Jr., "Predictive quantizing systems (differential pulse code modulation) for the transmission of television signals", Bell Sys. Tech. J., vol. 45, pp. 689-721, May-June 1966.

40. J.B. O'Neal Jr., "A bound on signal-to quantizing noise ratios for digital encoding systems", Proc. IEEE, vol. 55, pp. 287-291, March 1967.

41. R.W. Donaldson and D. Chan, "Analysis and subjective evaluation of differential pulse code modulation voice communication systems", IEEE Trans. Communication Technology, vol. COM-17, pp. 10-19, February 1969.

42. R.W. Donaldson and R.J. Douville, "Analysis, subjective evaluation, optimization and comparison of the performance capabilities of PCM, DPCM, ΔM, AM, and PM voice communication systems", IEEE Trans. Communication Technology, vol. Com-17, pp. 421-431, August 1969.

43. T.J. Goblick, Jr., "Analog source digitization: A comparison of theory and practice", IEEE Trans. Information Theory, vol. IT-13, pp. 323-326, April 1967.

44. R.G. Gallagher, Information Theory and Reliable Communication. New York: J. Wiley and Sons, 1968, ch. 3.

45. B. Smith, "Instantaneous companding of quantized signals", Bell Sys. Tech.

vol. 27, pp. 446-472, July 1948.

46. B.G. Cramer, "Optimum linear filtering of analog signals in noisy channels", IEEE Trans. Audio and Electroacoustics, vol. AU-14, pp. 3-15, March 1966.

47. R.F. Purton, "A survey of telephone speech signal statistics and their significance in the choice of a PCM companding law", Proc. IEE, vol. 109B, pp. 60-66, January 1962.

48. E.E. David, Jr., M.V. Mathews, and H.S. McDonald, "Description and results of experiments with speech using digital computer simulation", Proc. NEC, Chicago, Ill., pp. 776-775, October 1958.

49. E.E. David, Jr., M.V. Mathews, and H.S. McDonald, "A high-speed data translator for computer simulation of speech and television devices", Western Joint Computer Conference, San Francisco, Calif., pp. 354-357, March 1959.

50. M.V. Mathews, "Extremal coding for speech transmission", IRE Trans. Information Theory, vol. IT-5, pp. 129-136, September 1959.

51. B.S. Atal and M.R. Schroeder, "Predictive coding of speech signals", IEEE Wescon Convention Record, pt. 8/2, August 1968.

52. J.F. Kaiser, "The digital filter and speech communication", IEEE Trans. Audio and Electroacoustics, vol. AU-16, pp. 180-183, June 1968.

53. G-AE Concepts Subcommittee, "On digital filtering", IEEE Trans. Audio and Electroacoustics, vol. AU-16, pp. 303-314, September 1968.

54. J.F. Kaiser, "Digital filters", in <u>Systems Analysis by Digital Computer</u>., F.F. Kuo and J.F. Kaiser, Eds. New York: J. Wiley and Sons, 1966, Ch.7.

55. C.M. Rader and B. Gold, "Digital filter design techniques in the frequency domain", Proc. IEEE, vol. 55, pp. 149-171, February 1967.

56. R.M. Golden, "Digital filter synthesis by sampled-data transformation", IEEE Trans. Audio and Electroacoustics, vol. AU-16, pp. 321-329, September 1968.

57. H.D. Helms, "Nonrecursive digital filters: Design methods for achieving specifications on frequency response", IEEE Trans. Audio and Electroacoustics, vol. AU-16, pp. 336-342, September 1968.

58. H.D. Helms, "Fast Fourier transform method of computing difference equations and simulating filters", IEEE Trans. Audio and Electroacoustics, vol. AU-15, pp. 85-90, June 1967.

59. G.D. Bergland, "A guided tour of the fast Fourier transform", IEEE Spectrum, vol. 6, pp. 41-52, July 1969.

60. P.I. Richards, "Computing reliable power spectra", IEEE Spectrum, vol. 4, pp. 83-90, January 1967.

61. C. Bingham, H.D. Godfrey, and J.W. Tukey, "Modern techniques of power spectrum estimation", IEEE Trans. Audio and Electroacoustics, vol. AU-15, pp. 56-66, June 1967.

62. P.D. Welch, "The use of fast Fourier transform for the estimation of power spectra: A method based on time averaging over short, modified periodograms", IEEE Trans. Audio and Electroacoustics, vol. AU-15, pp. 70-73, June 1967.

63. J.W. Cooley, "Finite complex Fourier transform", SHARE Program Library, PK FORT, SDA 3465, September 1966.

64. J.W. Cooley and J.W. Tukey, "An algorithm for the machine calculation of Fourier series", Math. Comp., vol. 19, pp. 297-301, April 1965.

65. E.H. Rothauser, G.E. Urbanek, and W.P. Pachl, "Isopreference method for speech evaluation", J. Acoust. Soc. Am., vol. 44, pp. 408-418, August 1968.

66. W.A. Munson and J.E. Karlin, "Isopreference method for evaluating speech-transmission circuits", J. Acoust. Soc. Am., vol. 34, pp. 762-774, June 1962.

67. W.H. Tedford, Jr., and T.V. Frazier, "Further study of iospreference method of circuit evaluation", J. Acoust. Soc. Am., vol 39, pp. 645-648, April 1966.

68. "IEEE Recommended Practice for Speech Quality Measurements", IEEE Trans. Audio and Electroacoustics, vol. AU-17, pp. 225-246, September 1969.

69. M.R. Schroeder, "Reference signal for speech quality studies", J. Acoust. Soc. Am., vol. 44, pp. 1735-1736, December 1968.

70. W.S. Torgerson, <u>Theory and Methods of Scaling</u>. New York: J. Wiley, 1958.

71. R.W. Benson, and I.J. Hirsh, "Some variables in audio spectrometry", J. Acoust. Soc. Am., vol. 25, pp. 499-505, May 1953.

72. D.L. Richards, "Statistical properties of speech signals", Proc. IEE, vol. 111, pp. 941-949, May 1964.

73. J.P. Guilford, <u>Psychometric Method</u>. New York: McGraw-Hill, 1954.

74. C.C. Mueller, "Numerical transformation in the analysis of experimental data", Psycho. Bull.,pp. 198-223, 1949.

75. M.E. Rose, "The analysis of angular correlation and angular distribution data", Phys. Rev., vol. 91, pp. 610-615, August 1953.

76. P.G. Hoel, <u>Introduction to Mathematical Statistics</u>. New York: J. Wiley, 1954, pp. 216-219.

77. R.A. McDonald, "Signal-to-noise and idle channel noise performance of differential pulse code modulation systems - Particular applications to voice signals", Bell Sys. Tech. J., vol. 45, pp. 1123-1151, September 1966.

78. D.S. Seraphin, "A fast random generator for IBM 360", Commun. Assoc. Comput. Mach., vol. 12, p. 695, December 1969.

79. J.B. O'Neal, Jr., "Delta modulation quantizing noise: Analytical and computer simulation results for Gaussian and television input signals", Bell Sys. Tech. J., vol. 45, pp. 117-141, January 1966.